LJI-R-84-329
June 15, 1985

La Jolla INSTITUTE
CENTER FOR STUDIES OF NONLINEAR DYNAMICS
3252 HOLIDAY COURT, SUITE 208
LA JOLLA, CALIFORNIA 92037 • PHONE (619) 587-6000
AFFILIATED WITH THE UNIVERSITY OF CALIFORNIA, SAN DIEGO

THEORETICAL STUDIES AND DATA ANALYSIS OF WAVE PROPAGATION IN RANDOM MEDIA

Semiannual Technical Report
for Period of December 1, 1984 to May 31, 1985

Sponsored by
Defense Advanced Research Projects Agency (DoD)
ARPA Order No. 4852

Under Contract No. MDA903-83-C-0515 issued by
Department of Army, Defense Supply Service-Washington,
Washington, DC 20310

Effective Date of Contact: December 1, 1984
Expiration Date: September 30, 1985

Principal Investigator: Stanley M. Flatté
Telephone (619) 587-6013

La Jolla Institute
Center for Studies of Nonlinear Dynamics*
3252 Holiday Ct., Suite 208
La Jolla, CA 92037

"The views and conclusions contained in this document are those of the authors and should not be interpreted as representing the official policies, either expressed or implied, of the Defense Advanced Research Projects Agency or the U.S. Government."

*Affiliated with the University of California, San Diego

LJI-R-84-329
June 15, 1985

THEORETICAL STUDIES AND DATA ANALYSIS OF WAVE PROPAGATION IN RANDOM MEDIA

Semiannual Technical Report
for Period of December 1, 1984 to May 31, 1985

Sponsored by
Defense Advanced Research Projects Agency (DoD)
ARPA Order No. 4852

Under Contract No. MDA903-83-C-0515 issued by
Department of Army, Defense Supply Service-Washington,
Washington, DC 20310

Effective Date of Contact: December 1, 1984
Expiration Date: September 30, 1985

Principal Investigator: Stanley M. Flatté
Telephone (619) 587-6013

La Jolla Institute
Center for Studies of Nonlinear Dynamics*
3252 Holiday Ct., Suite 208
La Jolla, CA 92037

*Affiliated with the University of California, San Diego

(cont'd p 1)

TABLE OF CONTENTS

in WPRM;

WPRM;

A

B

THEORETICAL STUDIES AND DATA ANALYSIS OF WAVE PROPAGATION IN RANDOM MEDIA

SEMIANNUAL TECHNICAL REPORT FOR PERIOD OF

December 1, 1984 to May 31, 1985

Contract No. MDA903-83-C-0515

Principal Investigator: Stanley M. Flatté

I. SUMMARY

The objective of this work is to develop a general theoretical framework for calculating fluctuations of signals on waves propagated through random media (WPRM) and to apply this framework to sound through the ocean; light through the atmosphere; radio waves through the ionosphere, solar wind, or interstellar plasma; and any other similar case of waves propagating through continuous media. Comparison with real data is an important aspect of the effort.

The two most common signals sent on a carrier are the phase and amplitude of a nearly monochromatic wave. If enough bandwidth is available, one can send a pulse, and one can speak of the intensity and arrival time of that pulse. The technical problem is then to explain the statistical behavior of the intensity and arrival time in terms of medium fluctuations, where the medium is described statistically, usually by a power spectrum covering a large dynamic range of scales. Papers include: → (top B)

The eventual practical applications of an understanding of WPRM to science and to the defense department are myriad. The phase of a light wave from an astronomical object or a satellite is used by a telescope to focus to a detector; the quality of the focus depends on the state of the atmosphere - a random medium. A ground-based laser with large optics attempts to focus on a small

spot for a period of time; the atmosphere spreads out the spot by its action on the phase of the wave. Determination of pulsar parameters depends on observations of radio pulses through a distorting random medium-interstellar plasma. Communication with spacecraft by radio pulses using radio telescopes depends on coding schemes and antenna control that must contend with effects due to the solar wind and the earth's ionosphere. Communication with earth satellites must contend with the ionosphere, and the effects of a disturbed ionosphere (due, e.g., to nuclear explosions) must be predicted. Probing ocean processes, from large-scales (Gulf stream) on down (internal waves and microstructure) depends on understanding acoustic propagation through a random medium; for example, a favored method is to send pulses over long range and observe their arrival-time variations. Detection of submarines by passive acoustics is limited by ocean fluctuations that control the maximum antenna size and integration time that can be used for coherent signal integration. Active sonar for communication has a limited bandwidth due to ocean fluctuations. Determination of the characteristics of earthquakes, thought to be important for earthquake prediction, is done solely by seismic detection. The earth through which the seismic waves travel has randomness, and this limits the information that can be gleaned from seismic signals. The same effect limits our ability to distinguish between underground nuclear explosions and earthquakes, and thus affects our political stance vis-a-vis nuclear test bans. On the other hand, the distortions of seismic waves due to the earth's random properties can be used as a probe of those properties and hence can lead to a better understanding of earth structure.

The path-integral method for treating wave propagation has been successfully used by the principal investigator for the analysis of many experiments in ocean acoustics.[1] This method is therefore utilized extensively in our work.

Another school of wave propagation theory, which began in the early 1960's in order to explain experiments in light transmission through the turbulent atmosphere, utilizes a different technique involving partial differential equations for the moments of the wave field.[2] The moment equations and the path integral have now been used by enough researchers that the value of both approaches is appreciated, but the relations between the two methods has remained confusing to many people.

A first step in WPRM is characterizing the statistics of the random medium. In this report we will speak of the spectrum of medium fluctuations, which would be obtained by dragging an index-of-refraction sensor through the medium and taking a Fourier transform of the resulting time (= space) series. This spectrum is characterized by a power law (e.g. -5/3 for Kolmogorov turbulence) that implies much more variation at large scales than at small scales. It is likely that a sensor dragged in different directions will observe different spectra even on the average. In that case we speak of an anisotropic spectrum. For example, the strength of the ocean spectrum is much higher in the vertical than the horizontal for the same wave-number. Finally it is important to know that the spectrum cannot continue indefinitely at either large or small scales. At the "outer scale" the spectrum cuts off due usually to finite container size – the height of the atmosphere or the depth of the ocean. At the "inner scale" the spectrum cuts off due to physical processes; for example, viscosity becomes important at scales of order a few millimeters in the atmosphere and ocean.

This technical report covers the third six months of our contract effort. The next several paragraphs summarize the technical results we have obtained: more details are given in following sections. The work has been carried out under the direction of Dr. Stanley Flatté, and involves effort by Dr. Flatté, senior scientist Dr. Frank Henyey, two post-doctoral researchers Drs. Dennis Creamer

and Rod Frehlich, and a graduate student (in the UCSD Electrical Engineering and Computer Science Department) Johanan Codona.

Our progress in understanding the travel time of pulses in random media has resulted in a paper ACCEPTED for publication,[3] as well as results that will lead to later publication. Pulses sent through a fluctuating medium arrive earlier or later than they would in the absence of fluctuations, depending on the particular realization of the medium. The variance of arrival time can be calculated by straightforward methods in the geometrical optics limit. Our dramatic new result is for the average arrival time, which we find advanced in weak media. Heretofore, researchers were of the opinion that pulses were delayed on the average. This effect is of little importance in communication applications where the average arrival time is usually less important than the variance. However, the effect can be important in probing a random medium for large-scale variations by their effect on average travel time. Our result implies a possible confusion between a changing turbulence level and a change in the average index of refraction on a large scale. For example, ocean acoustic tomography attempts to measure the warming of a 100-km-square area of the ocean by an expected change in travel time of about 20 ms. However we find a change in average travel time of about 10 ms, due to an internal-wavefield that has no average warming at all. We have recently studied the range dependence of this effect, and have found that it grows as the square of the range. This implies that experiments being planned in the 1000-4000 km region will have major difficulties sorting out the effects of internal waves from the effects of large-scale structure. Most importantly, the determinations of internal-wave effects will NOT be contaminated by the large-scale effects.

Moving from arrival time, which is related to phase, we discuss amplitude or intensity. We have developed a method for calculating the spatial correlation

function of intensity on a transverse plane through a receiver. This is a long-standing problem that is of great importance in using wave propagation for probing the structure of a random medium, because measuring intensity is often the observation that can be made most easily. In addition, an amplitude-modulated signal will be degraded by intensity fluctuations due to the medium. The standard theory develops a series solution for the intensity spatial spectrum. The first few terms are an accurate representation of the small-wave-number end of the spectrum. In order to calculate the high-wave-number region many terms of the series had to be evaluated. We have determined a different series expansion, whose first few terms give the high-wave-number section of the spectrum. Hence the evaluation of the full spectrum is simplified considerably. A paper describing our results has been SUBMITTED to Radio Science.[5]

We have also made considerable progress toward evaluating the intensity spectrum for an arbitrary source distribution, going beyond the standard procedure of considering the special cases of a point source or an incident plane wave. Our general case will include a source that is extended over a large aperture. We also treat the two-frequency case.[6] An example of a coherent source of large aperture would be a large-aperture laser beam. An example of an incoherent source is a planet, or an illuminated satellite, or an infrared plume from an ascending booster.

Because researchers favoring the moment-equation method or the path-integral method typically knew only one of the methods in any depth, the relation between the two methods has been a mystery to many. We have expended quite a bit of effort to understand this relation. We have a paper in REVIEW by the Journal of Mathematical Physics that will show that the two methods are mathematically equivalent,[7] in much the same way that the Heisenberg and

Schrödinger approaches to quantum mechanics were shown to be mathematically equivalent. A better analogy for those familiar with quantum mechanics is the equivalence of the Schrödinger and Feynman approaches to quantum mechanics. The equivalence extends to the equivalence term by term of the series solutions for the intensity spectra mentioned earlier.

In nearly all cases, in order to compare theory to experimental data in WPRM, we must use a model spectrum for the medium fluctuations. We have developed phenomenological spectra, as a function of wave vector, that allow for an anisotropic component added to a turbulent isotropic component.[8] This model is meaningful both for the ocean, where the anisotropic component represents internal waves, and the ionosphere, where the anisotropy is due to electrons preferentially moving along magnetic field lines. We are in the process of calculating intensity spectra in the weak fluctuation region using these model spectra. We have data from an ocean-acoustic experiment that will be used for comparison purposes; the experiment utilized 10-70 kHz sound over several hundred meters under the Arctic ice.[9] We should note that the weak-fluctuation regime is one in which the intensity series solution for the low-wave-number regime is the only relevant one.

For more than one hundred years, eclipse observers have noted "mysterious" bands of shadows moving on the ground just before and after an eclipse. Many exotic theories of these shadow bands have been put forward, but most observers agree that they are probably due to atmospheric scintillation that becomes visible when the crescent of the eclipsed moon becomes thin enough (a few minutes before and after an eclipse). Johanan Codona, the graduate student associated with this project, has made the first systematic application of WPRM theory to eclipse shadow-band observations.[10] He explains the orientation and

contrast of the bands as a function of time, and describes the effects of eclipse geometry and the importance of wind direction. He relates shadow-band observations to stellar-scintillation observations. One important conclusion he draws is that as the illuminated crescent gets thinner, the shadow-band observations probe higher into the atmosphere. Recently published data[11] from the eclipse of February 16, 1980 in India agrees with Codona's predictions. Further data from the annular eclipse of May 30, 1984 in Georgia should soon be forthcoming.

We have begun the analysis of seismic data from the Center for Seismic Studies. Two nuclear explosions in the Soviet Union with good detections on the NORESS array, which has about twenty elements spaced out to a few kilometers have been obtained. The first look shows rather small travel-time fluctuations, somewhat at odds with the large amplitude fluctuations that have been suggested previously. We have looked at the data as a function of frequency up to about 20 Hz, and have seen no obvious systematic differences in travel time between the different frequencies, except for an unusual change in the arrival structure between 5 and 10 Hz.

As discussed in our last six-month report, this period and the next few months are primarily periods of preparation of manuscripts for publication. We will be presenting this work at a number of conferences, including a meeting of the Union of Radio Scientists at Vancouver (June 1985).

We will continue to be directly involved in comparison between theory and experiment over the next year. Spacecraft data from the Stanford Center for Radar Astronomy, satellite data from SRI-International, and seismic data from the Center for Seismic Studies (Virginia) will be included, along with our ongoing ocean-data effort.

Our longer-term goals will include the implementation of our new theoretical results into computer codes for calculation of general phase and amplitude fluctuations. Two directions are contemplated that will require large-scale computing. The first is propagating waves through individual realizations of random media to compare with our theoretical results and to extrapolate those results into parameter regimes in which the theory is not valid. This propagation can be done via a parabolic wave equation, so that it is a marching solution. The second involves evaluating the theoretical formulas which involve either multidimensional ordinary integrals, or in some cases, path integrals. We have begun some computer work on simulation of WPRM using our VAX, and we plan to implement the code on an IBM-PC that has two FFT hardware boards that should allow uninterrupted calculations at about twice the speed of a VAX. These efforts are in preparation for proposals to do simulation calculations on a CRAY.

REFERENCES

1. S.M. Flatté, et al., Sound Transmission through a Fluctuating Ocean, Cambridge University Press, 1979.

2. V.I. Tatarskii, The Effects of the Turbulent Atmosphere on Wave Propagation, Israel Program for Scientific Translation: Jerusalem, Israel, 1971.

3. J.L. Codona, D.B. Creamer, S.M. Flatté, R.G. Frehlich and F.S. Henyey, "Average Arrival Time of Wave Pulses through Continuous Random Media," accepted for publication in Physical Review Letters, May, 1985.

4. S.M. Flatté, "The Effect of Internal Waves on the Travel-Time of Acoustic Pulses over Long Ranges in the Ocean," in preparation.

5. J.L. Codona, D.B. Creamer, S.M. Flatté, R.G. Frehlich, and F.S. Henyey, "Solution for the Fourth Moment of Waves Propagating in Random Media," submitted for publication in Radio Science, May, 1985.

6. J.L. Codona, et al., "Two-frequency Intensity Correlation of an Extended Source seen through a Strongly Scattering Phase Screen" abstract submitted to U.R.S.I.

7. J.L. Codona, et al., "Comparison of Path-Integral and Moment-Equation Techniques for Wave Propagation in Random Media," submitted for publication in the Journal of Mathematical Physics.

8. See Section V.

9. M. Schulkin, G.R. Garrison, and T. Wen, "High-frequency Acoustic Variability in the Arctic, preprint from the University of Washington Applied Physics Laboratory.

10. J.L. Codona, "The Scintillation Theory of Eclipse Shadowbands," in preparation.

11. L.A. Marschall, R. Mahon, and R.C. Henry, "Observations of Shadow Bands at the Total Solar Eclipse of 16 February 1980," Applied Optics, **23**, 4390-93, 1984.

II. EQUIVALENCE OF PATH INTEGRAL AND MOMENT EQUATIONS

Two approaches have yielded many results for WPRM. These are the moment equation approach and the path integral approach. Although they both start with the parabolic wave equation, approximation are made in each to derive the fundamental equation or expression for any statistical moment of the wave field. These approximations are in the nature of assuming that correlation lengths are not too long. The relationship between the two approaches has not been clear.

We show that the two approaches are, in fact, equivalent. By using the method that Feynman used to show his path integral was equivalent to Schrödinger's equation, we derive an equation equivalent to the path integral, and find that this equation is the moment equation used in practice as a starting point in WPRM studies.

In some applications, both approaches yield expansions of the moment in some variable. Since the approaches are equivalent, the expansions are equal term by term. In other applications, one or the other approach might yield a desired expansion or approximation more readily than the other. For example, corrections to the "semiclassical" result are more easily obtained from the path integral.

The following manuscript is our finished paper on this subject. It has been submitted for publication in the Journal of Mathematical Physics.

LJI-P-84-294R1

Moment-Equation and Path-Integral Techniques for Wave Propagation in Random Media

by

Johanan L. Codona, Dennis B. Creamer, Stanley M. Flatté,*
R.G. Frehlich, and Frank S. Henyey

Center For Studies of Nonlinear Dynamics†
La Jolla Institute
3252 Holiday Court, Suite 208
La Jolla, California 92037

March 1985

---

*On leave from the University of California, Santa Cruz, CA 95064
†Affiliated with the University of California, San Diego.

Abstract

Differential equations for all moments of the field of a wave propagating through a random medium are derived under the parabolic approximation and the Markov approximation, but including anisotropy in the random medium and a deterministic background refractive index. Mathematical equivalence is demonstrated between these moment equations and path-integral expressions for the moments obtained under the same approximations. A discussion of approximations that are weaker than Markov is given.

I. Introduction

Many problems in wave propagation through random media concern phenomena in which there is no significant backscatter, so that a parabolic approximation may be made to the wave equation.[1] In these cases a further approximation, called the Markov approximation,[2] leads to relatively tractable mathematical expressions for moments of the field that can be used for practical calculations. Two quite different formalisms have been used in this context: the moment-equation and path-integral techniques.

A path-integral expression for a general moment of the field of a wave propagating through an inhomogeneous, anisotropic medium in the presence of a deterministic background refractive index has been derived,[3] and the expression has been used for specific calculations.[4,5,6]

Moment equations in coordinate representation have been derived for homogeneous isotropic media in the absence of a deterministic background.[2] Treatments of inhomogeneity, anisotropy, and deterministic background by moment-equation techniques have heretofore been confined to special cases involving the first and second moments.[7,8]

We present here general moment equations in coordinate representation that account for inhomogeneity, anisotropy, and deterministic background, but require the Markov approximation. We derive these equations using the time-ordered-product method of Van Kampen,[9] which also provides a derivation of equations that are valid under conditions more general than the Markov approximation. The modified equations are more complicated than those that require the Markov approximation: a special case was previously derived by Besieris and Tappert.[10]

We also show that our new general moment equations derived under the Markov approximation are mathematically equivalent to the path-integral expressions for the moments that have been previously presented. Thus, the two popular formalisms, under the Markov approximation, are not different in content.

The plan of the paper is as follows: in Section II we establish notation, present our new moment equations, and present path-integral expressions for the moments in similar notation. In Section III we establish the mathematical equivalence between the two techniques. In Section IV we present the derivation of our moment equations, and, along the way, derive the modified equations. In Section V, for completeness, we rederive the path-integral expressions for the moments. In Section VI we comment on the use of different coordinate systems (such as cylindrical or spherical) in the writing of moment equations. A summary concludes the paper.

II. Notation and Markov-Approximation Results

Consider waves travelling predominantly in the z direction. Let $\underline{x}$ be a transverse coordinate (e.g. two-dimensional, but in fact general), and k be a reference wave number ($k = 2\pi\omega/C_0$), where ω is the wave frequency and C_0 is a reference wave speed). Express the full wave field as

$$u(\underline{x},z,t) = \psi(\underline{x},z)\exp[ik(z - C_0 t)] \tag{1}$$

Let the wave speed (a function of position only) be

$$C(\underline{x},z) = C_0[1-2U_0(\underline{x})-2\mu(\underline{x},z)]^{-\frac{1}{2}} \approx C_0[1 + U_0(\underline{x}) + \mu(\underline{x},z)] \tag{2}$$

where U_0 represents the deterministic background and μ represents the fluctuating random medium, assumed to be a realization of a zero-mean Gaussian process.

Then, the parabolic equation (in rectangular coordinates) for the reduced wave function ψ is :

$$ik\partial_z\psi = -\frac{1}{2}\nabla^2\psi + k^2U_0(\underline{x})\psi + k^2\mu(\underline{x},z)\psi \tag{3}$$

where ∇^2 is the transverse Laplacian.

A moment Γ is the ensemble expectation value of a product of ψ's and ψ^*'s where each ψ or ψ^* is evaluated at a different position $\underline{x}_j$ and wavenumber k_j. We write, in abbreviated form,

$$\Gamma_{mn} = \langle \psi_1^* \cdots \psi_m^* \psi_{m+1} \cdots \psi_{m+n} \rangle \tag{4}$$

Define an operator L_0 such that

$$L_0 = \sum_{j=1}^{m+n} \pm \frac{1}{k_j}\left[-\frac{1}{2}\nabla_j^2 + k_j^2 U_{0j}\right] \tag{5}$$

The terms that apply to the ψ's use the plus sign and those that apply to the ψ^*'s use the minus sign. The subscript j requires that ∇_j^2 operate only on $\underline{x}_j$ and $U_{0j} \equiv U_0(\underline{x}_j)$.

Define the important combination of fluctuation quantities as

$$M(z) = \sum_{j=1}^{m+n} \pm k_j \mu(\underline{z}_j, z) \tag{6}$$

Our general moment equation under the Markov approximation can be written

$$\partial_z \Gamma_{mn}(z) = -iL_0 \Gamma_{mn}(z) - \frac{1}{2} \int_{-\infty}^{\infty} dz' \langle M(z) M_{shift}(z') \rangle \Gamma_{mn}(z) \tag{7}$$

where $M_{shift}(z')$ is obtained by evaluating $M(z)$ with all the $\underline{z}_j$ at z shifted by the transverse distance that a deterministic ray through $(\underline{z}_j, z)$ moves in travelling from z to z' (see Figure 1). In other words $M_{shift}(z')$ is evaluated at point B: i.e. $\underline{z}_j = \underline{z}_{ray}(z')$ where the ray is forced to go through $\underline{z}_j(z)$. The particular ray is determined not only by the local position $(\underline{z}_j, z)$, but also by the initial conditions on the moment; for example, the location of a point source, or the direction of a plane wave. The unphysical assumption of delta-correlated medium fluctuations along the propagation direction would imply that $M_{shift}(z')$ would be evaluated at point C: i.e. $\underline{z}_j(z)$ (and z'). In the isotropic case (or in the case of propagation along a principal axis of the anisotropy) the difference between evaluating $M_{shift}(z')$ at $\underline{z}_j(z)$ and $\underline{z}_{ray}(z')$ is negligible, and the delta-correlated assumption is adequate. In the anisotropic case, the necessity of defining the unperturbed ray makes (7) somewhat complicated to apply for general initial conditions. However, since (7) is a linear equation, superposition can be used whether the source is a point, an incident plane wave, or an arbitrary coherent or incoherent sum of point sources. Equation (7), which is one of the principal results of this paper, is derived in Section IV.

We now turn to the path integral method. Equation (3) has the formal solution

$$\psi = \int D\underline{z}(z) e^{iS} \tag{8}$$

where $\int D\underline{z}(z)$ means integration over paths, $\underline{z}(z)$ is a transverse vector indicating the position of the path at z, and

$$S = k \int_0^R dz \left[\frac{1}{2} \left(\frac{d\underline{z}}{dz} \right)^2 - U_0(\underline{z}) - \mu(\underline{z}, z) \right] \tag{9}$$

In order to obtain a given moment, expressions like (8) (or its complex conjugate) are multiplied together, and the ensemble average is taken:

$$\Gamma_{mn} = \int \prod_{j=1}^{m+n} D\mathcal{Z}_j(z) < e^{\sum \pm i S_j} > \tag{10}$$

The Markov approximation yields (See Section V):

$$\Gamma_{mn} = \int \prod_{j=1}^{m+n} D\mathcal{Z}_j(z) \exp \int_0^R dz \left[\sum_j \pm ik_j \left\{ \frac{1}{2} \left(\frac{d\mathcal{Z}_j}{dz} \right)^2 - U_{0j} \right\} - \frac{1}{2} \int_{-\infty}^{\infty} dz' < M(z) M_{shift}(z') > \right] \tag{11}$$

We show in the next section that the moment equations (7) and the path integral expressions (11) are mathematically equivalent.

III. Equivalence of Path Integral and Moment Equations under the Markov Approximation

We follow the technique that Feynman[11] used to show that his path-integral expression for nonrelativistic quantum mechanics is equivalent to the Schrödinger equation. The key to this demonstration is an understanding of how the important paths behave transversely as they move in z from a particular point. Feynman found that these paths resembled random walks in that

$$|\underline{x}(z') - \underline{x}(z)| \sim (z' - z)^{\frac{1}{2}} \tag{12}$$

as z' gets close to z. Given this behavior, it is easy to expand (11) in a Taylor series and obtain a differential equation which will turn out to be (7). We give the demonstration of (12) in the Appendix.

The path integral is defined as the limit of an integration over a set of "phase screens." These screens are at values $z_N = N\delta z$. The derivative $\frac{d\underline{x}}{dz}$ at $z = z_N$ is defined as $(\underline{x}(z_N + \delta z) - \underline{x}(z_N))/\delta z = \frac{\delta \underline{x}}{\delta z}$. The limit $\delta z \to 0$ is taken after the integrals are evaluated. The differential equation is obtained by considering the integral over the very last phase screen. The last integral in (11) can be written in terms of $\underline{x}_j' = \underline{x}_j(R - \delta z)$ and $\underline{x}_j = \underline{x}_j(R)$. Also, we define $\delta \underline{x}_j = \underline{x}_j - \underline{x}_j'$. Then Γ_{mn} can be expressed as:

$$\Gamma_{mn}(\{\underline{x}\}, R) = \tag{13}$$

$$N \int \prod_j d\underline{x}_j' \exp\left\{\delta z \left[\sum_j \pm i k_j \left[\frac{1}{2}\left[\frac{\delta \underline{x}_j}{\delta z}\right]^2 - U_{0j}\right] - \frac{1}{2}\int dz' < M(R) M_{shift}(z') > \right]\right\}$$

$$\Gamma_{mn}(\{\underline{x}'\}, R - \delta z)$$

where $\{\underline{x}\}$ denotes the set of $m+n$ $\underline{x}_j$'s. The first term in the exponent, $\pm \frac{ik_j}{2} \frac{(\delta \underline{x}_j)^2}{\delta z}$, is O(1) for small δz, because of (12). The exponent of the remaining terms can be expanded, since they have an explicit δz, as well as higher order terms. This results in

$$\Gamma_{mn}(\{z\},R) = \tag{14}$$

$$N\int\prod_j (d\delta z_j \exp\{\pm ik_j(\delta z_j)^2/2\delta z\})$$

$$\left[1-\delta z\left(\sum_j \pm ik_j U_{0j}(R)+\frac{1}{2}\int_{-\infty}^{\infty} dz' <M(R)M_{shift}(z')>\right)\right]\Gamma_{mn}(\{z'\},R-\delta z) + O(\delta z^{\frac{3}{2}})$$

We now have a relationship between the moment at R and the moment at $R-\delta z$, which we derived from our path-integral expression. But since the moment is a differentiable function we can find another relationship by Taylor expansion as follows:

$$\Gamma_{mn}(\{z'\},R-\delta z) = \left[1 - \delta z\,\partial_R - \sum_j \delta z_j\cdot\nabla_j + \frac{1}{2}\left(\sum_j \delta z_j\cdot\nabla_j\right)^2\right]\Gamma_{mn}(\{z\},R) \tag{15}$$

$$+ O(\delta z^{\frac{3}{2}})$$

Substituting (15) into (14) we find

$$\Gamma_{mn}(\{z\},R) = N\int\prod_j \left\{d\delta z_j \exp\{\pm ik_j(\delta z_j^2)/2\delta z\}\right. \tag{16}$$

$$\left.\left[1-\sum_j \delta z_j\cdot\nabla_j+\frac{1}{2}\left(\sum_j \delta z_j\cdot\nabla_j\right)^2-\delta z\,\partial_R-\delta z\left(\sum_j \pm ik_j U_{0j}(R)+\frac{1}{2}\int_{-\infty}^{\infty} dz' < M(R)M_{shift}(z') >\right)\right]\right\}$$

$$\Gamma_{mn}(\{z\},R) + O(\delta z^{\frac{3}{2}})$$

The term linear in $\sum_j \delta z_j\cdot\nabla_j$ is odd in δz_j and therefore gives zero due to the δz_j integral. The term that is quadratic in δz_j can be integrated by parts, yielding, to order δz:

$$\Gamma_{mn}(\{z\},R) = N\int\prod_j (d\delta z_j \exp\{\pm ik_j(\delta z_j)^2/2\delta z\})$$

$$\cdot\left\{1+\delta z\left|-\partial_R - \frac{1}{2}\sum_j \frac{1}{\pm ik_j}\nabla_j^2 - \sum_j \pm ik_j U_{0j}(R)\right.\right.$$

$$\left.\left. - \frac{1}{2}\int_{-\infty}^{\infty} dz' < M(R) M_{shift}(z') > \right\}\right| \Gamma_{mn}(\{z\},R) \quad . \tag{17}$$

The only way (17) can be true for all δz is for the coefficient of δz within the curly brackets operating on Γ_{mn} to give zero. Therefore, setting $R \to z$,

$$\partial_z \Gamma_{mn}(\{z\},z) = -i\sum \pm \frac{1}{k_j}(-\frac{1}{2}\nabla_j^2 + k_j^2 U_{0j})\Gamma_{mn}(\{z\},z)$$

$$- \frac{1}{2}\int_{-\infty}^{\infty} dz' < M(z) M_{shift}(z') > \Gamma_{mn}(\{z\},z) \tag{18}$$

which is identical to (7), as required. Thus, we have derived the moment equation (7) from the path integral expression (11). This shows that the path-integral expression (11) is a solution of the moment equation (7) and hence the two techniques are equivalent.

IV. Moment-Equation Derivation

We derive our moment equations by the method of Van Kampen.[9] The advantage of his method is that the physical basis for each approximation is readily apparent. He bases his method on techniques that were developed for quantum mechanics.

We shall find that the Markov approximation requires that the dimensionless number $L_p^2 M_t^2$ be small where L_p is the medium correlation length in the direction of the wave propagation, and M_t is the "typical" value of M, defined by (6) and called the "interaction strength." For the first moment $M = k\mu$, but for higher moments M is the sum and difference of a number of $k\mu$'s at different positions, and with different values of k.

We start with the parabolic wave equation (3) and the definition of L_0 and M, and write:

$$i\partial_z \psi_1^* \psi_2^* \cdots \psi_{m+n} = (L_0 + M)\psi_1^* \psi_2^* \cdots \psi_{m+n} \tag{19}$$

The "interaction representation" is defined by:

$$(\psi_1^* \psi_2^* \cdots \psi_{m+n})_I = e^{iL_0 z} \psi_1^* \psi_2^* \cdots \psi_{m+n} \tag{20}$$

and

$$M_I(z) = e^{iL_0 z} M(z) e^{-iL_0 z} \tag{21}$$

With these definitions, (19) becomes

$$i\partial_z (\psi_1^* \psi_2^* \cdots \psi_{m+n})_I = M_I(z)(\psi_1^* \psi_2^* \cdots \psi_{m+n})_I \tag{22}$$

This equation is linear and has the formal solution

$$(\psi_1^* \psi_2^* \cdots \psi_{m+n})_I = T\exp\left(-i \int_0^z M_I(z')dz'\right) \Gamma_{mn}(0) \tag{23}$$

$\Gamma_{mn}(0)$ is the initial condition. The "time-ordering" symbol T requires explanation. One notices that M_I is an operator, not just a function of space. $M_I(z_1)$ and $M_I(z_2)$ do not, in general, commute. If they did the solution of (22) would be given by (23) without the T symbol. The T symbol means that a product of

operators to the right is not applied in the usual order, but in such a way that operators with smaller values of z' are to be applied first. Thus there is an ordering in z. (The T-symbol was invented for solving problems in quantum mechanics where the analog of the longitudinal direction z is the time.) For example,

$$T\exp\Big(-i\int_0^z M_I(z')dz'\Big) = \tag{24}$$

$$\Big[T\exp\Big(-i\int_{z_1}^z M_I(z')dz'\Big)\Big]\Big[T\exp\Big(-i\int_0^{z_1} M_I(z')dz'\Big)\Big]$$

for $0 \le z_1 \le z$. Another example is

$$T\,\frac{(-i)^k}{k!}\left[\int_0^z M_I(z')dz'\right]^k = (-i)^k \int M_I(z_k)\ldots M_I(z_2)\,M_I(z_1)dz_1\,dz_2\ldots dz_k \tag{25}$$

where the integration region on the right side of (25) is $0 < z_1 < z_2 \ldots < z_k < z$, which is $k!$ times smaller than that of the left side, cancelling the factor of $k!$. Using either (24) or (25), one readily checks that (23) is a formal solution of (22).

We are assuming that M is a Gaussian process. The result that the expectation of the exponential of a zero-mean Gaussian random variable is the exponential of half the variance follows from combinatorial factors and remains true for a time-ordered exponential. Thus

$$(\Gamma_{mn})_I = T\exp\left[-\frac{1}{2}<\left[\int_0^z M_I(z')dz'\right]^2>\right]\Gamma_{mn}(0) \tag{26}$$

Although this is a formal expression for Γ_{mn}, it is not immediately useful for calculations, since there is no simple algorithm for evaluating a time-ordered exponential (in contrast to a normal exponential). Van Kampen proceeds by differentiating (26):

$$\partial_z(\Gamma_{mn})_I = \tag{27}$$

$$-T<M_I(z)\int_0^z dz' M_I(z')>\exp-\frac{1}{2}<\left[\int_0^z M_I(z'')dz''\right]^2>\Gamma_{mn}(0)$$

The $M_I(z)$ has the largest z, so it is written in the proper ordered position. The $M_I(z')$ that it is correlated with, however, might occur anywhere relative to the $M_I(z'')$'s in the exponential. If $L_p^2 M_t^2 \ll 1$, very little error is made by assuming that the first two M_I's are in the proper order, so that the T symbol can be brought through the first expectation value, yielding:

$$\theta_s(\Gamma_{mn})_I = - < M_I(z) \int_0^z dz' M_I(z') > (\Gamma_{mn})_I \tag{28}$$

This may be shown by expanding the exponential operators in (26) or (27) and discussing the order of M's in each term. The Nth term in the expansion has 2N occurrences of M_I, and is of a magnitude

$$< (\int_0^z M_I dz')^2 >^N / N! \tag{29}$$

where typical eigenvalues of the operators are implied. The terms beyond

$$N \approx 4 < (\int_0^z M_I dz')^2 > \tag{30}$$

become negligible compared to the original exponential, so we have to deal with at most N pairs of M_I's from source to range z. The two M_I's in a correlated pair must be within L_p of each other to give a nonzero correlation. The number of pairs may be estimated as

$$N \approx 4 L_p z M_t^2 \tag{31}$$

where M_t^2 is a typical value of M_I^2. (See Figure 2 for a schematic representation.) Our approximation reduces to saying it is unlikely to find a third occurrence of an M_I in between a pair that are within L_p of each other. This probability is roughly

$$\text{Probability} \approx \frac{L_p N}{z} \approx L_p^2 M_t^2 \quad . \tag{32}$$

Thus if the fluctuations are weak enough (M_t small), the approximation is valid, and (28) is justified.

We call (28) "first order perturbation theory." In typical situations, z is much larger than L_p, and the lower limit can be replaced by $-\infty$, making the equation independent of the source position. Moreover, the integral from $-\infty$ to z can be replaced by half the integral from $-\infty$ to ∞, when the correlation is a much slower function of $\frac{1}{2}(z+z')$ than of $z-z'$. The result is used, not in the interaction representation, but in the original representation. The exponentials of (20) and (21) are removed, giving

$$\partial_z \Gamma_{mn}(z) = \tag{33}$$

$$-iL_0\Gamma_{mn}(z) - \int_{-\infty}^{z} dz' \, \langle M(z) e^{-iL_0(z-z')} M(z') e^{iL_0(z-z')} \rangle \Gamma_{mn}(z)$$

For the second moment, this equation is related to an expression of Besieris and Tappert.[10] Although their work was for the second moment, we can generalize it directly; therefore in the rest of our comments we treat the general moment Γ_{mn} where Besieris and Tappert treated only Γ_{11}. Their equation 3.2 was expressed in a Fourier-transformed domain, but can be expressed in our notation as

$$\partial_z \Gamma_{mn}(z) = -iL_0\Gamma_{mn}(z) - \int_{-\infty}^{z} dz' \, \langle M(z) e^{-iL_0(z-z')} M(z') \rangle \Gamma_{mn}(z') \,. \tag{34}$$

This equation is equivalent to (33) to order $L_p^2 M_i^2$. Unlike (33), (34) implies a "memory" effect in which the gradient of the moment depends explicitly on the moment at all previous z's. The Markov approximation leads to (7), which eliminates the memory effect and requires only a correlation function of the medium along a specified (shifted) direction. Besieris and Tappert pointed out that a weaker approximation, called the "long-time Markov" approximation leads to a local (non-memory) equation (their equation 3.3), that in our notation is expressed as

$$\partial_z \Gamma_{mn} = -iL_0\Gamma_{mn}(z) - \left\{ \int_{-\infty}^{z} dz' \, \langle M(z) e^{-iL_0(z-z')} M(z') \rangle \right\} \Gamma_{mn}(z) \,. \tag{35}$$

We are only considering situations in which the parabolic wave equation is valid. It has been shown that in that case the long-time Markov is valid,[10] and

therefore (35) is as valid as (33).

Because L_0 is an operator, the integrals in (33-35) involve the medium correlation function in all directions, or, in the Fourier-transform domain, require a scattering kernel as a function of scattering angle. The Markov approximation to (33) consists of simplifying the deterministic propagation operator $e^{-iL_0(z-z')}$ for $z - z'$ on the order of L_p. Instead of correlating $M(z)$ with all possible transverse positions of $M(z')$, the Markov approximation corresponds to choosing only one transverse position for $M(z')$. (See Figure 1, where point A represents an arbitrary transverse position.) If the wave represented by $\Gamma_{mn}(z)$ were the unperturbed solution, then deterministic propagation would move the phase in the direction of the unperturbed ray. If the wave energy is traveling close to the unperturbed ray this operator retains its behavior to first approximation. As a result, deterministic propagation approximates a shift along the unperturbed ray to point B, i.e., $\underline{x}(z') = \underline{x}_{ray}(z')$, where the ray is forced to go through $\underline{x}(z)$. Hence $e^{-iL_0(z-z')}M(z')e^{iL_0(z-z')}$ can be approximated by $M_{shift}(z')$. This is the appropriate definition of the Markov approximation (rather than assuming the medium is delta-correlated along the z axis) and it immediately yields (7) from (33). In practice, instead of using the actual unperturbed ray, the tangent to the ray at z is often used.

If the delta-correlated assumption were made, it would correspond to evaluating $M_{shift}(z')$ at point C, which is strictly valid only if there is a single unperturbed ray travelling along the z-axis. If the medium fluctuations are isotropic, the correlation of any point at z' with the point P at z will give the same result because of the parabolic approximation, and hence the delta-correlated assumption is as good as any other choice. However, for an anisotropic medium it is important that point B (and hence (7)) be used, even when the Markov approximation is invoked. Note that (7) can be used in the presence of a deterministic background refractive index.

The difference between (33) and (7) can be caused by directions different from the unperturbed ray becoming important. A transverse wavenumber k_T, coming, for example, from M, causes the angle to change by $\delta\vartheta = k_T / k$. A transverse error in position of about $k_T L_p / k$ is made by assuming the

direction of the unperturbed ray. Thus, in order for the Markov approximation to be valid, it is required that $k_T L_p / k \ll L_T$, where L_T is the transverse scale of concern. Since $L_T \approx 1/k_T$, the Markov approximation fails at sufficiently small $k \approx L_p / L_f^2$. The parameter $\alpha = kL_f^2 / L_p$ introduced by Beran and McCoy[12] and discussed further in Flatté[4] reflects these considerations. For small α, one can use (33) or its equivalent.

V. Path-Integral Derivation

We recapitulate the derivation of the path-integral expression (7) from (10). Using the assumed Gaussian behavior of the fluctuations, we obtain from (10)

$$\Gamma_{mn} = \int \prod_{j=1}^{n} D\xi_j(z)\, e^{\sum_j \pm i S_{0j}}\, e^{V} \tag{36}$$

where S_0 is the part of S in (9) that does not involve μ, and

$$V = -\frac{1}{2}\int dz\, dz' < M(z) M(z') > \tag{37}$$

The expression (36) is an exact representation of the moment of the solution of the parabolic equation with Gaussian fluctuations. It is not used in practice as it stands because V depends on the paths at two values of z, namely z and z'.

The Markov approximation for the path integral comes from assuming that the paths do not stray far in transverse space over a distance L_P; they all move approximately parallel to the unperturbed ray. Thus, in the Markov approximation

$$V = -\frac{1}{2}\int dz\, dz' < M(z) M_{shift}(z') > \tag{38}$$

which only requires knowledge of the path at z. The final result (11) follows directly.

VI. Coordinate Systems

Moment equations can be formulated in a variety of coordinate systems, while path integrals require a rectangular coordinate system. There has been a fair amount of effort expended on using polar coordinate systems, especially for point source problems.

The same results (for point sources among others) can be obtained in either polar or rectangular coordinates. Thus, the results of Shishov[13] on the intensity correlation, derived in spherical polar coordinates, can be seen to be identical (after an appropriate transformation) to the results of Codona *et al.*,[14] derived in rectangular coordinates. It was necessary for Shishov to make small angle approximations in addition to the parabolic approximation of dropping the second derivative in the propagation direction, whereas Codona *et al.* only require the single parabolic approximation.

VII. Summary

We have derived moment equations in coordinate representation under the Markov approximation that apply in anisotropic, inhomogeneous media with deterministic background. The derivation shows the relationship between these moment equations and modified equations that are valid under approximations weaker than Markov; the second-moment equation of Besieris and Tappert is a special case of these modified equations.

In a hierarchy of approximations we begin with the parabolic wave equation itself. A path integral with non-local exponent can be written as an exact solution, although it is not yet useful in practice. The next level is the approximation that the interaction strength over a correlation length is small—this "first-order perturbation theory" leads to the modified moment equations, and in homogeneous, isotropic media, to the standard moment equations and path-integral expressions. In anisotropic, inhomogeneous media, however, a further approximation is necessary to obtain the moment equations and path integral expressions. This further approximation is that the significant flow of wave energy, or the important paths, are parallel to the unperturbed ray; we call this the Markov approximation because its violation implies the appearance of correlations between successive scatterings. We have shown that the moment equations and the path-integral expressions for the moments are mathematically equivalent under the Markov approximation. Thus the two formalisms have exactly the same physical content. In an anisotropic medium, the moment equation involves a shift operation to calculate the medium correlation function along the unperturbed ray; this form of the moment equation has not been given before.

We have also pointed out that all appropriate formulae can be derived in a rectangular coordinate system (even for point sources).

Acknowledgement: This work was supported by DARPA.

Appendix

We must show that the scaling $|\delta \underline{x}_j| \sim (\delta z)^{\frac{1}{2}}$ holds for integrals of the form

$$\int \prod d\delta \underline{x}_j \exp\left[\sum \pm i k_j \frac{\delta x_j^2}{2\delta z}\right] F(\underline{x}_j) \qquad (A.1)$$

If F is expandable in a power series (even if the radius of convergence is zero) this result follows immediately. One expands F and integrates term by term, obtaining a power series in $(\delta z)^{\frac{1}{2}}$. By standard methods in the theory of asymptotic expansions, only the low order terms need to be retained as $\delta z \to 0$.

For singular functions, a demonstration is not as simple . One may worry about cancellations between terms in the exponent, since the signs might differ.

We will content ourselves with a demonstration in the case likely to arise in practice. It is common to model a random medium as having a power law structure function. Thus as two x's become equal, a singularity $|x_i - x_j|^p$ with $p > 0$ might occur in the integrand. In order to have possible cancellations in the exponent, we assume that $k_i = k_j = k$, and the exponential factor is $\exp(ik(\delta x_i^2 - \delta x_j^2)/2\delta z)$. We assume, for simplicity, that x_i and x_j are one-dimensional; higher dimensional singularities are effectively weaker.

Define $\nu = (\delta x_i + \delta x_j)/2$, $\mu = \delta x_i - \delta x_j$, $\alpha = x_i - x_j$. The singularity from the previous step, $x_j' = x_j - \delta x_j$ is $|\mu - \alpha|^p$. The integral to be evaluated is

$$\int d\mu d\nu \, e^{i\mu\nu/\delta z} f(\alpha,\mu,\nu) |\mu - \alpha|^p \qquad (A.2)$$

We would like to ignore the μ dependence in f. However, spurious large-μ contributions would arise, even though we are only interested in contributions from μ close to α. To drop the μ dependence of f and also to simplify the analysis, we introduce a convergence factor $\exp(-a(\mu^2 + \nu^2)/\delta z^{1-\varepsilon})$. As long as $\mu, \nu \sim \delta z^{\frac{1}{2}}$, this factor does not change the integral as $\delta z \to 0$ (we are assuming $\varepsilon > 0$). Conversely, if the integral in the limit $\delta z \to 0$ does not depend on a and ε, then μ and ν are of order $\delta z^{\frac{1}{2}}$.

The integral is then

$$I = \int d\mu d\nu \, e^{ik\mu\nu/\delta z} \exp[-a(\mu^2 + \nu^2)/\delta z^{1-\varepsilon}] \, |\mu - \alpha|^p \, f(\alpha,\nu) \qquad (A.3)$$

The μ integral can be done:

$$I = C_1 \int d\nu \, e^{ik\alpha\nu/\delta z} \exp[-a(\alpha^2 + \nu^2)/\delta z^{1-\varepsilon}] \qquad (A.4)$$

$$f(\alpha,\nu) \, a^{-(1+p)/2} \, \delta z^{(1+p)(1-\varepsilon)/2} \, M\left(\frac{p+1}{2}, \frac{1}{2}, -\frac{(\nu+2i\delta z^{\varepsilon} a\alpha)^2}{4a\delta z^{1+\varepsilon}}\right)$$

where M is a confluent hypergeometric function and C_1 is a constant independent of δz, ε, and a (as are C_2 and C_3, below). The hypergeometric function has a part that behaves as the exponential of its argument for large (positive) values of its argument, a part that falls as a power (since $(p+1)/2$ is positive) and a part at small values of the argument. These last two parts can be combined into a bounded part. We show that the exponential part gives the leading behavior and the bounded part is a higher power of δz.

The contribution I_1 from the exponential asymptotic part of M is

$$I_1 = C_2 \int d\nu e^{ik\alpha\nu/\delta z} \exp[-a(\alpha^2 + \nu^2)/\delta z^{1-\varepsilon}] \qquad (A.5)$$

$$f(\alpha,\nu) \, a^{-(1+p)/2} \, \delta z^{(1+p)(1-\varepsilon)/2} \exp\left(\frac{(2\delta z^{\varepsilon} a\alpha - ik\nu)^2}{4a\delta z^{1-\varepsilon}}\right)$$

The exponential from M cancels much of the first two exponentials:

$$I_1 = C_2 \int d\nu \exp\left\{-\nu^2\left[\frac{a}{\delta z^{1-\varepsilon}} + \frac{k^2}{4a\delta z^{1+\varepsilon}}\right]\right\} f(\alpha,\nu) \, a^{-(1+p)/2} \, \delta z^{(1+p)(1-\varepsilon)/2} \qquad (A.6)$$

which can be done explicitly. Only the first term in the exponential survives as $\delta z \to 0$. The result is independent of a and ε, and is

$$I_1 = C_3 \delta z \, f(\alpha,0) |\alpha|^p \qquad (A.7)$$

exactly as would be obtained from the Taylor series expansion for I.

We now turn to the contribution I_2 from the bounded part of M. We show I_2 has a higher power of δz than I_1. We can set ε to any positive value. At large ε we depend on the fact that $e^{ik\alpha\nu/\delta z}$ averages to zero for $\nu \sim \delta z^{1+\delta}$ for any positive

δ, but it would be necessary to examine the detailed behavior of M to use this fact. On the other hand, for small enough ε, it suffices to bound the integral by the integral of the absolute value of the integrand. The convergence factor provides a cutoff at $\nu \sim \delta z^{1-\varepsilon/2}$. Thus $\int d\nu \exp[-a\nu^2/\delta z^{1-\varepsilon}] f(a,\nu)$ gives a contribution scaling like $\delta z^{1-\varepsilon/2}$. Thus I_2 is bounded by an expression which scales as

$$I_2 \sim \delta z^{(1-\varepsilon)/2 + (1+p)(1-\varepsilon)/2} = \delta z^{(1+p/2)(1-\varepsilon)} \qquad \text{(A.8)}$$

As long as we have chosen ε small enough, the exponent of δz is larger than 1, and I_2 can be neglected relative to I_1. Thus we have established the necessary scaling of μ and ν even in the singular case.

References

1. V.A. Fock, "Theory of Radio-Wave Propagation in an Inhomogeneous Atmosphere for a Raised Source," *Bulletin de l'Académie des Sciences de l'URSS*, 70, 1950. Translated as Ch. 14 of *Electromagnetic Diffraction and Propagation Problems*, by V.A. Fock, Permagamon Press, Oxford, 1965.

2. V.I. Tatarskii, *The Effects of the Turbulent Atmosphere on Wave Propagation*, p. 223, Israel Program For Scientific Translation, Jerusalem, 1971.

3. R. Dashen, "Path Integrals for Waves in Random Media," *J. Math. Phys.*, vol. 20, 894-920, May 1979.

4. S.M. Flatté, R. Dashen, W.H. Munk, K.M. Watson, and F. Zachariasen, *Sound Transmission Through a Fluctuating Ocean*, Cambridge University Press, New York, 1979.

5. S.M. Flatté, "Wave Propagation Through Random Media: Contributions from Ocean Acoustics," *Proceedings of the IEEE*, vol. 71, 1267-1294, 1983.

6. S. M. Flatté, D.R. Bernstein, and R. Dashen, "Intensity Moments by Path Integral Techniques for Wave Propagation Through Random Media, with Application to Sound in the Ocean," *Physics of Fluids*, vol. 26, 1701-1713, 1983.

7. M.J. Beran, A.M. Whitman, and S. Frankenthal, "Scattering Calculations Using the Characteristic Rays of the Coherence Function," *J. Acoust. Soc. Am.*, vol. 71, 1124, 1982.

8. R.N. Baer, J.S. Perkins, E.B. Wright, and J.J. McCoy, "Stochastic Propagation of the Mutual Coherence Function in the Deep Ocean," *J. Acoust. Soc. Am.*, vol. 75, 1407, 1984.

9. N.G. Van Kampen, *Stochastic Processes in Physics and Chemistry*, North Holland, New York, 1981.

10. I.M. Besieris and F.D. Tappert, "Kinetic Equations for the Quantized Motion of a Particle in a Randomly Perturbed Potential Field," *J Math. Phys.*, vol. 14, 1829, 1973.

11. R.P. Feynman and A.R. Hibbs, *Quantum Mechanics and Path Integrals*, McGraw-Hill, New York, 1965.

12. M.J. Beran and J.J. McCoy, "Propagation through an anisotropic random medium," *J. Math. Phys.*, vol. 15, 1901-1912, 1974.

13. V.I. Shishov, "Strong Fluctuations of the Intensity of a Plane Wave Propagating in a Random Medium," *Soviet Physics JETP*, vol. 34, 744, 1972.

14. J.L. Codona, D.B. Creamer, S.M. Flatté, R.G. Frehlich, and F.S. Henyey, *Solution for the Fourth Moment of Waves Propagating in Random Media*, in preparation, 1985.

Figure Captions

Figure 1a. Moment-equation expression of the Markov approximation. The correlation should be taken between a point at z (point P) and an arbitrary point at z' (point A). Instead it is taken with the point B, obtained by extrapolating along the unperturbed ray from P. The assumption of delta-correlated medium fluctuations leads to the incorrect formulation of correlations between points P and C. The dashed lines indicate the idea of a scattering as a function of angle from point P.

Figure 1b. Path-integral expression of the Markov approximation. The general path at z' (point A) is approximated by the path at z extrapolated along the unperturbed ray (point B).

Figure 2a. Typical z values of the interactions from a Taylor series term in (9) are indicated by x's. Dashed lines show which interactions are correlated. It is assumed that $L_p^2 M_t^2 \ll 1$.

Figure 2b. A portion of a contribution to (9) which is improperly ordered in "first order perturbation theory." Such contributions are small if $L_p^2 M_t^2 \ll 1$.

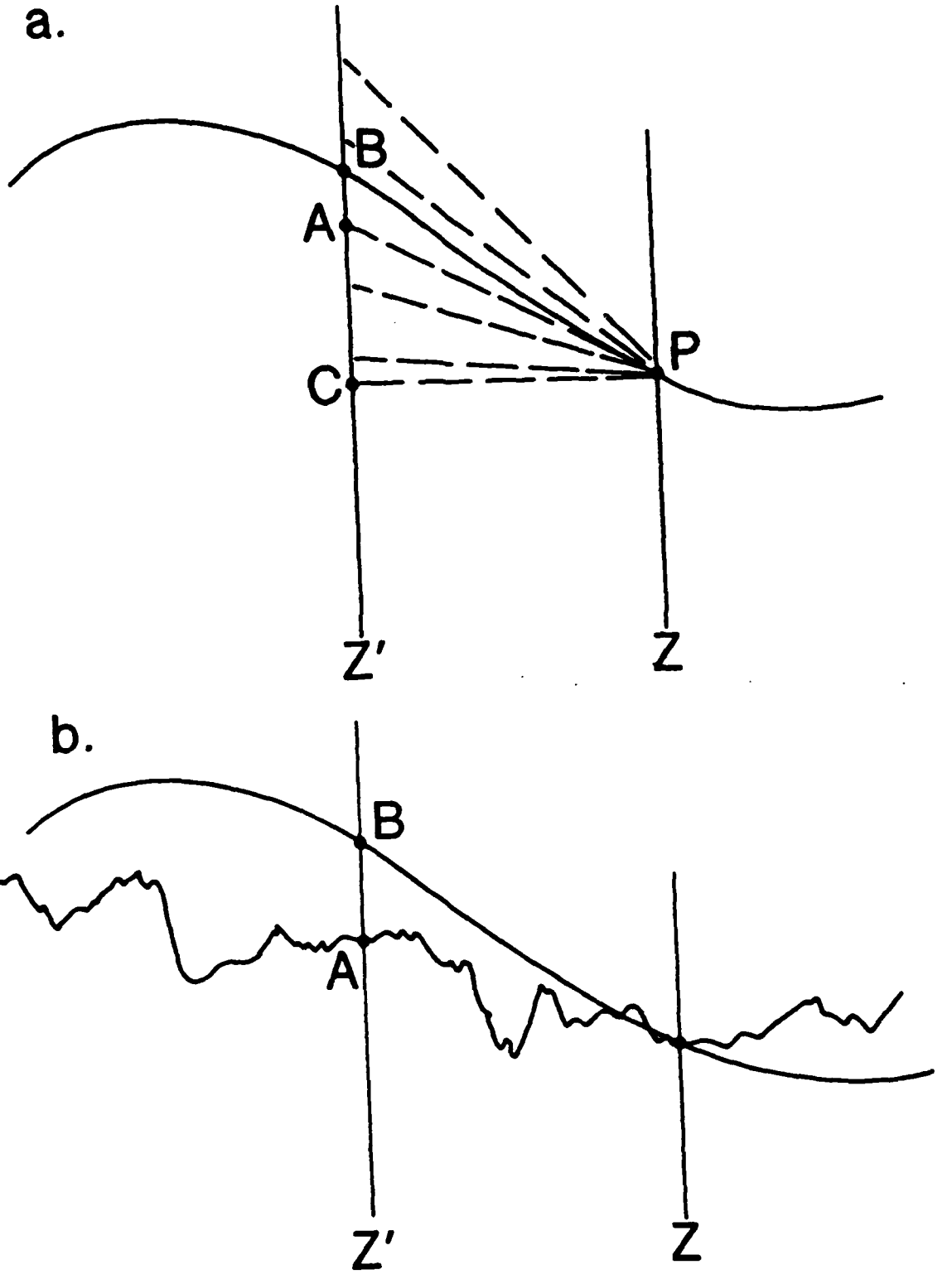

Figure 1

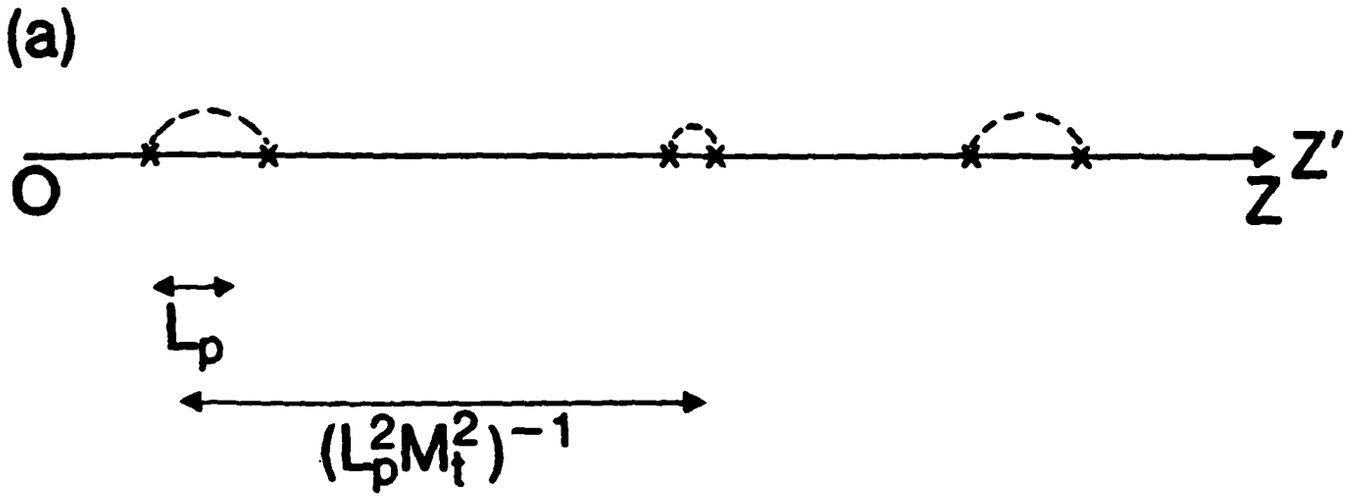

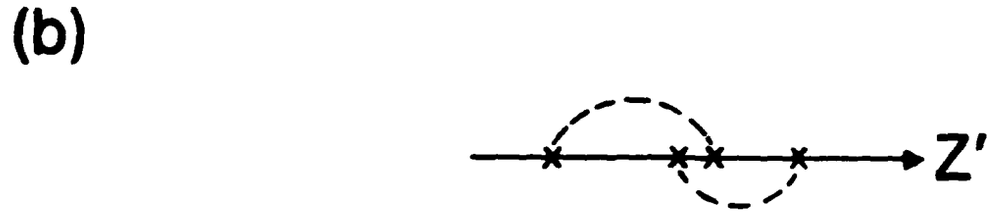

Figure 2

III. INTENSITY CORRELATIONS

The following section is a paper on a new treatment of the fourth moment that allows calculations in the high-frequency region by only a few terms of an expansion. It has been submitted to Radio Science.

IV. ECLIPSE SHADOW BANDS

The following is an unfinished draft paper on eclipse shadow bands, by J. Codona.

LJI-P-84-295

Solution for the Fourth Moment of Waves Propagating in Random Media

Johanan L. Codona, Dennis B. Creamer, Stanley M. Flatté[a],
R.G. Frehlich, and Frank S. Henyey

Center For Studies of Nonlinear Dynamics[b]
La Jolla Institute
La Jolla, California *92037*

Abstract

A series expression is developed for the fourth moment of a beamed field incident on a random phase screen or an extended medium. The series has a symmetry that allows its first few terms to generate useful approximations at both low and high spatial frequency. The parabolic wave equation, the Markov approximation, and Gaussian refractive index fluctuations are assumed. The result for the phase screen is obtained by Green's-function techniques. The extended-medium result is derived in an analogous manner using path integral methods. The same results are also derived by moment-equation methods. The behavior of the leading terms is compared to previous results for plane-wave and point-source geometries.

PACS numbers: 03.40.Kf, 05.40.+j, 42.20.Cc, 92.10.Vz

a. On leave from the University of California, Santa Cruz, CA 95064
b. Affiliated with the University of California, San Diego.

1. INTRODUCTION

Many years of research have been devoted to the study of wave propagation in random media (WPRM). The first comprehensive review of the field was by Tatarskii [1971], followed by Prokhorov et al [1975], Ishimaru [1978], and Fante [1975,1980]. The propagation of radio waves through the ionosphere is reviewed by Yeh and Liu [1982]. The phenomenon of interstellar scintillation is reviewed by Rickett [1977] and Rickett et al [1984]. Sound propagation through the ocean and path integral techniques are discussed by Flatte et al [1979] and Flatte [1983].

We consider waves propagating from an arbitrary source distribution in a random medium. We assume the statistics of the medium are locally homogeneous, and we make the Markov approximation; i.e. the field fluctuations induced within a correlation length along the propagation direction are weak. For a more complete discussion see Codona et al, [1985]. The wave propagation is characterized by narrow angular scattering due to the small random fluctuations in refractive index. It is then convenient to write the complex monochromatic scalar field as $E(\boldsymbol{\rho},z)e^{ikz}$ where z is the propagation direction, $\boldsymbol{\rho}$ is the transverse coordinate and k is the wavenumber of the wave with no refractive index fluctuations.

The random nature of the fields is conveniently described by statistical moments evaluated in the transverse plane located at distance R. Ensemble averages of random variables are denoted by <>. The first moment

$$\Gamma_1(\boldsymbol{\rho},R) = \langle E(\boldsymbol{\rho},R)\rangle \tag{1}$$

or average of the field and the second moment

$$\Gamma_2(\boldsymbol{\rho}_1,\boldsymbol{\rho}_2,R) = \langle E(\boldsymbol{\rho}_1,R)E^*(\boldsymbol{\rho}_2,R)\rangle \tag{2}$$

or mutual coherence function are well understood [Tatarskii, 1971]. However, there are few analytic results for the fourth moment

$$\Gamma_4(\boldsymbol{\rho}_1,\boldsymbol{\rho}_2,\boldsymbol{\rho}_3,\boldsymbol{\rho}_4,R) = \langle E(\boldsymbol{\rho}_1,R)E^*(\boldsymbol{\rho}_2,R)E(\boldsymbol{\rho}_3,R)E^*(\boldsymbol{\rho}_4,R)\rangle \tag{3}$$

Previous theoretical work concentrated on plane-wave and point-source geometry. We present three main results for arbitrary source distribution.

A series expression for the fourth moment is derived as an expansion of the Green's function for the fourth moment, thus avoiding the difficulties associated with the source distribution. For the thin-screen problem, the expansion quantity is a combination of phase structure functions. For the extended random media, the expansion quantity is an analogous combination of phase structure function densities. The Green's function is expressed as a multiple path integral. The resulting series of path integrals is evaluated with a useful identity.

Our second result is the generation of two series for the intensity correlation or intensity spectrum. The fourth moment $\Gamma_4(\boldsymbol{\rho}_1,\boldsymbol{\rho}_2,\boldsymbol{\rho}_3,\boldsymbol{\rho}_4,R)$ has the obvious symmetries that it is unchanged by interchanging $\boldsymbol{\rho}_1$ and $\boldsymbol{\rho}_3$ or by interchanging $\boldsymbol{\rho}_2$ and $\boldsymbol{\rho}_4$. Each term of the series expansion does not share the symmetry of the entire expression. Thus two separate series are obtained by invoking symmetry. In principle, either series could be summed to give Γ_4. We demonstrate, however, that it is better to consider both series in order to describe the fourth moment with the fewest number of terms. This assertion is demonstrated for the second moment of intensity or intensity correlation, $C(\boldsymbol{\rho}_1,\boldsymbol{\rho}_2,R)$, which is a special case of the fourth moment, i.e.

$$C(\boldsymbol{\rho}_1,\boldsymbol{\rho}_2,R) = \langle I(\boldsymbol{\rho}_1,R)I(\boldsymbol{\rho}_2,R)\rangle = \Gamma_4(\boldsymbol{\rho}_1,\boldsymbol{\rho}_1,\boldsymbol{\rho}_2,\boldsymbol{\rho}_2) = \Gamma_4(\boldsymbol{\rho}_1,\boldsymbol{\rho}_2,\boldsymbol{\rho}_2,\boldsymbol{\rho}_1) \tag{4}$$

Note that the symmetry of the fourth moment has been explicitly indicated. A clear presentation of the behavior of the intensity correlation series obtained from the fourth moment expansion requires the introduction of a spatial spectrum of intensity fluctuations for a spatially nonstationary random process. We adopt the definition

$$\Phi(\boldsymbol{\alpha},\boldsymbol{\kappa},R) = \frac{1}{(2\pi)^2}\int_{-\infty}^{\infty} C(\boldsymbol{\alpha},\boldsymbol{\beta},R)e^{-i\boldsymbol{\kappa}\cdot\boldsymbol{\beta}}\,d\boldsymbol{\beta} \tag{5}$$

where

$$\boldsymbol{\alpha} = \frac{1}{2}(\boldsymbol{\rho}_1 + \boldsymbol{\rho}_2) \qquad \boldsymbol{\beta} = \boldsymbol{\rho}_1 - \boldsymbol{\rho}_2 \tag{6}$$

(Note the free format of the argument list of functions). The spectrum has the property

$$\int_{-\infty}^{\infty} \Phi(\underline{\rho}, \underline{q}, R)\, d\underline{q} = C(\underline{\rho}, 0, R) = \langle I(\underline{\rho}, R)^2 \rangle \qquad (7)$$

It should be noted that the spatial spectrum may depend on the centroid $\underline{\rho}$.

Since there are two series for the intensity correlation there are also two series for the intensity spectrum. The leading terms of one series for $\Phi(\underline{\rho}, \underline{q}, R)$ describe the small $\underline{q}$ behavior while the other series is valid at high $\underline{q}$. The rate of convergence of each series provides a criterion for merging the two results to produce a complete expression for the intensity spectrum. In general, an analogous treatment of the intensity correlation series is not possible since the leading terms of both series do not converge to the variance as the spatial separation approaches zero.

Our third result is the demonstration of the equivalence of path integral and moment-equation methods. Early theoretical work on WPRM concentrated on geometrical optics and the method of small perturbations [Barabanenkov, 1971; Tatarskii, 1971]. These two approaches were limited to weak scattering conditions. This restriction was removed with the introduction of differential equations for the moments of the field [Prokhorov, 1975]. Functional techniques of high energy physics (path integrals and operator methods) provided another point of view to WPRM [Klyatskin, 1973; Dashen, 1979]. The moment equation method and functional techniques are equivalent [Codona et al, 1985] and must generate identical results when expansions are performed in the same quantity. This equivalence is demonstrated by deriving the same fourth moment series expression using moment-equation methods.

The thin-screen case is considered in section 2. The second and fourth moment are analyzed with Green's function techniques and the behavior of the intensity correlation is investigated. The same analysis for the extended medium case is presented in section 3. Here we use the path integral representation of the Green's function. Identical results for the fourth moment are derived with moment equation methods in section 4. The main results of the paper are summarized in section 5.

2. GREEN'S FUNCTION APPROACH TO THE THIN SCREEN PROBLEM

2.1 Introduction

One of the first WPRM problems considered was the propagation of plane waves through a random phase screen [Mercier, 1962; Salpeter, 1967; Bramley, 1967; Gochelashvily and Shishov, 1971, 1972, 1975; Rumsey, 1975; Rino, 1979a, b; Uscinski and Macaskill, 1983a, b]. The propagation of radio waves through the ionosphere and the solar wind are two applications of this model. The theory of scintillation from a point source viewed through a random phase screen has been investigated by Lee [1977]. The case of a Gaussian beam focussed on the observation plane has been considered by Gochelashvily [1974]. Previous work concentrated on plane-wave and point-source geometries. We analyze the more general problem of an arbitrary beam incident on a phase screen using Green's function methods. The following analysis is presented in a fashion that permits a clear extension to the more complex problem of wave propagation in extended random media. We review Green's function methods with a discussion of the second moment. A series expression for the fourth moment is presented as an expansion of the Green's function for the fourth moment. The behavior of the resulting series for the intensity correlation is then discussed.

Consider the scalar wave field, $E(\boldsymbol{\rho},z)$, incident on a thin random phase screen situated at the plane z=0. The field, $E(\boldsymbol{\rho},0+)$, emerging from this screen is given by

$$E(\boldsymbol{\rho},0+) = E(\boldsymbol{\rho},0)e^{i\theta(\boldsymbol{\rho})} \tag{8}$$

where $E(\boldsymbol{\rho},0)$ is the field just before the interface of the screen and the phase fluctuations are

$$\theta(\boldsymbol{\rho}) = k\int_{0}^{0+} n(\boldsymbol{\rho},z)dz \tag{9}$$

where $n(\boldsymbol{\rho},z)$ is the random fluctuations in refractive index. Assume $\theta(\boldsymbol{\rho})$ is a zero mean Gaussian random variable with homogeneous statistics and correlation function

$$C_\theta(\boldsymbol{\varrho}) = \langle\theta(\boldsymbol{\rho})\theta(\boldsymbol{\rho}+\boldsymbol{\varrho})\rangle = \int_{-\infty}^{\infty}\Phi_\theta(\boldsymbol{\kappa})e^{i\boldsymbol{\kappa}\cdot\boldsymbol{\varrho}}d\boldsymbol{\kappa} \tag{10}$$

where $\Phi_\theta(\vec{q})$ is the spectrum of phase fluctuations. The structure function of phase fluctuations, $D_\theta(\vec{\beta})$, is defined by

$$D_\theta(\vec{\beta}) = \langle[\theta(\vec{x}) - \theta(\vec{x}+\vec{\beta})]^2\rangle = 2[C_\theta(0) - C_\theta(\vec{\beta})] = 2\int_{-\infty}^{\infty}[1-\cos(\vec{q}\cdot\vec{\beta})]\Phi_\theta(\vec{q})\,d\vec{q} \tag{11}$$

For narrow angular scattering the scalar field satisfies the parabolic wave equation

$$2ik\frac{\partial E}{\partial z} + \nabla^2 E = 0 \tag{12}$$

The solution of the field at a distance R from the screen is

$$E(\vec{x},R) = \int_{-\infty}^{\infty} E(\vec{x}',0)G(\vec{x}\vec{x}',R)\,d\vec{x}' \tag{13}$$

where the Green's function is

$$G(\vec{x}\vec{x}',R) = e^{i\theta(\vec{x}')}G^f(\vec{x}\vec{x}',R) \tag{14}$$

with the free space Green's function

$$G^f(\vec{x}\vec{x}',R) = \frac{k}{2\pi iR}\exp[\frac{ik}{2R}(\vec{x}-\vec{x}')^2] \tag{15}$$

2.2 Green's-Function Approach to the Second Moment

Since the random fields have a Green's function solution, the moments of the field also have a Green's function representation. Consider the second moment of the field or mutual coherence function, $\Gamma_2(\vec{x}_1,\vec{x}_2,R)$, given by

$$\Gamma_2(\vec{x}_1,\vec{x}_2,R) = \langle E(\vec{x}_1,R)E^*(\vec{x}_2,R)\rangle = \int_{-\infty}^{\infty}\int_{-\infty}^{\infty}\Gamma_2(\vec{x}'_1,\vec{x}'_2,0)\langle G(\vec{x}_1;\vec{x}'_1,R)G^*(\vec{x}_2;\vec{x}'_2,R)\rangle\,d\vec{x}'_1\,d\vec{x}'_2 \tag{16}$$

The Green's function for the second moment is identified as the expression inside the $\langle\rangle$, i.e.

$$G_2(\vec{x}_1;\vec{x}'_1,R) = G_2^f(\vec{x}_1;\vec{x}'_1,R)\langle\exp[i(\hat{\theta}(\vec{x}'_1) - \hat{\theta}(\vec{x}'_2))]\rangle \tag{17}$$

where

$$G_2^f(\mathfrak{L}_i;\mathfrak{L}'_i,R) = G^f(\mathfrak{L}_1;\mathfrak{L}'_1,R)G^{f^*}(\mathfrak{L}_2;\mathfrak{L}'_2,R) = \frac{k^2}{(2\pi R)^2}\exp\left[\frac{ik}{2R}[(\mathfrak{L}_1-\mathfrak{L}'_1)^2-(\mathfrak{L}_2-\mathfrak{L}'_2)^2]\right] \quad (18)$$

is the free space Green's function for the second moment. Here, $\mathfrak{L}'_i$ and $\mathfrak{L}_i$ denote the set of $\mathfrak{L}'$ and $\mathfrak{L}$ coordinates respectively. The expectation over the random phase is performed with the identity

$$\langle e^{i\theta}\rangle = e^{-\frac{1}{2}\langle\theta^2\rangle} \quad (19)$$

which is valid for zero mean Gaussian random variables. The Green's function for the second moment is then

$$G_2(\mathfrak{L}_i;\mathfrak{L}'_i,R) = G_2^f(\mathfrak{L}_i;\mathfrak{L}'_i,R)\exp\left[-\frac{1}{2}D_\theta(\mathfrak{L}'_1-\mathfrak{L}'_2)\right] \quad (20)$$

and the second moment is given by

$$\Gamma_2(\mathfrak{L}_1,\mathfrak{L}_2,R) = \frac{k^2}{(2\pi R)^2}\int_{-\infty}^{\infty}\int_{-\infty}^{\infty}\Gamma_2(\mathfrak{L}'_1,\mathfrak{L}'_2,0)e^{\frac{ik}{2R}[(\mathfrak{L}_1-\mathfrak{L}'_1)^2-(\mathfrak{L}_2-\mathfrak{L}'_2)^2]}e^{-\frac{1}{2}D_\theta(\mathfrak{L}'_1-\mathfrak{L}'_2)}d\mathfrak{L}'_1\,d\mathfrak{L}'_2 \quad (21)$$

2.3 Green's-function Approach to the Fourth Moment

Previous work on the fourth moment has concentrated on plane-wave conditions [Zavorotnyi, 1979a]. We address the full fourth moment with an arbitrary source distribution. Following the previous analysis of the second moment, the Green's function for the fourth moment is given by

$$G_4(\mathfrak{L}_i;\mathfrak{L}'_i,R) = G_4^f(\mathfrak{L}_i;\mathfrak{L}'_i,R) \quad (22)$$

$$\exp\left[-\frac{1}{2}[D_\theta(\mathfrak{L}'_1-\mathfrak{L}'_2)+D_\theta(\mathfrak{L}'_3-\mathfrak{L}'_4)+D_\theta(\mathfrak{L}'_1-\mathfrak{L}'_4)+D_\theta(\mathfrak{L}'_2-\mathfrak{L}'_3)-D_\theta(\mathfrak{L}'_2-\mathfrak{L}'_4)-D_\theta(\mathfrak{L}'_1-\mathfrak{L}'_3)]\right]$$

where $G_4^f(\mathfrak{L}_i;\mathfrak{L}'_i,R)$ is the free space Green's function for the fourth moment. It is convenient to apply the unitary coordinate transformation [Rumsey, 1975]

$$2\vec{\alpha} = \vec{\xi}_1 + \vec{\xi}_2 + \vec{\xi}_3 + \vec{\xi}_4 \qquad 2\vec{\xi}_1 = \vec{\alpha} + \vec{\beta} + \vec{\gamma} + \vec{\delta}$$

$$2\vec{\beta} = \vec{\xi}_1 + \vec{\xi}_2 - \vec{\xi}_3 - \vec{\xi}_4 \qquad 2\vec{\xi}_2 = \vec{\alpha} + \vec{\beta} - \vec{\gamma} - \vec{\delta}$$

$$2\vec{\gamma} = \vec{\xi}_1 - \vec{\xi}_2 - \vec{\xi}_3 + \vec{\xi}_4 \qquad 2\vec{\xi}_3 = \vec{\alpha} - \vec{\beta} - \vec{\gamma} + \vec{\delta}$$

$$2\vec{\delta} = \vec{\xi}_1 - \vec{\xi}_2 + \vec{\xi}_3 - \vec{\xi}_4 \qquad 2\vec{\xi}_4 = \vec{\alpha} - \vec{\beta} + \vec{\gamma} - \vec{\delta} \tag{23}$$

The set $(\vec{\alpha}', \vec{\beta}', \vec{\gamma}', \vec{\delta}')$, will denote the same transformation on the coordinate set $(\vec{\xi}'_1, \vec{\xi}'_2, \vec{\xi}'_3, \vec{\xi}'_4)$. The Green's function for the fourth moment then becomes

$$G_4(\vec{\xi}_i; \vec{\xi}'_i, R) = G_4^f(\vec{\xi}_i; \vec{\xi}'_i, R) \tag{24}$$

$$\exp\left[-\frac{1}{2}\left[D_\phi(\vec{\gamma}' + \vec{\delta}') + D_\phi(\vec{\gamma}' - \vec{\delta}') + D_\phi(\vec{\beta}' + \vec{\delta}') + D_\phi(\vec{\beta}' - \vec{\delta}') - D_\phi(\vec{\beta}' + \vec{\gamma}') - D_\phi(\vec{\beta}' - \vec{\gamma}')\right]\right]$$

where

$$G_4^f(\vec{\xi}_i; \vec{\xi}'_i, R) = \frac{k^4}{(2\pi R)^4} \exp\left[\frac{ik}{2R}\left[(\vec{\xi}_1 - \vec{\xi}'_1)^2 - (\vec{\xi}_2 - \vec{\xi}'_2)^2 + (\vec{\xi}_3 - \vec{\xi}'_3)^2 - (\vec{\xi}_4 - \vec{\xi}'_4)^2\right]\right]$$

$$= \frac{k^4}{(2\pi R)^4} \exp\left[i\frac{k}{R}\left[(\vec{\alpha} - \vec{\alpha}') \cdot (\vec{\delta} - \vec{\delta}') + (\vec{\beta} - \vec{\beta}') \cdot (\vec{\gamma} - \vec{\gamma}')\right]\right] \tag{25}$$

is the free space Green's function for the fourth moment. This expression is intractable, both analytically and numerically. Marians [1975], numerically calculated the intensity spectrum of plane-waves incident on a two-dimensional phase screen.

The plane-wave case was considered by Zavorotnyi et al [1977]. They noted that a combination of structure functions was small in the important regions of integration. A series expression was then obtained as a Taylor series expansion. For the general case, we identify that same expansion quantity as

$$Q = -\frac{1}{2}\left[D_\phi(\vec{\beta}' + \vec{\delta}') + D_\phi(\vec{\beta}' - \vec{\delta}') - D_\phi(\vec{\beta}' + \vec{\gamma}') - D_\phi(\vec{\beta}' - \vec{\gamma}')\right] \tag{26}$$

$$= 2\int_{-\infty}^{\infty} \Phi_\phi(\vec{\kappa})\left[\cos(\vec{\delta}' \cdot \vec{\kappa}) - \cos(\vec{\gamma}' \cdot \vec{\kappa})\right] e^{i\vec{\beta}' \cdot \vec{\kappa}}\, d\vec{\kappa}$$

We will investigate the behavior of Q for a structure function that is power law above the inner scale l_0. The exponent in (24) is large unless two of the first four structure functions are small. (The other two can nearly cancel the last two structure functions). The only way the exponent can be small , while allowing the cancellations, is for

$$\vec{\delta}' = O(s_0) \quad \text{and} \quad \vec{\beta}' = O(s_0) \quad \text{or} \quad \gamma' = O(s_0) \tag{27}$$

where s_0 is the field correlation distance defined by $D_\Phi(s_0) = 1$. The remaining variable ($\vec{\beta}'$ or γ') is typically of order of the scattering disk

$$W = \Theta_0 R = \frac{R}{s_0 k} \tag{28}$$

where Θ_0 is the width of the angular spectrum. When the inner scale is larger than W, there is little scintillation. Therefore, we consider the case $s_0 \ll W$, $l_0 \ll W$, $\gamma' = O(s_0)$,and $\vec{\beta}' = O(W)$. A Taylor series expansion about $\vec{\beta}'$ reduces Q to

$$Q = \frac{1}{2}(\vec{\delta}'^2 + \gamma'^2) D_\Phi''(\vec{\beta}') \tag{29}$$

For a power-law structure function

$$D_\Phi(\vec{\beta}') = (\vec{\beta}'/s_0)^p \tag{30}$$

Q becomes

$$Q = \frac{p(p-1)}{2}\left(\frac{\vec{\delta}'^2 + \gamma'^2}{\vec{\beta}'^2}\right)\left(\frac{\vec{\beta}'}{s_0}\right)^p = O\left(\frac{s_0}{W}\right)^{2-p} \tag{31}$$

On the other hand, the other terms in the exponent are $O(D_\Phi(s_0)) = O(1)$, which was the condition which caused γ' and $\vec{\delta}'$ to be order s_0. Thus, if $s_0 < W$, a Taylor series in Q is appropriate, but a Taylor series in the entire exponent requires many more terms.

The other possibility, $\vec{\beta}' = O(s_0)$, and $\gamma' = O(W)$ requires an expansion in another variable, Q', obtained from Q by interchanging $\vec{\beta}'$ with γ'. This alternate expansion is the fundamental reason that two different series are required.

We now return to the Taylor series expansion in Q, with the result

$$G_4(\boldsymbol{\rho}_1;\boldsymbol{\rho}_1,R) = \sum_{n=0}^{\infty} G_{4_n}(\boldsymbol{\rho}_1;\boldsymbol{\rho}_1;z) = G_4^f(\boldsymbol{\rho}_1;\boldsymbol{\rho}_1,R)\exp\left[-\tfrac{1}{2}[D_\Phi(\boldsymbol{\gamma}+\boldsymbol{\delta}')+D_\Phi(\boldsymbol{\gamma}-\boldsymbol{\delta}')]\right] \qquad (32)$$

$$\left[1+\sum_{n=1}^{\infty}\frac{z^n}{n!}\int_{-\infty}^{\infty}d\boldsymbol{\rho}_1 \quad \int_{-\infty}^{\infty}d\boldsymbol{\rho}_n \exp\left[i\sum_{j=1}^{n}\boldsymbol{\rho}_j\cdot\boldsymbol{\beta}'\right]\prod_{j=1}^{n}\Phi_\Phi(\boldsymbol{\rho}_j)[\cos(\boldsymbol{\delta}'\cdot\boldsymbol{\rho}_j)-\cos(\boldsymbol{\gamma}'\cdot\boldsymbol{\rho}_j)]\right]$$

This series should converge quickly when the quantity Q is small over the important region of integration. Note that the symmetry of the full fourth moment expression (24) does not hold for each term of the expansion. The equivalent moment-equation derivation is presented in section 4.1.

The first term of (32) reduces to

$$G_{4_0}(\boldsymbol{\rho}_1;\boldsymbol{\rho}_1,R) = G_4^f(\boldsymbol{\rho}_1;\boldsymbol{\rho}_1,R)e^{-\frac{1}{2}[D_\Phi(\boldsymbol{\rho}_1-\boldsymbol{\rho}_2)+D_\Phi(\boldsymbol{\rho}_3-\boldsymbol{\rho}_4)]} = G_2(\boldsymbol{\rho}_1,\boldsymbol{\rho}_2,\boldsymbol{\rho}_1,\boldsymbol{\rho}_2,R)G_2(\boldsymbol{\rho}_3,\boldsymbol{\rho}_4,\boldsymbol{\rho}_3,\boldsymbol{\rho}_4,R) \qquad (33)$$

Thus, for spatially coherent sources, the first term of the fourth moment is a product of two *second moments*, i.e.

$$\Gamma_{4_0}(\boldsymbol{\rho}_1,\boldsymbol{\rho}_2,\boldsymbol{\rho}_3,\boldsymbol{\rho}_4,R) = \Gamma_2(\boldsymbol{\rho}_1,\boldsymbol{\rho}_2,R)\Gamma_2(\boldsymbol{\rho}_3,\boldsymbol{\rho}_4,R) \qquad (34)$$

The next term of the Green's function expansion is

$$G_{4_1}(\boldsymbol{\rho}_1;\boldsymbol{\rho}_1,R) = 2G_4^f(\boldsymbol{\rho}_1;\boldsymbol{\rho}_1,R)\exp\left[-\tfrac{1}{2}[D_\Phi(\boldsymbol{\gamma}+\boldsymbol{\delta}')+D_\Phi(\boldsymbol{\gamma}-\boldsymbol{\delta}')]\right] \qquad (35)$$

$$\int_{-\infty}^{\infty}\Phi_\Phi(\boldsymbol{\rho})[\cos(\boldsymbol{\delta}'\cdot\boldsymbol{\rho})-\cos(\boldsymbol{\gamma}'\cdot\boldsymbol{\rho})]e^{i\boldsymbol{\beta}'\cdot\boldsymbol{\rho}}\,d\boldsymbol{\rho}$$

These two terms contain the useful first-order description of the fourth moment. The rate of convergence of the series is determined by the higher order terms. For the plane-wave case, the fourth-moment expressions generated from (34) and (35) are identical to the asymptotic results of Zavorotnyi [1979a Eq (7)].

2.4 Intensity Correlation

There are few measurements of the full fourth moment of WPRM [Gurvich et al, 1978, 1979a]. However, the intensity correlation, a special case of the fourth moment, is commonly observed. We will now demonstrate that our fourth-moment series (32) generates two different expressions for the intensity correlation (4), one valid at low spatial frequency, the other valid at high spatial frequency.

The low frequency version of the intensity correlation is obtained from the fourth moment (3) by setting $\vec{x}_1 = \vec{x}_2$ and $\vec{x}_3 = \vec{x}_4$ or by setting $\vec{\delta} = 0$ and $\vec{\gamma} = 0$. The n=0 term produces

$$C_0^{\gamma}(\vec{\alpha},\vec{\beta},R) = \frac{k^4}{(2\pi R)^4}\int_{-\infty}^{\infty}\Gamma_4(\vec{\alpha}',\vec{\beta}',\vec{\gamma}',\vec{\delta}',0)\exp\left[-i\frac{k}{R}[(\vec{\alpha}-\vec{\alpha}')\cdot\vec{\delta}' + (\vec{\beta}-\vec{\beta}')\cdot\vec{\gamma}']\right] \tag{36}$$

$$\exp\left[-\tfrac{1}{2}[D_\theta(\vec{\gamma}+\vec{\delta}') + D_\theta(\vec{\gamma}-\vec{\delta}')]\right] d\vec{\alpha}'\, d\vec{\beta}'\, d\vec{\gamma}'\, d\vec{\delta}'$$

For spatially coherent sources

$$C_0^{\gamma}(\vec{\alpha},\vec{\beta},R) = \langle I(\frac{\vec{\alpha}+\vec{\beta}}{2},R)\rangle\langle I(\frac{\vec{\alpha}-\vec{\beta}}{2},R)\rangle = \langle I(\vec{x}_1,z)\rangle\langle I(\vec{x}_3,z)\rangle \tag{37}$$

or

$$\Phi_0^{\gamma}(\vec{\mu},\vec{q},R) = \frac{1}{(2\pi)^2}\int_{-\infty}^{\infty}\langle I(\vec{\mu}+\frac{\vec{\beta}}{2},R)\rangle\langle I(\vec{\mu}-\frac{\vec{\beta}}{2},R)\rangle\, e^{-i\vec{\beta}\cdot\vec{q}}\, d\vec{\beta} \tag{38}$$

which normally describes the smallest spectral scale of the process. Indeed, for plane-wave conditions $\Phi_0^{\gamma}(\vec{\mu},\vec{q},R) = \langle I\rangle^2\delta(\vec{q})$ since the average intensity, $\langle I\rangle$, is a constant.

The corresponding terms for n=1 may be written as

$$C\Gamma(\vec{\alpha},\vec{\beta},R) = \frac{2k^4}{(2\pi R)^4}\int_{-\infty}^{\infty}\Gamma_4(\vec{\alpha}',\vec{\beta}',\vec{\gamma}',\vec{\delta}',0)\exp\left[-i\frac{k}{R}[(\vec{\alpha}-\vec{\alpha}')\cdot\vec{\delta}' + (\vec{\beta}-\vec{\beta}')\cdot\vec{\gamma}']\right] \tag{39}$$

$$\exp\left[-\frac{1}{2}[D_\Phi(\vec{\gamma}'+\vec{\delta}') + D_\Phi(\vec{\gamma}'-\vec{\delta}')]\right]\Phi_\Phi(\vec{\kappa})[\cos(\vec{\delta}'\cdot\vec{\kappa}) - \cos(\vec{\gamma}'\cdot\vec{\kappa})]e^{i\vec{\beta}'\cdot\vec{\kappa}}\, d\vec{\alpha}'\, d\vec{\beta}'\, d\vec{\gamma}'\, d\vec{\delta}'\, d\vec{\kappa}$$

and

$$\Phi_I^{(2)}(\vec{\alpha},\vec{q},R) = \frac{2k^2}{(2\pi)^4R^2}\int_{-\infty}^{\infty}\Gamma_4(\vec{\alpha}',\vec{\beta}',\vec{\gamma}' = -\vec{q}\frac{R}{k},\vec{\delta}',0)\exp[-i\frac{k}{R}(\vec{\alpha}-\vec{\alpha}')\cdot\vec{\delta}']e^{i(\vec{q}-\vec{\alpha})\cdot\vec{\beta}'} \tag{40}$$

$$\exp\left[-\frac{1}{2}[D_\Phi(\vec{q}\frac{R}{k}+\vec{\delta}') + D_\Phi(\vec{q}\frac{R}{k}-\vec{\delta}')]\right]\Phi_\Phi(\vec{\kappa})[\cos(\vec{\delta}'\cdot\vec{\kappa}) - \cos(\vec{\gamma}'\cdot\vec{\kappa})]\; d\vec{\alpha}'\, d\vec{\beta}'\, d\vec{\delta}'\, d\vec{\kappa}$$

For the case of plane waves, (40) reduces to the familiar result

$$\Phi_I^{(2)}(\vec{\alpha},\vec{q},R) = \Phi_\Phi(\vec{q})\exp[-D_\Phi(\vec{q}\frac{R}{k})]\sin^2[q^2\frac{R}{2k}] \tag{41}$$

which also describes the low q behavior of $\Phi(\vec{\alpha},\vec{q},R)$. The Born, or weak-scattering approximation is obtained by ignoring the exponential term. Similarly, the Born approximation for the general case is obtained from (40) by ignoring the last exponential term.

The high frequency version of the intensity correlation is obtained from the fourth moment (3) by setting $\vec{x}_1 = \vec{x}_4$ and $\vec{x}_2 = \vec{x}_3$ or by setting $\vec{\delta} = 0$ and $\vec{\beta} = 0$. The n=0 term produces

$$C\Gamma^{(2)}(\vec{\alpha},\vec{\gamma},R) = \frac{k^4}{(2\pi R)^4}\int_{-\infty}^{\infty}\Gamma_4(\vec{\alpha}',\vec{\beta}',\vec{\gamma}',\vec{\delta}',0)\exp\left[-i\frac{k}{R}[(\vec{\alpha}-\vec{\alpha}')\cdot\vec{\delta}' + (\vec{\gamma}-\vec{\gamma}')\cdot\vec{\beta}']\right] \tag{42}$$

$$\exp\left[-\frac{1}{2}[D_\Phi(\vec{\gamma}'+\vec{\delta}') + D_\Phi(\vec{\gamma}'-\vec{\delta}')]\right] d\vec{\alpha}'\, d\vec{\beta}'\, d\vec{\gamma}'\, d\vec{\delta}'\, d\vec{\kappa}$$

For spatially coherent sources

$$C\Gamma^{(2)}(\vec{x}_1,\vec{x}_2,R) = \Gamma_2(\vec{x}_1,\vec{x}_2,R)\Gamma_2^*(\vec{x}_1,\vec{x}_2,R) \tag{43}$$

This expression is the high frequency approximation, i.e. the intensity correlation is the square of the mutual coherence function, and may also be derived by assuming that the

complex electric fields are zero mean Gaussian random variables.

The n=1 term reduces to

$$C_1^{\mathcal{N}}(\vec{\alpha},\vec{\gamma},R) = \frac{2k^4}{(2\pi R)^4}\int_{-\infty}^{\infty}\Gamma_4(\vec{\alpha}',\vec{\beta}',\vec{\gamma}',\vec{\delta}',0)\exp\left[-i\frac{k}{R}[(\vec{\alpha}-\vec{\alpha}')\cdot\vec{\delta}'+(\vec{\gamma}-\vec{\gamma}')\cdot\vec{\beta}']\right] \tag{44}$$

$$\exp\left[-\tfrac{1}{2}[D_\Phi(\vec{\gamma}'+\vec{\delta}')+D_\Phi(\vec{\gamma}'-\vec{\delta}')]\right]\Phi_\Phi(\vec{\kappa})[\cos(\vec{\delta}'\cdot\vec{\kappa})-\cos(\vec{\gamma}'\cdot\vec{\kappa})]e^{i\vec{\beta}'\cdot\vec{\kappa}}\,d\vec{\alpha}'\,d\vec{\beta}'\,d\vec{\gamma}'\,d\vec{\delta}'\,d\vec{\kappa}$$

and

$$\Phi_1^{\mathcal{N}}(\vec{\alpha},\vec{q},R) = \frac{2k^2}{(2\pi)^4R^2}\int_{-\infty}^{\infty}\Gamma_4(\vec{\alpha}',\vec{\beta}'=-\vec{q}\frac{R}{k},\vec{\gamma}',\vec{\delta}',0)\exp[-i\frac{k}{R}(\vec{\alpha}-\vec{\alpha}')\cdot\vec{\delta}']e^{-i(\vec{\gamma}'+\vec{\alpha}\frac{R}{k})\cdot\vec{q}} \tag{45}$$

$$\exp\left[-\tfrac{1}{2}[D_\Phi(\vec{\gamma}'+\vec{\delta}')+D_\Phi(\vec{\gamma}'-\vec{\delta}')]\right]\Phi_\Phi(\vec{\kappa})[\cos(\vec{\delta}'\cdot\vec{\kappa})-\cos(\vec{\gamma}'\cdot\vec{\kappa})]\;d\vec{\alpha}'\,d\vec{\gamma}'\,d\vec{\delta}'\,d\vec{\kappa}$$

Thus we have shown how the fourth-moment series generates two expressions for the intensity correlation: one ($\vec{\delta}=0,\vec{\gamma}=0$) useful at low spatial frequencies, and the other ($\vec{\delta}=0,\vec{\beta}=0$) useful at high spatial frequencies. The region of validity depends on the statistics of the phase fluctuations and the initial source distribution. The case of plane waves incident on a random phase screen with a power-law spectrum has been investigated by Gochelashvily and Shishov [1975]. Their calculations of the first few terms of the intensity spectrum [Figure 1] imply the two series converge quickly when the quantity Q is small over the important region of integration. The rate of convergence is difficult to determine a priori; the contribution to the intensity spectrum from the higher terms is the best indication of convergence. The intensity correlation series is more difficult to interpret since the errors of the expansion accumulate in the region of small spacing but in the spectral domain, these errors appear in the central regions of the spectrum [cf Figure 1].

3. PATH INTEGRAL TECHNIQUES FOR EXTENDED RANDOM MEDIA

3.1 Introduction

We now consider the more complex problem of wave propagation in a random media that is locally homogeneous with statistics that vary slowly in the direction of propagation. Laser propagation in the atmosphere, radio propagation through the interstellar medium, and sound propagation through the ocean with no deterministic background are common examples of this phenomena. The application of path integral techniques to problems of wave propagation in random media was introduced by Klyatskin and Tatarskii [1970], Zavorotnyi et al [1977] and Dashen [1979]. Path integral methods have been successfully applied to the difficult problem of WPRM for anisotropic, inhomogeneous medium with deterministic background of refractive index [Flatte et al, 1979]. A functional operator form of the path integral was used by Tatarskii and Zavorotnyi [1980], to extend thin-screen analysis to the problem of wave propagation in extended random media for the plane-wave case. We use the path integral representation of the Green's function to illustrate this connection because one obtains a clear presentation of the role of the source distribution. Note that the operator formalism is equivalent to the path integral method and produces the same results.

The path integral technique is introduced by a review of the second-moment derivation. The reduction of path integrals to familiar Reimann integrals is performed by a useful identity [cf (59)]. Using this identity, we present a series expression for the fourth moment that is analogous to the thin-screen results of section 2.2. The behavior of the resulting correlation series is then discussed.

For narrow angular scattering, the scalar field satisfies the parabolic wave equation

$$2ik\frac{\partial E}{\partial z} + \nabla^2 E + 2k^2 n(\underline{x},z)E = 0 \tag{46}$$

where $n(\underline{x},z)$ denotes the refractive index fluctuations. We define the correlation of refractive index fluctuations, $B_n(\underline{s},t,z)$, as

$$B_n(\boldsymbol{\rho},\ell,z) = \langle n(0,z)n(\boldsymbol{\rho},z+\ell)\rangle \tag{47}$$

The path integral formulation for the Green's function was developed by Feynman [1948], and may be written as

$$G(\boldsymbol{\rho}';\boldsymbol{\rho},R) = \int D\boldsymbol{\rho}(z)\exp\left[i\frac{k}{2}\int_0^R[\dot{\boldsymbol{\rho}}(z)]^2dz - ik\int_0^R n[\boldsymbol{\rho}(z),z]dz\right] \tag{48}$$

where $D\boldsymbol{\rho}(z)$ denotes the infinite dimensional integration over all possible paths, $\boldsymbol{\rho}(z)$, connecting the points $(\boldsymbol{\rho}',0)$ and $(\boldsymbol{\rho},R)$ and $\dot{\boldsymbol{\rho}}(z) = \frac{d\boldsymbol{\rho}}{dz}$.

If there are no refractive index fluctuations, the Green's function becomes the free space Green's function.

$$G^f(\boldsymbol{\rho};\boldsymbol{\rho}',R) = \int D\boldsymbol{\rho}(z)\exp\left[i\frac{k}{2}\int_0^R[\dot{\boldsymbol{\rho}}(z)]^2dz\right] = \frac{k}{2\pi iR}\exp\left[\frac{ik}{2R}(\boldsymbol{\rho}-\boldsymbol{\rho}')^2\right] \tag{49}$$

3.2 Second Moment by Path Integral Techniques

The Green's function for the moments of the field are easily expressed in terms of the path integral. The Green's function for the first and second moment were derived by Dashen [1979]. These results were obtained under the Mar'kov approximation [Zavorotnyi, 1978]. We review the derivation for the Green's function for the second moment, which is given by

$$G_2(\boldsymbol{\rho}_1,\boldsymbol{\rho}_2;\boldsymbol{\rho}'_1,\boldsymbol{\rho}'_2,R) = \langle G(\boldsymbol{\rho}_1;\boldsymbol{\rho}'_1,R)G^*(\boldsymbol{\rho}_2;\boldsymbol{\rho}'_2,R)\rangle \tag{50}$$

$$= \int\int D\boldsymbol{\rho}_1(z)\,D\boldsymbol{\rho}_2(z)\exp\left[i\frac{k}{2}\int_0^R([\dot{\boldsymbol{\rho}}_1(z)]^2-[\dot{\boldsymbol{\rho}}_2(z)]^2)dz\right]\left\langle\exp\left[-ik\int_0^R[n(\boldsymbol{\rho}_1(z),z)-n(\boldsymbol{\rho}_2(z),z)]dz\right]\right\rangle$$

Applying (19) and the Markov approximation results in

$$G_2(\boldsymbol{\rho}_i;\boldsymbol{\rho}'_i,R) = \frac{k^2}{(2\pi R)^2}\int\int D\boldsymbol{\rho}_1(z)\,D\boldsymbol{\rho}_2(z) \tag{51}$$

$$\exp\left[i\frac{k}{2}\int_0^R([\dot{\boldsymbol{\rho}}_1(z)]^2-[\dot{\boldsymbol{\rho}}_2(z)]^2)dz - \frac{1}{2}\int_0^R d[\boldsymbol{\rho}_1(z)-\boldsymbol{\rho}_2(z),z]dz\right]$$

and the phase structure function density is given by

$$d(\vec{\beta},z) = 2k^2 \int_{-\infty}^{\infty} [B_n(0,t,z) - B_n(\vec{\beta},t,z)]dt$$

$$= 4\pi k^2 \int_{-\infty}^{\infty} [1 - \cos(\vec{\beta}\cdot\vec{q})]\Phi_n(\vec{q},q_z=0,z)\, d\vec{q} \tag{52}$$

where

$$\Phi_n(\vec{q},q_z,R) = \frac{1}{(2\pi)^3}\int_{-\infty}^{\infty}\int_{-\infty}^{\infty} B_n(\vec{\rho},z,R)\exp[-i(\vec{\rho}\cdot\vec{q}+zq_z)]\, d\vec{\rho}\, dz \tag{53}$$

is the refractive index spectrum. Change path variables to

$$\vec{\rho}(z) = \frac{1}{2}[\vec{r}_1(z)+\vec{r}_2(z)] - \frac{1}{2}(\vec{\rho}_1+\vec{\rho}_2)\frac{z}{R} - \frac{1}{2}(\vec{\rho}'_1+\vec{\rho}'_2)(1-\frac{z}{R}) \tag{54}$$

$$\vec{\beta}(z) = \vec{r}_1(z) - \vec{r}_2(z) - \vec{\gamma}(z) \tag{55}$$

where

$$\vec{\gamma}(z) = (\vec{\rho}_1-\vec{\rho}_2)\frac{z}{R} + (\vec{\rho}'_1-\vec{\rho}'_2)(1-\frac{z}{R}) \tag{56}$$

Then $\vec{\rho}(0) = \vec{\rho}(R) = \vec{\beta}(0) = \vec{\beta}(R) = 0$ and

$$G_2(\vec{\rho}_1;\vec{\rho}'_1,R) = \exp\left[\frac{i}{2k}[(\vec{\rho}'_1-\vec{\rho}_1)^2-(\vec{\rho}'_2-\vec{\rho}_2)^2]\right]\int\int D\vec{\rho}(z)\, D\vec{\beta}(z)$$

$$\exp\left[ik\int_0^R \vec{\rho}(z)\cdot\vec{\beta}(z)dz - \frac{1}{2}\int_0^R d[\vec{\beta}(z)+\vec{\gamma}(z),z]dz\right] \tag{57}$$

Integrating the first path term in the exponential by parts and substituting the free space Green's function results in

$$G_2(\underline{\rho}_1;\underline{\rho}'_1,R) = \frac{(2\pi R)^2}{k^2} G^{\prime}(\underline{\rho}_1;\underline{\rho}'_1,R) G^{\prime *}(\underline{\rho}_2,\underline{\rho}'_2,R) \int\int D\hat{\underline{\rho}}(z)\, D\hat{\underline{\beta}}(z)$$

$$\exp\left[-ik\int_0^R \hat{\underline{\rho}}(z)\cdot\hat{\underline{\beta}}(z)dz - \frac{1}{2}\int_0^R d(\hat{\underline{\beta}}(z)+\hat{\gamma}(z),z)dz \right] \tag{58}$$

This path integral is evaluated with the identity

$$\int\int D\hat{\underline{\rho}}(z)\, D\hat{\underline{\beta}}(z) F[\hat{\underline{\beta}}(z)] \exp\left[ik\int_0^R \hat{\underline{\rho}}(z)\cdot[\hat{\underline{\beta}}(z)-\underline{\beta}(z)]dz \right] = \frac{k^2}{(2\pi R)^2} F[\underline{g}(z)] \tag{59}$$

where $\underline{g}(z)$ is the solution of $\ddot{\underline{g}}(z) = \underline{\beta}(z)$ that satisfies the appropriate boundary conditions. Identity (59) reduces (58) to

$$G_2(\underline{\rho}_1;\underline{\rho}'_1,R) = G^{\prime}(\underline{\rho}_1;\underline{\rho}'_1,R) G^{\prime *}(\underline{\rho}_2;\underline{\rho}'_2,R) \exp\left[-\frac{1}{2}\int_0^R d[\hat{\gamma}(z),z]dz \right] \tag{60}$$

and $\underline{g}(z) = 0$ is the solution of $\ddot{\underline{g}}(z) = 0$, that satisfies the required boundary conditions. Using this Green's function, the expression for the second moment becomes

$$\Gamma_2(\underline{\rho}_1,\underline{\rho}_2,R) = \int_{-\infty}^{\infty}\int_{-\infty}^{\infty} \Gamma_2(\underline{\rho}'_1,\underline{\rho}'_2,0) G_2(\underline{\rho}_1,\underline{\rho}_2;\underline{\rho}'_1,\underline{\rho}'_2,R)\, d\underline{\rho}'_1\, d\underline{\rho}'_2 \tag{61}$$

For plane-wave input

$$\Gamma_2(\underline{\rho}_1,\underline{\rho}_2,R) = \langle I\rangle \exp\left[-\frac{1}{2}\int_0^R d[(\underline{\rho}_1-\underline{\rho}_2),z]dz \right] \tag{62}$$

and a point source gives

$$\Gamma_2(\underline{\rho}_1,\underline{\rho}_2,R) = \langle I(R)\rangle \exp\left[\frac{ik}{2R}[\underline{\rho}_1^2-\underline{\rho}_2^2] - \frac{1}{2}\int_0^R d[(\underline{\rho}_1-\underline{\rho}_2)\frac{z}{R},z]dz \right] \tag{63}$$

3.3 Fourth Moment by Path Integral Techniques

We derive a series expression for the fourth moment in a manner analogous to the thin-screen derivation. The Green's function for the fourth moment is given by the multiple path integral

$$G_4(\boldsymbol{\rho}_1;\boldsymbol{\rho}'_1,R) = \langle G(\boldsymbol{\rho}_1;\boldsymbol{\rho}'_1,R)G^*(\boldsymbol{\rho}_2,\boldsymbol{\rho}'_2,R)G(\boldsymbol{\rho}_3;\boldsymbol{\rho}'_3,R)G^*(\boldsymbol{\rho}_4,\boldsymbol{\rho}'_4,R)\rangle = \int D\boldsymbol{\rho}_1\, D\boldsymbol{\rho}_2\, D\boldsymbol{\rho}_3\, D\boldsymbol{\rho}_4$$

$$\exp\left[i\frac{k}{2}\int_0^R[\boldsymbol{\rho}_1^2-\boldsymbol{\rho}_2^2+\boldsymbol{\rho}_3^2-\boldsymbol{\rho}_4^2]dz\right]\langle\exp[-ik\int_0^R[n(\boldsymbol{\rho}_1,z)-n(\boldsymbol{\rho}_2,z)+n(\boldsymbol{\rho}_3,z)-n(\boldsymbol{\rho}_4,z)]dz\,]\rangle \qquad (64)$$

If $\int_0^R[n(\boldsymbol{\rho}_1,z)-n(\boldsymbol{\rho}_2,z)+n(\boldsymbol{\rho}_3,z)-n(\boldsymbol{\rho}_4,z)]dz$ is a zero mean Gaussian random variable (19) and the Markov approximation is valid, the last term of (64) becomes

$$\exp[-\tfrac{1}{2}\int_0^R[d(\boldsymbol{\rho}_1-\boldsymbol{\rho}_2,z)+d(\boldsymbol{\rho}_3-\boldsymbol{\rho}_4,z)+d(\boldsymbol{\rho}_1-\boldsymbol{\rho}_4,z)+d(\boldsymbol{\rho}_2-\boldsymbol{\rho}_3,z)-d(\boldsymbol{\rho}_2-\boldsymbol{\rho}_4,z)-d(\boldsymbol{\rho}_1-\boldsymbol{\rho}_3,z)]dz\,].$$

Change path variables to

$$2\hat{\boldsymbol{\alpha}}(z)=\boldsymbol{\rho}_1(z)+\boldsymbol{\rho}_2(z)+\boldsymbol{\rho}_3(z)+\boldsymbol{\rho}_4(z) \qquad 2\boldsymbol{\rho}_1(z)=\hat{\boldsymbol{\alpha}}(z)+\hat{\boldsymbol{\beta}}(z)+\hat{\boldsymbol{\gamma}}(z)+\hat{\boldsymbol{\delta}}(z)$$

$$2\hat{\boldsymbol{\beta}}(z)=\boldsymbol{\rho}_1(z)+\boldsymbol{\rho}_2(z)-\boldsymbol{\rho}_3(z)-\boldsymbol{\rho}_4(z) \qquad 2\boldsymbol{\rho}_2(z)=\hat{\boldsymbol{\alpha}}(z)+\hat{\boldsymbol{\beta}}(z)-\hat{\boldsymbol{\gamma}}(z)-\hat{\boldsymbol{\delta}}(z)$$

$$2\hat{\boldsymbol{\gamma}}(z)=\boldsymbol{\rho}_1(z)-\boldsymbol{\rho}_2(z)-\boldsymbol{\rho}_3(z)+\boldsymbol{\rho}_4(z) \qquad 2\boldsymbol{\rho}_3(z)=\hat{\boldsymbol{\alpha}}(z)-\hat{\boldsymbol{\beta}}(z)-\hat{\boldsymbol{\gamma}}(z)+\hat{\boldsymbol{\delta}}(z)$$

$$2\hat{\boldsymbol{\delta}}(z)=\boldsymbol{\rho}_1(z)-\boldsymbol{\rho}_2(z)+\boldsymbol{\rho}_3(z)-\boldsymbol{\rho}_4(z) \qquad 2\boldsymbol{\rho}_4(z)=\hat{\boldsymbol{\alpha}}(z)-\hat{\boldsymbol{\beta}}(z)+\hat{\boldsymbol{\gamma}}(z)-\hat{\boldsymbol{\delta}}(z) \qquad (65)$$

Then

$$G_4(\boldsymbol{\rho}_1;\boldsymbol{\rho}'_1,R) = \int D\hat{\boldsymbol{\alpha}}\, D\hat{\boldsymbol{\beta}}\, D\hat{\boldsymbol{\gamma}}\, D\hat{\boldsymbol{\delta}}\ \exp\left[ik\int_0^R(\hat{\boldsymbol{\alpha}}\cdot\hat{\boldsymbol{\delta}}+\hat{\boldsymbol{\beta}}\cdot\hat{\boldsymbol{\gamma}})dz\right]$$

$$\exp\left[-\frac{1}{2}\int_0^R[d(\hat{\boldsymbol{\gamma}}+\hat{\boldsymbol{\delta}},z)+d(\hat{\boldsymbol{\gamma}}-\hat{\boldsymbol{\delta}},z)+d(\hat{\boldsymbol{\beta}}+\hat{\boldsymbol{\delta}},z)+d(\hat{\boldsymbol{\beta}}-\hat{\boldsymbol{\delta}},z)-d(\hat{\boldsymbol{\beta}}+\hat{\boldsymbol{\gamma}},z)-d(\hat{\boldsymbol{\beta}}-\hat{\boldsymbol{\gamma}},z)]dz\right] \qquad (66)$$

Change variables again to paths about the straight lines connecting the points $(\boldsymbol{\rho}'_i,0)$ to $(\boldsymbol{\rho}_i,R)$ i.e.

$$\vec{a}_1(z) = \vec{a}(z) - \vec{l}(\vec{a},z)$$

$$\vec{\beta}_1(z) = \vec{\beta}(z) - \vec{l}(\vec{\beta},z)$$

$$\vec{\gamma}_1(z) = \vec{\gamma}(z) - \vec{l}(\vec{\gamma},z)$$

$$\vec{\delta}_1(z) = \vec{\delta}(z) - \vec{l}(\vec{\delta},z) \tag{67}$$

where

$$\vec{l}(\vec{a},z) = \vec{a}(0)(1-\frac{z}{R}) + \vec{a}(z)\frac{z}{R} = \vec{a}'(1-\frac{z}{R}) + \vec{a}\frac{z}{R} \tag{68}$$

is the straight line path from $(\vec{a}',0)$ to $(\vec{a},R)$. In order to simplify the large expressions, $[\vec{a}',\vec{\beta}',\vec{\gamma}',\vec{\delta}']$ will replace $[\vec{a}(0),\vec{\beta}(0),\vec{\gamma}(0),\vec{\delta}(0)]$ and $[\vec{a},\vec{\beta},\vec{\gamma},\vec{\delta}]$ will replace $[\vec{a}(R),\vec{\beta}(R),\vec{\gamma}(R),\vec{\delta}(R)]$ Then

$$G_4(\vec{x}_1;\vec{x}'_1,R) = \frac{(2\pi R)^4}{k^4} G_1'(\vec{x}_1;\vec{x}'_1,R)\int D\vec{a}_1\, D\vec{\beta}_1\, D\vec{\gamma}_1\, D\vec{\delta}_1 \exp\left[ik\int_0^R(\vec{a}_1\cdot\vec{\delta}_1 + \vec{\beta}_1\cdot\vec{\gamma}_1)dz\right] \tag{69}$$

$$\exp\left[-\frac{1}{2}\int_0^R[d(\vec{\gamma}_1+\vec{\delta}_1+\vec{a}(\vec{\gamma},\vec{\delta}),z) + d(\vec{\gamma}_1-\vec{\delta}_1+\vec{b}(\vec{\gamma},\vec{\delta}),z) + d(\vec{\beta}_1+\vec{\delta}_1+\vec{a}(\vec{\beta},\vec{\delta}),z)\right.$$

$$\left. + d(\vec{\beta}_1-\vec{\delta}_1+\vec{b}(\vec{\beta},\vec{\delta}),z) - d(\vec{\beta}_1+\vec{\gamma}_1+\vec{a}(\vec{\beta},\vec{\gamma}),z) - d(\vec{\beta}_1-\vec{\gamma}_1+\vec{b}(\vec{\beta},\vec{\gamma}),z)]dz\right]$$

with

$$\vec{a}(\vec{a},\vec{\beta}) = \vec{l}(\vec{a},z) + \vec{l}(\vec{\beta},z)$$

$$\vec{b}(\vec{a},\vec{\beta}) = \vec{l}(\vec{a},z) - \vec{l}(\vec{\beta},z) \tag{70}$$

Substituting (integration by parts)

$$ik\int_0^R(\vec{a}_1\cdot\vec{\delta}_1 + \vec{\beta}_1\cdot\vec{\gamma}_1)dz = -ik\int_0^R(\vec{a}_1\cdot\vec{\delta}_1 + \vec{\beta}_1\cdot\vec{\gamma}_1)dz \tag{71}$$

and performing the integration over the paths $\vec{\alpha}_1$ and $\vec{\delta}_1$ using (59) results in

$$G_4(\vec{\rho}_4;\vec{\rho}_4',R) = \frac{(2\pi R)^2}{k^2} G_1'(\vec{\rho}_4;\vec{\rho}_4',R) \int\int D\vec{\beta}_1\, D\vec{\gamma}_1 \exp\left[-ik\int_0^R \vec{\beta}_1 \cdot \vec{\gamma}_1 dz \right]$$

$$\exp\left[-\frac{1}{2}\int_0^R [d(\vec{\gamma}_1 + \vec{a}(\vec{\gamma},\vec{\delta}),z) + d(\vec{\gamma}_1 + \vec{b}(\vec{\gamma},\vec{\delta}),z) + d(\vec{\beta}_1 + \vec{a}(\vec{\beta},\vec{\delta}),z) \right. \tag{72}$$

$$\left. + d(\vec{\beta}_1 + \vec{b}(\vec{\beta},\vec{\delta}),z) - d(\vec{\beta}_1 + \vec{\gamma}_1 + \vec{a}(\vec{\beta},\vec{\gamma}),z) - d(\vec{\beta}_1 - \vec{\gamma}_1 + \vec{b}(\vec{\beta},\vec{\gamma}),z)]dz \right]$$

Note that (72) is similar to (24) of the thin-screen derivation. The analogous expansion parameter is identified as the combination of phase structure function densities

$$Q = -\frac{1}{2}\int_0^R [d(\vec{\beta}_1 + \vec{a}(\vec{\beta},\vec{\delta}),z) + d(\vec{\beta}_1 + \vec{b}(\vec{\beta},\vec{\delta}),z) - d(\vec{\beta}_1 + \vec{\gamma}_1 + \vec{a}(\vec{\beta},\vec{\gamma}),z) - d(\vec{\beta}_1 - \vec{\gamma}_1 + \vec{b}(\vec{\beta},\vec{\gamma}),z)]dz$$

$$= 4\pi k^2 \int_0^R \int_{-\infty}^{\infty} \Phi_n(\vec{q},q_z = 0,z) \exp[i\vec{q}\cdot[\vec{\beta}_1 + \vec{l}(\vec{\beta},z)]][\cos(\vec{q}\cdot\vec{l}(\vec{\delta},z)) - \cos(\vec{q}\cdot[\vec{\gamma}_1 + \vec{l}(\vec{\gamma},z)])]\, d\vec{q}\, dz \tag{73}$$

For a point source, this expression is small in the contributing regions of path space [Dashen, 1979]. Performing the Taylor series in Q results in

$$G_4(\vec{\rho}_4;\vec{\rho}_4',R) = G_1'(\vec{\rho}_4;\vec{\rho}_4',R) \int\int D\vec{\beta}_1\, D\vec{\gamma}_1 \exp\left[-\frac{1}{2}\int_0^R [d(\vec{\gamma}_1(z) + \vec{a}(\vec{\gamma},\vec{\delta}),z) + d(\vec{\gamma}_1(z) + \vec{b}(\vec{\gamma},\vec{\delta}),z)]dz \right]$$

$$\left[\exp[-ik\int_0^R \vec{\beta}_1(z)\cdot\vec{\gamma}_1(z)dz] + \sum_{n=1}^{\infty} \frac{(4\pi k^2)^n}{n!} \int_0^R dz_1 \cdots \int_0^R dz_n \int_{-\infty}^{\infty} d\vec{q}_1 \cdots \int_{-\infty}^{\infty} d\vec{q}_n \right.$$

$$\exp\left[-ik\int_0^R \vec{\beta}_1(z)\cdot[\vec{\gamma}_1(z) - \sum_{j=1}^{n} \frac{\vec{q}_j}{k}\delta(z - z_j)]dz + i\sum_{j=1}^{n} \vec{l}(\vec{\beta},z_j)\cdot\vec{q}_j \right]$$

$$\left. \prod_{j=1}^{n} \Phi_n(\vec{q}_j,q_z = 0,z_j)[\cos(\vec{q}_j\cdot\vec{l}(\vec{\delta},z_j)) - \cos(\vec{q}_j\cdot(\vec{\gamma}_1(z_j) + \vec{l}(\vec{\gamma},z_j)))] \right] \tag{74}$$

Applying identity (59) yields

$$G_4(\vec{x}_1;\vec{x}'_1,R) = G_4^f(\vec{x}_1;\vec{x}'_1,R)\left\{\exp\left[-\frac{1}{2}\int_0^R [d(\vec{x}(\gamma,\delta),z) + d(\vec{x}'(\gamma,\delta),z)]dz\right] + \right.$$

$$\sum_{n=1}^{\infty} \frac{(4\pi k^2\eta)^n}{n!} \int_0^R dz_1 \cdots \int_0^R dz_n \int_{-\infty}^{\infty} d\vec{q}_1 \cdots \int_{-\infty}^{\infty} d\vec{q}_n \qquad (75)$$

$$\exp\left[i\sum_{j=1}^{n} \vec{l}(\vec{\beta},z_j)\cdot\vec{q}_j - \frac{1}{2}\int_0^R [d(\sum_{m=1}^{n}\frac{\vec{q}_m}{k}h(z;z_m) + \vec{x}(\gamma,\delta),z) + d(\sum_{m=1}^{n}\frac{\vec{q}_m}{k}h(z;z_m) + \vec{x}'(\gamma,\delta),z)]dz\right]$$

$$\left.\prod_{j=1}^{n}\Phi_n(\vec{q}_j,q_z=0,z_j)[\cos(\vec{q}_j\cdot\vec{l}(\vec{\delta},z_j)) - \cos(\vec{q}_j\cdot(\sum_{m=1}^{n}\frac{\vec{q}_m}{k}h(z_j,z_m) + \vec{l}(\gamma,z_j)))]\right\} = \sum_{n=0}^{\infty} G_{4_n}(\vec{x}_1;\vec{x}'_1,R)$$

where $h(z;z_1)$ is the solution of

$$\ddot{h}(z;z_1) = \delta(z - z_1) \qquad (76)$$

that is

$$h(z;z_1) = z\left(\frac{z_1}{R} - 1\right) \qquad z < z_1$$

$$h(z;z_1) = z_1\left(\frac{z}{R} - 1\right) \qquad z > z_1 \qquad (77)$$

The free space Green's function for the fourth moment, $G_4^f(\vec{x}_1;\vec{x}'_1,R)$, is given by (25).

The first term of (75)

$$G_{4_0}(\vec{x}_1;\vec{x}'_1,R) = G_4^f(\vec{x}_1;\vec{x}'_1,R)e^{-\frac{1}{2}\int_0^R [d(\vec{x}(\gamma,\delta),z) + d(\vec{x}'(\gamma,\delta),z)]dz} = G_2(\vec{x}_1,\vec{x}_2;\vec{x}'_1,\vec{x}'_2,R)G_2(\vec{x}_3,\vec{x}_4;\vec{x}'_3,\vec{x}'_4,R) \qquad (78)$$

is analogous to the thin-screen result (33).

The n=1 term is more complex.

$$G_{4_1}(\vec{x}_1;\vec{x}'_1,R) = 4\pi k^2 G_4^f(\vec{x}_1;\vec{x}'_1,R)\int_0^R\int_{-\infty}^{\infty}\Phi_n(\vec{q},q_z=0,z_1)[\cos(\vec{q}\cdot\vec{l}(\vec{\delta},z_1)) - \cos(\vec{q}\cdot[\frac{\vec{q}}{k}h(z_1,z_1) + \vec{l}(\gamma,z_1)])]$$

$$e^{i\vec{q}\cdot\vec{l}(\vec{\beta},z_1)}\exp\left[-\frac{1}{2}\int_0^R [d(\frac{\vec{q}}{k}h(z;z_1) + \vec{x}(\gamma,\delta),z) + d(\frac{\vec{q}}{k}h(z;z_1) + \vec{x}'(\gamma,\delta),z)]dz\right] d\vec{q}\,dz_1 \qquad (79)$$

The higher order terms of the fourth-moment Green's function are obtained from (75) but become more intractable. However, the first order description of the fourth moment is given by the leading terms of the series expansion. We now compare these expressions to previous results for the fourth moment. The point-source result is obtained from the Green's function by setting Γ_1 to zero. This reproduces the iterated series of Shishov [1972 Eq (13)] that was derived using moment-equation methods in a spherical coordinate system. Appling the plane-wave initial condition generates the series expression of Shishov [1971 Eq (20)]. Gurvich et al [1979b] proved this series was convergent. It can be shown that the point-source series is also convergent. Applying the plane-wave case to (79) with $\vec{\alpha} = 0$ and $\vec{\delta} = 0$, reproduces the strong scattering results of Fante [1975 Eq (B1)] and Zavorotnyi [1979b Eq (3)].

3.4 Intensity Correlation

Furutsu [1972] derived expressions for the intensity correlation from a Gaussian beam propagating in a random medium with a square-law structure function. This case describes random wander of a beam [Wandzura, 1980]. Weak scattering results for intensity correlation from a Gaussian beam are presented by Ishimaru [1969]. We now consider the intensity correlation following the thin screen analysis of section 2.3.

The fourth-moment series generates two expressions for the intensity correlation; one is obtained by setting $\vec{\delta} = 0$ and $\vec{\gamma} = 0$ (the low spatial frequency region) and the other by setting $\vec{\delta} = 0$ and $\vec{\beta} = 0$ (the high spatial frequency region). The resulting expressions for the n=0 term are

$$C_0^{\gamma}(\vec{\alpha},\vec{\beta},R) = \frac{k^4}{(2\pi R)^4}\int_{-\infty}^{\infty}\Gamma_4(\vec{\alpha}',\vec{\beta}',\vec{\gamma}',\vec{\delta}',0)\exp\left[-i\frac{k}{R}[(\vec{\alpha}-\vec{\alpha}')\cdot\vec{\delta}'+(\vec{\beta}-\vec{\beta}')\cdot\vec{\gamma}']\right] \qquad (80)$$

$$\exp\left[-\frac{1}{2}\int_0^R[\,d((\vec{\gamma}'+\vec{\delta}')(1-\frac{z}{R}),z)+d((\vec{\gamma}'-\vec{\delta}')(1-\frac{z}{R}),z)]dz\right] d\vec{\alpha}'\,d\vec{\beta}'\,d\vec{\gamma}'\,d\vec{\delta}'$$

and

$$C_0^{\gamma\gamma}(\vec{\alpha},\vec{\gamma},R) = \frac{k^4}{(2\pi R)^4}\int_{-\infty}^{\infty}\Gamma_4(\vec{\alpha}',\vec{\beta}',\vec{\gamma}',\vec{\delta}',0)\exp[-i\frac{k}{R}[(\vec{\alpha}-\vec{\alpha}')\cdot\vec{\delta}'+(\vec{\gamma}-\vec{\gamma}')\cdot\vec{\beta}']] \tag{81}$$

$$\exp\left[-\frac{1}{2}\int_0^R[\,d((\vec{\gamma}'+\vec{\delta}')(1-\frac{z}{R})+\vec{\gamma}\frac{z}{R},z)+d((\vec{\gamma}'-\vec{\delta}')(1-\frac{z}{R})+\vec{\gamma}\frac{z}{R},z)]dz\right] d\vec{\alpha}'\,d\vec{\beta}'\,d\vec{\gamma}'\,d\vec{\delta}'$$

For spatially coherent sources, these expressions reduce to

$$C_0^{\gamma\gamma}(\vec{\alpha},\vec{\beta},R) = \langle I(\frac{\vec{\alpha}+\vec{\beta}}{2},R)\rangle\langle I(\frac{\vec{\alpha}-\vec{\beta}}{2},R)\rangle = \langle I(\vec{\rho}_1,z)\rangle\langle I(\vec{\rho}_2,z)\rangle \tag{82}$$

and

$$C_0^{\gamma\gamma}(\vec{\rho}_1,\vec{\rho}_2,R) = \Gamma_2(\vec{\rho}_1,\vec{\rho}_2,R)\Gamma_2^*(\vec{\rho}_1,\vec{\rho}_2,R) \tag{83}$$

which are analogous to the thin-screen results (37) and (43).

The corresponding expressions for the n=1 term are given by

$$C_1^{\gamma\gamma}(\vec{\alpha},\vec{\beta},R) = \frac{4\pi k^6}{(2\pi R)^4}\int_0^R\int_{-\infty}^{\infty}\Gamma_4(\vec{\alpha}',\vec{\beta}',\vec{\gamma}',\vec{\delta}',0)e^{-i\frac{k}{R}[(\vec{\alpha}-\vec{\alpha}')\cdot\vec{\delta}'+(\vec{\beta}-\vec{\beta}')\cdot\vec{\gamma}']}e^{i\vec{q}\cdot[\vec{\beta}'(1-\frac{z_1}{R})+\vec{\beta}\frac{z_1}{R}]}\Phi_n(\vec{q},z_1)$$

$$\exp\left[-\frac{1}{2}\int_0^R[d(\frac{\vec{q}}{k}h(z;z_1)+(\vec{\gamma}'+\vec{\delta}')(1-\frac{z}{R}),z)+d(\frac{\vec{q}}{k}h(z;z_1)+(\vec{\gamma}'-\vec{\delta}')(1-\frac{z}{R}),z)]dz\right]$$

$$[\cos(\vec{q}\cdot\vec{\delta}'(1-\frac{z_1}{R}))-\cos(\vec{q}\cdot(\frac{\vec{q}}{k}h(z_1,z_1)+\vec{\gamma}'(1-\frac{z_1}{R})))]\,d\vec{\alpha}'\,d\vec{\beta}'\,d\vec{\gamma}'\,d\vec{\delta}'\,d\vec{q}\,dz_1 \tag{84}$$

and

$$C_1^{\gamma\gamma}(\vec{\alpha},\vec{\gamma},R) = \frac{4\pi k^6}{(2\pi R)^4}\int_0^R\int_{-\infty}^{\infty}\Gamma_4(\vec{\alpha}',\vec{\beta}',\vec{\gamma}',\vec{\delta}',0)e^{-i\frac{k}{R}[(\vec{\alpha}-\vec{\alpha}')\cdot\vec{\delta}'+\vec{\beta}'\cdot(\vec{\gamma}-\vec{\gamma}')]}e^{i\vec{q}\cdot\vec{\beta}'[1-\frac{z_1}{R}]}\Phi_n(\vec{q},z_1)$$

$$\exp\left[-\frac{1}{2}\int_0^R[d(\frac{\vec{q}}{k}h(z;z_1)+(\vec{\gamma}'+\vec{\delta}')(1-\frac{z}{R})+\vec{\gamma}\frac{z}{R},z)+d(\frac{\vec{q}}{k}h(z;z_1)+(\vec{\gamma}'-\vec{\delta}')(1-\frac{z}{R})+\vec{\gamma}\frac{z}{R},z)]dz\right]$$

$$\left[\cos[\vec{q}\cdot\vec{\delta}'(1-\frac{z_1}{R})]-\cos[\vec{q}\cdot(\frac{\vec{q}}{k}h(z_1,z_1)+\vec{\gamma}'(1-\frac{z_1}{R})+\vec{\gamma}\frac{z_1}{R})]\right]d\vec{\alpha}'\,d\vec{\beta}'\,d\vec{\gamma}'\,d\vec{\delta}'\,d\vec{q}\,dz_1 \tag{85}$$

The corresponding expressions for the intensity spectrum are obtained from (44). The Born approximation is secured from (84) by ignoring the last exponential term.

The low-frequency series for the intensity spectrum has been investigated for a power-law spectrum of refractive index fluctuations and plane-wave [Gochelashvily and Shishov, 1971, 1974] and point-source [Gochelashvily et al, 1974] geometries. The qualitative behavior of the intensity spectrum is similar to the thin screen result [Figure 1]. In weak scattering, the first two terms describe the complete intensity spectrum. In strong scattering the intensity spectrum is characterized by two components. The low frequency region is described by $\Phi^{W}(\vec{q},R)$. The high frequency behavior was first determined by summing the low-frequency series, which yields the high frequency approximation $\Phi_{\delta}^{W}(\vec{q},R)$. The derivation presented here generates this same result plus higher correction terms without performing a complicated summation.

Uscinski [1982] derived an approximate expression for the intensity spectrum for the case of plane waves by summing a perturbation series for the fourth moment equation. Macaskill [1983] derived the same result using the two-scale expansion [Beran et al, 1982]. In our notation, their expression for the intensity spectrum is

$$\Phi(\vec{q},R)=\frac{1}{(2\pi)^2}\int_{-\infty}^{\infty}\exp\Big[-\int_0^R[\,d(\vec{x},z)+d(\frac{\vec{q}}{k}(R-z),z)$$

$$-\frac{1}{2}d(\vec{x}+\frac{\vec{q}}{k}(R-z),z)-\frac{1}{2}d(\vec{x}-\frac{\vec{q}}{k}(R-z),z)]dz\Big]e^{-i\vec{q}\cdot\vec{x}}\,d\vec{x} \qquad (86)$$

The low and high spatial frequency behavior is identical to that obtained from (84) and (83).

The intensity correlation from a point source embedded in a random medium with irregularities that are constant in one transverse dimension is obtained from the point-source result by the substitution $\Phi_n(\vec{q})=\Phi_n(q_x)\delta(q_y)$. The leading order terms of the intensity correlation series are

$$C_{\delta}^{W}(\beta,R)=\langle I\rangle^2\exp[-\int_0^R d(\beta\frac{z}{R})dz] \qquad (87)$$

$$C_I^{(1)}(\beta,R) = 8\pi k^2 \langle I \rangle^2 \int_0^R \int_{-\infty}^{\infty} \Phi_n(q,z_1) \sin^2\left[\frac{q^2}{2k} h(z_1,z_1)\right]$$

$$\exp\left[-\int_0^R d\left[\frac{q}{k} h(z;z_1),z\right] dz + i\beta q \frac{z_1}{R}\right] dq \; dz_1 \tag{88}$$

and

$$C_I^{(2)}(\beta,R) = 8\pi k^2 \langle I \rangle^2 \int_0^R \int_{-\infty}^{\infty} \Phi_n(q,z_1) \sin^2\left[q\beta \frac{z_1}{2R} + \frac{q^2}{2k} h(z_1,z_1)\right]$$

$$\exp\left[-\int_0^R d\left[\beta \frac{z}{R} + \frac{q}{k} h(z;z_1),z\right] dz + i\beta q \frac{z_1}{R}\right] dq \; dz_1 \tag{89}$$

Ignoring the exponential term of (88) reproduces the weak scattering (Rytov approximation) result of Tur and Beran [1983].

Fante [1983] investigated the effect of the inner scale of turbulence on scintillation for the case of strong scattering of plane waves by calculating the expression $C_I^{(1)}(\beta,R)$. The contribution of this term to the total intensity variance is appreciable over a wide range of parameter space. Therefore, higher terms are required for an accurate description of the intensity correlation.

4. MOMENT EQUATION APPROACH

4.1 Moment Equation Method for the Thin Screen

We now derive the fourth-moment result (24), using the moment-equation method. This method is based on partial differential equations for the transverse moments that are derived from the parabolic equation for the random fields. These differential equations may then be solved by transform methods [Rumsey, 1975] and the method of characteristics [Kiang and Liu, 1982]. There are, in general, many transforms that will simplify the problem. We choose one [Shishov, 1971] that permits an analogous derivation for the fourth moment of waves propagating through extended random media.

The fourth moment satisfies the differential equation

$$\frac{\partial \Gamma_4}{\partial z} = \frac{i}{2k}(\nabla_1^2 - \nabla_2^2 + \nabla_3^2 - \nabla_4^2)\Gamma_4 \tag{90}$$

with initial condition

$$\Gamma_4(\vec{\rho}_1,\vec{\rho}_2,\vec{\rho}_3,\vec{\rho}_4,0+) = \Gamma_4(\vec{\rho}_1,\vec{\rho}_2,\vec{\rho}_3,\vec{\rho}_4,0)\langle e^{i[\theta(\vec{\rho}_1)-\theta(\vec{\rho}_2)+\theta(\vec{\rho}_3)-\theta(\vec{\rho}_4)]}\rangle = \Gamma_4(\vec{\rho}_1,\vec{\rho}_2,\vec{\rho}_3,\vec{\rho}_4,0)$$

$$\exp\left[-\frac{1}{2}[D_\theta(\vec{\rho}_1-\vec{\rho}_2)+D_\theta(\vec{\rho}_3-\vec{\rho}_4)+D_\theta(\vec{\rho}_1-\vec{\rho}_4)+D_\theta(\vec{\rho}_2-\vec{\rho}_3)-D_\theta(\vec{\rho}_2-\vec{\rho}_4)-D_\theta(\vec{\rho}_1-\vec{\rho}_3)]\right] \tag{91}$$

Change variables to the coordinate system (23). Then

$$\frac{\partial \Gamma_4}{\partial z} = \frac{i}{k}(\nabla_\alpha\cdot\nabla_\beta + \nabla_\beta\cdot\nabla_\gamma)\Gamma_4 \tag{92}$$

This equation is solved in the Fourier transform domain

$$M(\vec{R},\vec{q},\vec{\gamma},\vec{\delta},R) = \frac{1}{(2\pi)^4}\int_{-\infty}^{\infty}\Gamma_4(\vec{\alpha},\vec{\beta},\vec{\gamma},\vec{\delta},R)e^{-i[\vec{R}\cdot\vec{\alpha}+\vec{q}\cdot\vec{\beta}]}\,d\vec{\alpha}\,d\vec{\beta} \tag{93}$$

which transforms (92) to

$$\frac{\partial M}{\partial z} = -\left(\frac{\vec{R}}{k}\cdot\nabla_\beta + \frac{\vec{q}}{k}\cdot\nabla_\gamma\right)M \tag{94}$$

Changing variables to

$$\vec{a} = k\vec{\delta} - \vec{R}z \qquad \vec{b} = k\vec{\gamma} - \vec{q}z \qquad \tau = z$$

$$\vec{\delta}(\tau) = \frac{\vec{a}+\vec{R}\tau}{k} \qquad \vec{\gamma}(\tau) = \frac{\vec{b}+\vec{q}\tau}{k} \qquad z = \tau$$

$$\nabla_\beta = k\nabla_a \qquad \nabla_\gamma = k\nabla_b \qquad \frac{\partial}{\partial z} = -\vec{q}\cdot\nabla_b - \vec{R}\cdot\nabla_a + \frac{\partial}{\partial \tau} \tag{95}$$

transforms (94) to

$$\frac{\partial M}{\partial \tau}(\vec{R},\vec{q},\vec{a},\vec{b},\tau) = 0 \tag{96}$$

Since M is independent of r, the solution in the original variables is

$$M(\xi,\alpha,\gamma,\beta,R) = M(\xi,\alpha,\gamma - \alpha\frac{R}{k},\beta - \xi\frac{R}{k},0+) \tag{97}$$

The fourth moment is the inverse Fourier transform of this expression. After some manipulation, the Green's function result, (24), is produced. The moment- equation method is based on the formulation of the free space Green's function in the Fourier transform domain. This transform technique will now be applied to the more difficult problem of wave propagation in an extended random medium.

4.2 Moment Equation Method for Extended Random Media

The moment-equation method was a major contribution to the theory of wave propagation in extended random media [Prokhorov et al 1975, Tatarskii, 1971]. Using moment-equation methods, a series expression for the fourth moment was derived for plane-wave [Shishov, 1971] and point-source [Shishov, 1972] conditions. For an arbitrary source distribution, we present an analogous expression that is identical to the path integral results of section 3.3, thus demonstrating the equivalence of the two methods.

The transverse moments of the electric field satisfy differential equations [de Wolf, 1967; Brown, 1967; Shishov, 1968; Dolin, 1968; Chernov, 1969; Tatarskii, 1969; Lee, 1974]. We follow the techniques of Shishov [1971] to solve the differential equation for the fourth moment

$$\frac{\partial \Gamma_4}{\partial z} - \frac{i}{2k}[\nabla_1^2 - \nabla_2^2 + \nabla_3^2 - \nabla_4^2]\Gamma_4 + V\Gamma_4 = 0 \tag{98}$$

where

$$2V = d(\boldsymbol{\rho}_1 - \boldsymbol{\rho}_2, z) + d(\boldsymbol{\rho}_1 - \boldsymbol{\rho}_4, z) + d(\boldsymbol{\rho}_2 - \boldsymbol{\rho}_3, z) + d(\boldsymbol{\rho}_3 - \boldsymbol{\rho}_4, z) - d(\boldsymbol{\rho}_1 - \boldsymbol{\rho}_3, z) - d(\boldsymbol{\rho}_2 - \boldsymbol{\rho}_4, z) \tag{99}$$

In the coordinate system of (23), the fourth moment satisfies

$$\frac{\partial \Gamma_4}{\partial z} - \frac{i}{k}[\nabla_\alpha \cdot \nabla_\beta + \nabla_\beta \cdot \nabla_\gamma]\Gamma_4 + V\Gamma_4 = 0 \tag{100}$$

with

$$2V = d(\vec{\gamma}+\vec{\delta},R) + d(\vec{\gamma}-\vec{\delta},R) + d(\vec{\beta}+\vec{\delta},R) + d(\vec{\beta}-\vec{\delta},R) - d(\vec{\beta}+\vec{\gamma},R) - d(\vec{\beta}-\vec{\gamma},R) \qquad (101)$$

We identify the last four structure function densities in V, i.e.

$$2S = d(\vec{\beta}+\vec{\delta},z) + d(\vec{\beta}-\vec{\delta},z) - d(\vec{\beta}+\vec{\gamma},z) - d(\vec{\beta}-\vec{\gamma},z) \qquad (102)$$

as the related quantity to the path integral expansion variable Q of (73). The Fourier transform (93) converts (100) to the integral equation

$$\frac{\partial M}{\partial z} + \frac{\vec{k}}{k}\cdot\nabla_{\vec{\beta}}M + \frac{\vec{q}}{k}\cdot\nabla_{\vec{\gamma}}M + \frac{1}{2}[d(\vec{\gamma}+\vec{\delta}) + d(\vec{\gamma}-\vec{\delta})]M = G(\vec{k},\vec{q},\vec{\gamma},\vec{\delta},z) \qquad (103)$$

where G is the convolution of M with the transform of S, i.e.

$$G(\vec{k},\vec{q},\vec{\gamma},\vec{\delta},z) = 4\pi k^2 \int \Phi_n(\vec{q}_1,z)[\cos(\vec{\delta}\cdot\vec{q}_1) - \cos(\vec{\gamma}\cdot\vec{q}_1)]M(\vec{k},\vec{q}-\vec{q}_1,\vec{\gamma},\vec{\delta},z)\,d\vec{q}_1 \qquad (104)$$

The change of variables (95) transforms (103) to

$$\frac{\partial M}{\partial \tau} + \frac{1}{2}[d(\vec{\gamma}(\tau)+\vec{\delta}(\tau),\tau) + d(\vec{\gamma}(\tau)-\vec{\delta}(\tau),\tau)]M = G(\vec{k},\vec{q},\vec{\gamma}(\tau),\vec{\delta}(\tau),\tau) \qquad (105)$$

This is an ordinary differential equation in r, with solution

$$M(\vec{k},\vec{q},\vec{b},\vec{a},\tau) = M(\vec{k},\vec{q},\frac{\vec{b}}{k},\frac{\vec{a}}{k},0)\exp\left[-\frac{1}{2}\int_0^\tau [d(\vec{\gamma}(z)+\vec{\delta}(z),z) + d(\vec{\gamma}(z)-\vec{\delta}(z),z)]dz\right]$$

$$+ \int_0^\tau \exp\left[-\frac{1}{2}\int_{z_1}^\tau [d(\vec{\gamma}(z)+\vec{\delta}(z),z) + d(\vec{\gamma}(z)-\vec{\delta}(z),z)]dz\right] G(\vec{k},\vec{q},\vec{\gamma}(z_1),\vec{\delta}(z_1),z_1)\,dz_1 \qquad (106)$$

Changing variables back to $\vec{\delta},\vec{\gamma},R$ results in

$$M(\vec{k},\vec{q},\vec{\gamma},\vec{\delta},R) = M(\vec{k},\vec{q},\vec{\gamma}_3,\vec{\delta}_3,0)\exp\left[-\frac{1}{2}\int_0^R [d(\vec{\gamma}_2+\vec{\delta}_2,z) + d(\vec{\gamma}_2-\vec{\delta}_2,z)]dz\right]$$

$$+ \int_0^R \exp\left[-\frac{1}{2}\int_{z_1}^R [d(\vec{\gamma}_2+\vec{\delta}_2,z) + d(\vec{\gamma}_2-\vec{\delta}_2,z)]dz\right] G(\vec{k},\vec{q},\vec{\gamma}_1,\vec{\delta}_1,z_1)\,dz_1 \qquad (107)$$

where

$$\boldsymbol{\rho}_1 = \boldsymbol{\rho}_0(R - z_1) \qquad \boldsymbol{\rho}_2 = \boldsymbol{\rho}_0(R - z) \qquad \boldsymbol{\rho}_3 = \boldsymbol{\rho}_0(R)$$

$$\boldsymbol{\delta}_1 = \boldsymbol{\delta}_0(R - z_1) \qquad \boldsymbol{\delta}_2 = \boldsymbol{\delta}_0(R - z) \qquad \boldsymbol{\delta}_3 = \boldsymbol{\delta}_0(R) \tag{108}$$

and

$$\boldsymbol{\rho}_0(z) = \boldsymbol{\rho} - \frac{\mathbf{q}}{k} z \qquad \boldsymbol{\delta}_0(z) = \boldsymbol{\delta} - \frac{\boldsymbol{\varepsilon}}{k} z \tag{109}$$

This expression can be written as the integral equation

$$M(\boldsymbol{\varepsilon}, \mathbf{q}, \boldsymbol{\rho}, \boldsymbol{\delta}, R) = Z(\boldsymbol{\varepsilon}, \mathbf{q}, \boldsymbol{\rho}, \boldsymbol{\delta}, R)$$

$$+ \int_0^R \iiint \mathrm{K}(\boldsymbol{\varepsilon}, \mathbf{q}, \mathbf{q}', \boldsymbol{\rho}, \boldsymbol{\rho}', \boldsymbol{\delta}, \boldsymbol{\delta}', R, z_1) M(\boldsymbol{\varepsilon}, \mathbf{q}', \boldsymbol{\rho}', \boldsymbol{\delta}', z_1)\, d\mathbf{q}'\, d\boldsymbol{\rho}'\, d\boldsymbol{\delta}'\, dz_1 \tag{110}$$

where

$$Z(\boldsymbol{\varepsilon}, \mathbf{q}, \boldsymbol{\rho}, \boldsymbol{\delta}, 0) = M(\boldsymbol{\varepsilon}, \mathbf{q}, \boldsymbol{\rho}_3, \boldsymbol{\delta}_3, 0) \exp\left[-\frac{1}{2} \int_0^R [d(\boldsymbol{\rho}_2 + \boldsymbol{\delta}_2, z) + d(\boldsymbol{\rho}_2 - \boldsymbol{\delta}_2, z)]\, dz \right] \tag{111}$$

and

$$\mathrm{K}(\boldsymbol{\varepsilon}, \mathbf{q}, \mathbf{q}', \boldsymbol{\rho}, \boldsymbol{\rho}', \boldsymbol{\delta}, \boldsymbol{\delta}', R, z_1) = 4\pi k^2 \Phi_n(\mathbf{q} - \mathbf{q}', z_1) \delta(\boldsymbol{\delta}' - \boldsymbol{\delta}_1) \delta(\boldsymbol{\rho}' - \boldsymbol{\rho}_1) \tag{112}$$

$$\exp\left[-\frac{1}{2} \int_{z_1}^R [d(\boldsymbol{\rho}_2 + \boldsymbol{\delta}_2, z) + d(\boldsymbol{\rho}_2 - \boldsymbol{\delta}_2, z)]\, dz \right] \left\{ \cos[\boldsymbol{\delta}' \cdot (\mathbf{q} - \mathbf{q}')] - \cos[\boldsymbol{\rho}' \cdot (\mathbf{q} - \mathbf{q}')] \right\}$$

The formal solution is written as a sum of terms which are obtained by the iteration

$$M_n(\boldsymbol{\varepsilon}, \mathbf{q}, \boldsymbol{\rho}, \boldsymbol{\delta}, R) = \int_0^R \iiint \mathrm{K}(\boldsymbol{\varepsilon}, \mathbf{q}, \mathbf{q}', \boldsymbol{\rho}, \boldsymbol{\rho}', \boldsymbol{\delta}, \boldsymbol{\delta}', R, z_1) M_{n-1}(\boldsymbol{\varepsilon}, \mathbf{q}', \boldsymbol{\rho}', \boldsymbol{\delta}', z_1)\, d\mathbf{q}'\, d\boldsymbol{\rho}'\, d\boldsymbol{\delta}'\, dz_1 \tag{113}$$

and $M_0 = Z$. This expression is a power series in the group of phase structure function densities denoted by Q, which is the same quantity as (73) of the path integral expansion; hence

the two series are equal, term by term. Unfortunately, for higher order terms, this equality is not obvious by examination since the functional form of the two series is very different: the moment equation series is essentially a multiple convolution, while the path integral result is not. However, with careful algebraic manipulation, the equality of the two series can be explicitly demonstrated.

The moment-equation method was first applied to the simple geometries of plane waves and point sources. Since the moments are then independent of the centroid coordinate, the differential equations simplify. Early work concentrated on moment-equation methods because of this simplification. Moment-equation techniques have also been used to investigate the validity of the Markov approximation [Klyatskin, 1969; Klyatskin and Tatarskii, 1971] and the effects of non-gaussian refractive index fluctuations under the Markov approximation [Klyatskin, 1975]. The Green's function formulation provides a clear connection between the thin screen and extended medium. The operator form of the path integral has also been useful for evaluating the corrections to the Markov approximation for the higher intensity moments [Zavorotnyi, 1978].

5. SUMMARY

A series expression has been derived for the fourth moment of waves incident on a phase screen or propagating through extended random media. The asymmetric terms of the expansion generate two expressions for the intensity correlation; one that approximates the low frequency region of the spatial spectrum and the other appropriate for the high frequencies. The rate of convergence of the two approximations can be used to produce a complete expression for the intensity spectrum valid for any initial source distribution. These results can be derived using moment-equation techniques or functional methods (path integral or operator).

Many problems of WPRM may now be attacked with renewed confidence since we have derived expressions that are valid for arbitrary source distributions. These include

a) The intensity statistics from beamed lasers, navigational beacons, radar, spacecraft and

satellite radio transmissions, compact astronomical sources and other extended wave sources.

b) The effects of slowly varying refractive index statistics along the propagation path, e.g. the turbulence profile of planetary atmospheres.

c) Comparison of thin-screen and extended-media results.

d) The relationship between intensity statistics and the form of the refractive index spectrum.

e) Imaging through random media.

Acknowledgements: This research was funded by DARPA.

References

Barabanenkov, Y.N., Y.A. Kravtsov, S.M. Rytov, and V.I. Tatarskii, Status of the theory of propagation of waves in randomly inhomogeneous medium, Sov. Phys. Usp., 13, 551-680, 1971.

Beran, M.J., A.M. Whitman, and S. Frankenthal, Scattering calculations using the characteristic rays of the coherence function, J. Acoust. Soc. Am., 71, 1124-1130, 1982.

Bramley, E.N., Diffraction of an angular spectrum of waves by a phase-changing screen, J. Atmos. Terr. Phys., 29, 1-28, 1967.

Brown, W.P., Propagation in random media- cumulative effect of weak inhomogeneities IEEE Trans. Ant. Prop., AP-15, 81-89, 1967.

Chernov, L.A., Equations for the statistical moments of the field in a randomly-inhomogeneous medium, Akust. Zh., 15, 594-603, 1969. English, Sov. Phys. Acoustics, 15, 511-517, 1970.

Codona, J.L., D.B. Creamer, S.M. Flatté, R.G. Frehlich, and F. Henyey, Moment-equation and path-integral techniques for wave propagation in random media, submitted to J. Math. Phys., 1985.

Dashen, R., Path integrals for waves in random media, J. Math. Phys., 20, 894-920, 1979.

de Wolf, D.A., Multiple scattering in a random continuum, Radio Science, 2, 1379-1392, 1967.

Dolin, L.S., Equations for the correlation functions of a wave beam in a randomly-inhomogeneous medium, Izv. VUZ. Radiofiz., 11, 840-849, 1968. English, Radiophysics and Quantum Electronics, 11, 486-491, 1968.

Fante, R.L., Electromagnetic beam propagation in turbulent media, Proc. IEEE, 63, 1669-1692, 1975.

Fante, R.L., Electromagnetic beam propagation in turbulent media: An update, Proc. IEEE, 68, 1424-1443, 1980.

Fante, R.L., Inner-scale size effect on the scintillations of light in the turbulent atmosphere, J. Opt. Soc. Am., 73, 277-281, 1983.

Feynman, R.P., Space-time approach to non-relativistic quantum mechanics, Rev. Mod. Phys., 20, 367-387, 1948.

Flatté, S.M., R. Dashen, W.H. Munk, K.M. Watson, and F. Zachariasen, Sound Transmission Through a Fluctuating Ocean, published by the Cambridge University Press in their series on Mechanics and Applied Mathematics, 1979.

Flatté, S.M., Wave propagation through random media: Contributions from ocean acoustics, Proc. IEEE, 71, 1267-1294, 1983.

Furutsu, K., Statistical theory of wave propagation in a random medium and the irradiance distribution function, J. Opt. Soc. Am., 62, 240-254, 1972.

Gochelashvily, K.S., and V.I. Shishov, Laser beam scintillation beyond a turbulent layer, Optica Acta, 18, 313-320, 1971.

Gochelashvily, K.S., and V.I. Shishov, Focused irradiance fluctuations beyond a layer of turbulent atmosphere, Optica Acta, 19, 327-332, 1972.

Gochelashvily, K.S., Propagation of focused laser radiation in a turbulent medium, Kvant. Elektron., 1, 848-857, 1974. English, Sov. J. Quant. Electron., 4, 465-470, 1974.

Gochelashvily, K.S., and V.I. Shishov, Saturated fluctuations in the laser radiance intensity in a turbulent medium, Zh. Eksp. Teor. Fiz., 66, 1237-1247, 1974. English, Sov. Phys. JETP, 39, 605-609, 1974.

Gochelashvily, K.S., V.G. Pevgov, and V.I. Shishov, Saturation of fluctuations of the intensity of laser radiation at large distances in a turbulent atmosphere Fraunhofer zone of transmitter Kvant. Elektron., 1, 1156-1165, 1974. English, Sov. J. Quant. Electron., 4, 632-637, 1974.

Gochelashvily, K.S., and V.I. Shishov, Saturation of laser irradiance fluctuations beyond a turbulent layer, Optical and Quantum Electronics, 7, 524-536, 1975.

Gurvich, A.S., and V. Kan, Measurement of four-point field coherence function in region of random focusing of laser emission, Izv. Vysh. Ucheb. Zaved. Radiofiz., 21, 398-407, 1978. English, Radiophysics and Quantum Electronics, 21, 274-281, 1978.

Gurvich, A.S., V. Kan, V.I. Tatarskii, and V.U. Zavorotnyi, Four-point field coherence function in

a turbulent medium, Optica Acta, 26, 543-553, 1979a.

Gurvich, A.S., B.S. Elenov, Vl. V. Pokasov, K.K. Sabel'fel'd, and V.I. Tatarskii, Spatial structure of strong fluctuations of light intensity in a turbulent medium, Izv. Vysh. Ucheb. Zaved. Radiofiz., 22, 198-207, 1979b. English, Radiophysics and Quantum Electronics, 22, 135-142, 1979b.

Ishimaru, Akira, Fluctuations of a focused beam wave for atmospheric turbulence probing, Proc. IEEE, 57, 407-414, 1969.

Ishimaru, Akira, Wave Propagation and Scattering in Random Media, Academic Press, 1978.

Kiang, Yean-Woei, and C.H. Liu, Propagation of beam waves through a turbulent layer, Radio Science, 17, 1211-1219, 1982.

Klyatskin, V.I. Applicability of the approximation of a markov random process in problems relating to the propagation of light in a medium with random inhomogeneities, Zh. Eksp. Teor. Fiz., 57, 952-958, 1969. English, Soviet Physics JETP, 30, 520-523, 1970.

Klyatskin, V.I., and V.I. Tatarskii, The parabolic equation approximation for propagation of waves in a medium with random inhomogeneities, Zh. Eksp. Teor. Fiz., 58, 624-634, 1970. English, Soviet Physics JETP, 31, 335-339, 1970.

Klyatskin, V.I., and Tatarskii, A new method of successive approximations in the problem of the propagation of waves in a medium having random large-scale inhomogeneities, Izv. Vysh. Ucheb. Zaved. Radiofiz., 14, 1400-1415, 1971. English, Radiophysics and Quantum Electronics, 14, 1100-1111, 1971.

Klyatskin, V.I., Statistical theory of light propagation in a randomly-inhomogeneous medium (Functional methods) (Review), Izv. Vysh. Ucheb. Zaved. Radiofiz., 16, 1629-1644, 1973. English, Radiophysics and Quantum Electronics, 16, 1261-1271, 1973.

Klyatskin, V.I., and V.I. Tatarskii, Statistical theory of light propagation in a turbulent medium (Review), Izv. Vysh. Ucheb. Zaved. Radiofiz., 15, 1433-1455, 1972. English, Radiophysics and Quantum Electronics, 15, 1095-1111, 1972.

Lee, L.C., Wave propagation in a random medium: A complete set of the moment equations with different wave numbers, J. Math. Phys., 15, 1431-1435, 1974.

Lee, L.C., Theory of thin-screen scintillations for a spherical wave, Astrophysical Journal, 218, 468-476, 1977.

Macaskill, C., An improved solution to the fourth moment equation for intensity fluctuations, Proc. R. Soc. Lond. A, 386, 461-474, 1983.

Marians, M. Computed scintillation spectra for strong turbulence, Radio Sci., 10, 115-119, 1975.

Mercier, R.P., Diffraction by a screen causing large random phase fluctuations, Proc. Camb. Phil. Soc., 58, 382-400, 1962.

Prokhorov, A.M., F.V.Bunkin, K.S. Gochelashvily, and V.I.Shishov, Laser irradiance propagation in turbulent media, Proc. IEEE, 63, 790-811 1975.

Rickett, B.J., Interstellar scattering and scintillation of radio waves, Ann. Rev. Astron. Astrophys., 15, 479-504, 1977.

Rickett, B.J., W.A. Coles and G. Bourgois, Slow scintillation in the interstellar medium, Astron. Astrophys., 134, 390-395, 1984.

Rino, C.L., A power law phase screen model for ionospheric scintillation 1. Weak scatter, Radio Science, 14, 1135-1145, 1979a.

Rino, C.L., A power law phase screen model for ionospheric scintillation 2. Strong scatter, Radio Science, 14, 1147-1155, 1979b.

Rumsey, V.H., Scintillations due to a concentrated layer with a power-law turbulence spectrum, Radio Science, 10, 107-114, 1975.

Salpeter, E.E., Interplanetary scintillations I. Theory, Astrophys. J., 147, 433-448, 1967.

Shishov, V.I., Theory of wave propagation in random media, Izv. Vuz. Radiofiz., 11, 866-875, 1968. English, Radiophysics Quantum Electronics, 11, 500-505, 1968.

Shishov, V.I., Strong fluctuations of the intensity of a plane wave propagating in a random refractive medium, Zh. Eksp. Teor. Fiz., 61, 1399-1409, 1971. English, Sov. Phys. JETP, 34, 744-748, 1972.

Shishov, V.I., Strong fluctuations of the intensity of a spherical wave propagating in a randomly refractive medium, Izv. Vysh. Ucheb. Zaved. Radiofiz., 15, 904-912, 1972. English, Radiophysics and Quantum Electronics, 15, 689-695, 1972.

Tatarskii, V.I., Light propagation in a medium with random refractive index inhomogeneities in the Markov random process approximation, Zh. Eksp. Teor. Fiz., 56, 2106-2117, 1969. English, Soviet Physics JETP, 29, 1133-1138, 1969.

Tatarskii, V.I., The Effects of the Turbulent Atmosphere on Wave Propagation, National Technical Information Service, Springfield, Va., 1971.

Tatarskii, V.I., and V.U. Zavorotnyi, Strong fluctuations in light propagation in a randomly inhomogeneous medium, E. Wolf, Progress in Optics XVIII, North-Holland, 1980.

Tur, Moshe, and Mark J. Beran, Wave propagation in random media: a comparison of two theories, J. Opt. Soc. Am., 73, 1343-1349, 1983.

Uscinski, B.J., Intensity fluctuations in a multiple scattering medium. Solution of the fourth moment equation, Proc. R. Soc. Lond. A., 380, 137-169, 1982.

Uscinski, B.J., and C. Macaskill, Intensity fluctuations due to a deeply modulated phase screen- I. Theory, J. Atmos. Terr. Phys., 45, 595-605, 1983a.

Uscinski, B.J., and C. Macaskill, Intensity fluctuations due to a deeply modulated phase screen-II. Results, J. Atmos. Terr. Phys., 45, 607-615, 1983b.

Wandzura, S.M., Meaning of quadratic structure functions, J. Opt. Soc. Am., 70, 745-747, 1980.

Yeh, Kung Chie, and Chao-Han Liu, Radio wave scintillations in the ionosphere, Proc. IEEE, 70, 324-360, 1982.

Zavorotnyi, V.U., V.I. Klyatskin, and V.I. Tatarskii Strong fluctuations of the intensity of electromagnetic waves in randomly inhomogeneous media, Zh. Eksp. Teor. Fiz., 73, 481-497, 1977. English, Soviet Physics JETP, 46, 252-260, 1977.

Zavorotnyi, V.U., Strong fluctuations of electromagnetic waves in a random medium with finite longitudinal correlation of the inhomogeneities, Zh. Eksp. Teor. Fiz., 75, 56-65, 1978. English, Soviet Physics JETP, 48, 27-31, 1978.

Zavorotnyi, V.U., Four-point coherence function of the field behind a phase screen for strong fluctuations of wave intensity, Izv. Vysh. Ucheb. Zaved. Radfiz., 22, 462-469, 1979a . English, Radiophysics and Quantum Electronics, 22, 318-323, 1979a.

Zavorotnyi, V.U., Four-point function for field-coherence in a turbulent medium in a region of strong fluctuations of wave intensity, Izv. Vysh. Ucheb. Zaved. Radfiz., 22, 979-988, 1979b. English, Radiophysics and Quantum Electronics, 22, 677-683, 1979b.

Figure Captions

Figure 1. The leading terms of the intensity spectrum versus normalized spatial frequency, qR_f, where $R_f = (R/k)^{\frac{1}{2}}$ is the Fresnel scale. The curves are calculated from expressions given by Gochelashvily and Shishov [1975] for the case of plane waves incident on a random phase screen with a Kolmogorov spectrum of phase fluctuations and $D_\phi(R_f) = 100$. The (-) sign indicates that $\Phi_1^{NF}(q)$ is negative at high frequency.

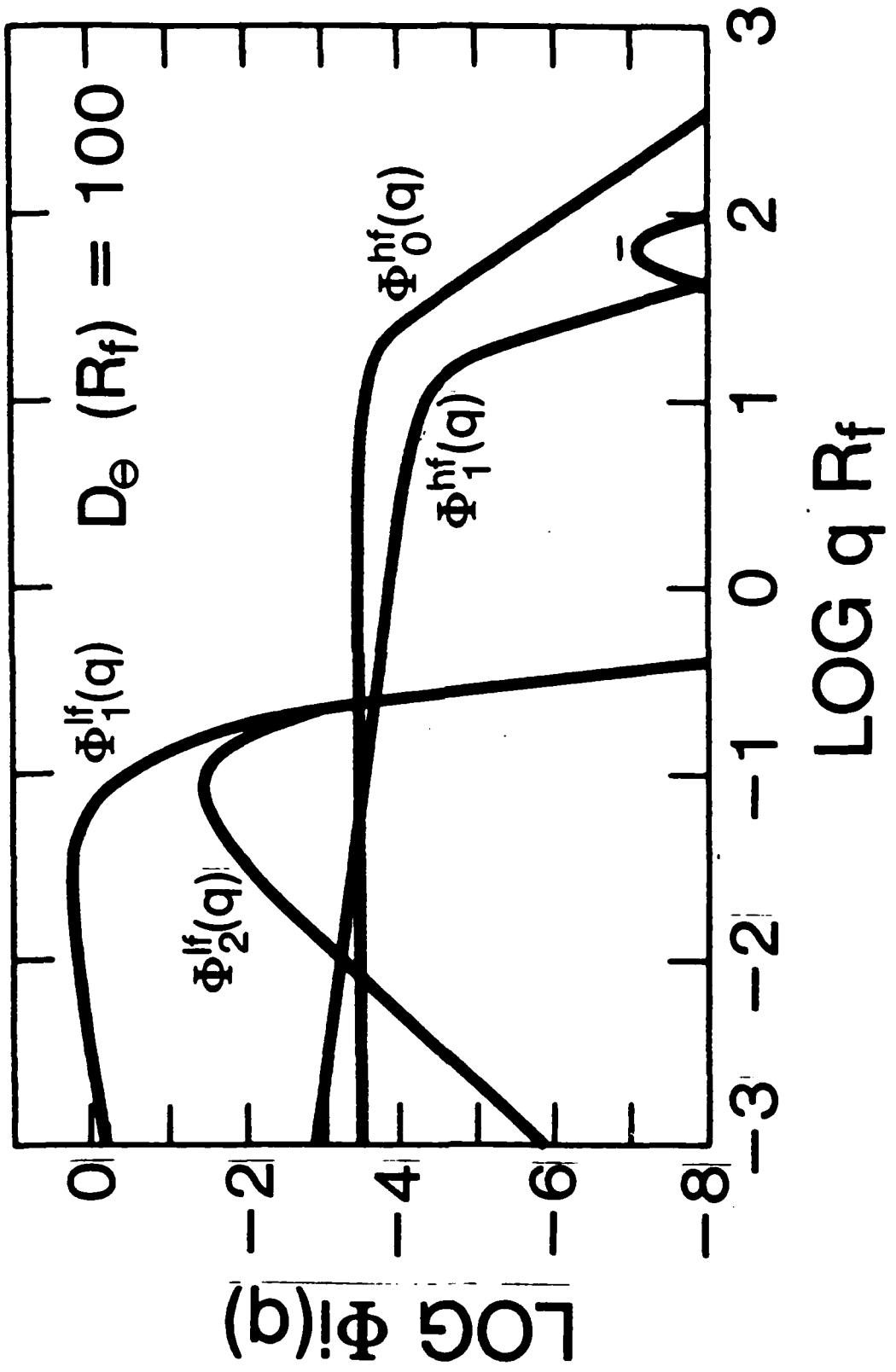
LOG φi(q)
0
−2
−4
−6
−8
−3
−2
−1
0
1
2
3
LOG q Rf
D_Θ (R_f) = 100
$\Phi_1^{lf}(q)$
$\Phi_2^{lf}(q)$
$\Phi_0^{hf}(q)$
$\Phi_1^{hf}(q)$

IV. UNEQUAL-FREQUENCY CORRELATION

The following section is a draft paper on the two-frequency intensity correlation. This subject is important for understanding the maximum bandwidth available in a communications channel. It is also valuable in preparing for understanding the connection between pulse propagation characteristics and the intervening random medium. It is not directly related to pulse width because that depends on the correlation of particular frequency derivatives of the fourth moment rather than the fourth moment itself.

LJI-P-85-321

Two Frequency Intensity Cross-Spectrum

Johanan L. Codona, Dennis B. Creamer, Stanley M. Flatté,*
R.G. Frehlich, and Frank S. Henyey

Center For Studies of Nonlinear Dynamics†
La Jolla Institute
3252 Holiday Court, Suite 208
La Jolla, California 92037

Abstract

The intensity cross-spectrum (spatial Fourier transform of the two frequency intensity correlation) for scintillations caused by a plane wave passing through a random phase screen is considered. By examining the two frequency fourth moment, we show that the "fully saturated" approximation of modelling this spectrum as the transform of the square of the second moment breaks down when the outer scale is large compared with the diameter of the scattering disk. A new approximation is obtained which has essentially the same limits of validity as the "fully saturated" approximation to the monochromatic fourth moment.

*On leave from the University of California, Santa Cruz, CA 95064
†Affiliated with the University of California, San Diego.

1. Introduction

The finite bandwidth of real sources and receivers has an important effect on the intensity variation of waves propagating in random media: scintillations will appear weaker than with an ideal narrow-band receiver due to intensity decorrelation at different wavelengths [Budden & Uscinski, 1970; Fante, 1977]. In weak scattering conditions, the decorrelation bandwidth is larger implying that the reduction of the intensity variance s minimal. However, in strong scattering the effect of this decorrelation can be substantial and is evident in observations of "dynamic spectra", e.g. radio frequency spectra as a function of time, which are commonly used in analysis of pulsars [Rickett, 1969]. This effect is particularly important when observing the intensity spread of propagating pulses (pulse jitter) [Liu & Yeh, 1971].

Previously, intensity decorrelations were studied using a "saturated scintillations" argument [Shishov, 1973; Lee, 1976]. When the intensity scintillations have saturated, it is argued that the real and imaginary parts of the field become zero-mean Gaussian random variables, implying that the intensity distribution is Rayleigh. The correlation of intensity fluctuations is then the magnitude squared of the second moment of the fields. This is reasonably well understood for the monochromatic intensity correlation (second moment of intensity), where it can be shown that the Rayleigh limit is reached in strong enough scattering [Tatarskii, 1971; Flatté, 1983; Codona et al, 1985]. When there is a finite bandwidth present, the major problem with the argument that the two-frequency intensity covariance is the magnitude squared of the two-frequency second moment (mutual coherence function) is the appearance of the mean-square phase shift in the result. Physically, this is unreasonable since the intensity of the wave shouldn't be affected by its integrated phase. This dependence on the phase shift also implies that, in situations where the important region of

scattering (scattering disk) is much smaller than the outer scale of the turbulent fluctuations, the result from the "saturated scintillations" argument depend sensitively on this outer scale (through the phase shift factor). Previously, this dilemma had been solved by dropping the phase factor entirely. In this paper we analyze the question of intensity decorrelation of a plane wave propagating through a random phase screen. A series representation of the two-frequency intensity correlation function will be derived. The nature of the above phase shift factor will be clarified and the conditions under which it can be ignored will be presented.

We consider plane waves normally incident on a phase screen and freely propagating a distance R beyond the screen to an observation plane. The refractive index fluctuations, $\mu(\underline{x})$, in the screen induce an random phase change, $\Theta = k\int \mu(\underline{x},z)dz$, as the field passes through the screen. Here z is the direction of the propagating wave, $\underline{x}$ is the co-ordinate transverse to this direction, and k is the wavenumber. The phase change Θ is assumed to be a zero-mean Gaussian random variable with locally homogeneous statistics, and the correlation function

$$C_\Theta(\underline{x}) = <\Theta(\underline{x}')\Theta(\underline{x}'+\underline{x})> = \int_{-\infty}^{\infty} \Phi_\Theta(\underline{q}) e^{i\underline{q}\cdot\underline{x}} d^2q \qquad (1)$$

where $\Phi_\Theta(\underline{q})$ is the spectrum of phase fluctuations and <> denotes ensemble averages. Since we are not dealing with monochromatic fields, it is important to remember that there is wavenumber dependence in the phase and is included in the phase spectrum. The wave propagation is characterized by narrow angular scattering in the phase screen due to the small fluctuations of the refractive index. Then the complex scalar wave field can be expressed as $E(\underline{x},z;k)e^{ikz}$, implying that, away from the screen, the field E satisfies the parabolic equation [

$$\frac{\partial E}{\partial z} = \frac{i}{2k}\frac{\partial^2}{\partial \underline{x}^2}E \qquad (2)$$

with the value on emerging from the screen

$$E(\underline{x},0+;k) = E(\underline{x},0;k)\, e^{i\theta(\underline{x})} \tag{3}$$

expressed in terms of the incident field $E(\underline{x},0;k)$. For a plane wave the incident field is a constant, which we set to one. The solution of the parabolic equation at the observation plane with the proper initial condition is then

$$E(\underline{x},R;k) = \frac{k}{2i\pi R}\int_{-\infty}^{\infty} e^{i\theta(\underline{x}')} \exp\left(\frac{ik(\underline{x}-\underline{x}')^2}{2R}\right) d^2x' \tag{4}$$

Averages of the random phase are simplified by the use of the identity

$$\langle e^{i\theta}\rangle = e^{-\frac{1}{2}\langle\theta^2\rangle} \tag{5}$$

valid for any zero-mean Gaussian random variable. This, for example, gives the average of the field as

$$\langle E(\underline{x},R;k)\rangle = \exp\left[-\frac{1}{2}\Phi^2\right] \tag{6}$$

where $\Phi^2 = C_\theta(\vec{0})$ is the mean square phase shift.

In Section 2 we introduce the general second and fourth moments of the field and the two-point, two-frequency (intensity) correlation function. In Section 3 we consider the "fully saturated" approximation to this correlation function. In Section 4 two different series representations for the intensity cross-spectrum (spatial Fourier transform of the intensity correlation) are presented. The first series describes the low spatial frequency behaviour of the cross-spectrum (i.e. it converges quickly in this region). The other series describes the high spatial frequency behaviour. These series are very similar to those which appear for the monochromatic intensity correlation. It is shown that the "fully saturated" approximation (with the mean-square phase shift factor) is only valid over a negligible portion of the intensity cross-spectrum. The conditions under which this phase shift factor may be omitted are detailed. Finally,

in Section 5 we accumulate the formulae which approximate the two-frequency intensity cross-spectrum. This approximation is sufficient to analyze most problems of intensity decorrelation caused by strongly scattering thin screens.

2. Second and Fourth Moments

The random nature of the fields is conveniently described by statistical moments evaluated in the observation plane. The moments of particular concern for the study of frequency decorrelation are the second and fourth moments. The general second moment is given by

$$\Gamma_2(\boldsymbol{\rho}_1,\boldsymbol{\rho}_2,R;k_1,k_2) \equiv \langle E(\boldsymbol{\rho}_1,R;k_1)E^*(\boldsymbol{\rho}_2,R;k_2)\rangle \tag{7}$$

$$= \frac{k_1k_2}{(2\pi R)^2}\int\int_{-\infty}^{\infty} e^{-\frac{1}{2}V_2}\exp\left[\frac{i}{2R}[k_1(\boldsymbol{\rho}_1-\boldsymbol{\rho}_1')^2-k_2(\boldsymbol{\rho}_2-\boldsymbol{\rho}_2')^2]\right]d^2x_1'd^2x_2'$$

where we have used the solution for the fields, (4). We have used (5) to obtain $\exp[-V_2/2]$, where

$$V_2(\boldsymbol{\rho}_1-\boldsymbol{\rho}_2;k_1,k_2) \equiv \langle[\int(k_1\mu(\boldsymbol{\rho}_1,z')-k_2\mu(\boldsymbol{\rho}_2,z'))dz']^2\rangle \tag{8}$$

$$= \left[\frac{k_1-k_2}{(k_1+k_2)/2}\right]^2\phi^2 + D(\boldsymbol{\rho}_1-\boldsymbol{\rho}_2)$$

We have expressed the quantity V_2 in terms of ϕ^2, which is the mean-square phase shift for a wave with the mean wave number $\bar{k}=(k_1+k_2)/2$, and D is the phase structure function associated with a wavenumber which is the geometric mean, $(k_1k_2)^{1/2}$, i.e.

$$D(\boldsymbol{\rho}_1-\boldsymbol{\rho}_2) = k_1k_2\langle[\int(\mu(\boldsymbol{\rho}_1,z')-\mu(\boldsymbol{\rho}_2,z'))\,dz']^2\rangle \tag{9}$$

It will be useful to explicitly display the wavenumber dependence of the phase structure function by expressing it in terms of a structure function for the integrated index of refraction fluctuations, D_μ, via $D=k_1k_2D_\mu$, where

$$D_\mu(\vec{x}_1-\vec{x}_2) = \langle[\int(\mu(\vec{x}_1,z')-\mu(\vec{x}_2,z'))\,dz']^2\rangle \tag{10}$$

It is convenient to express the second moment in terms of mean and difference variables for the co-ordinates in the observation plane

$$\vec{\alpha} = \frac{\vec{x}_1+\vec{x}_2}{2} \quad , \quad \vec{\beta} = \vec{x}_1-\vec{x}_2 \tag{11a}$$

with similar expressions for the (primed) co-ordinates on the screen. We also use combinations of the wavenumbers given by

$$\bar{k} = \frac{k_1 + k_2}{2} \quad , \quad \delta k = k_1 - k_2 \tag{11b}$$

Then the second moment is given by

$$\Gamma_2(\vec{\alpha},\vec{\beta},R;k_1,k_2) = \frac{k_1k_2}{(2\pi R)^2}\exp\left[-(\frac{\delta k}{\bar{k}})^2\frac{\Phi^2}{2}\right]\int\int_{-\infty}^{\infty} e^{-\frac{1}{2}D(\vec{\beta}')}$$

$$\exp\left[i\frac{\delta k}{2R}[(\vec{\alpha}-\vec{\alpha}')^2+(\vec{\beta}-\vec{\beta}')^2]+i\frac{\bar{k}}{R}(\vec{\alpha}-\vec{\alpha}')\cdot(\vec{\beta}-\vec{\beta}')\right]d^2\alpha'\,d^2\beta' \tag{12}$$

We can immediately do the α' integration since the phase structure function is independent of this variable. Note that this implies that Γ_2 is independent of $\vec{\alpha}$, which follows from the translation invariance of the problem for an incident plane wave. Performing the α' integration we secure for the second moment

$$\Gamma_2(\vec{\beta},R;k_1,k_2) = \frac{k_1k_2}{2\pi\,\delta k\,R}\exp[-(\frac{\delta k}{\bar{k}})^2\frac{\Phi^2}{2}]\int_{-\infty}^{\infty} e^{-\frac{1}{2}D(\vec{\beta}')}$$

$$\exp\left[\frac{ik_1k_2}{2\,\delta k\,R}(\vec{\beta}-\vec{\beta}')^2\right]d^2\beta' \tag{13}$$

The general fourth moment is given by

$$\Gamma_4(\vec{x}_1,\vec{x}_2,\vec{x}_3,\vec{x}_4,R;k_1,k_2,k_3,k_4) = \langle E(\vec{x}_1,R;k_1)E^*(\vec{x}_2,R;k_2)E(\vec{x}_3,R;k_3)E^*(\vec{x}_4,R;k_4)\rangle$$

$$= \int\int_{-\infty}^{\infty}\int\int\prod_{j=1}^{4}\left[d^2x_j'\exp[-i\frac{(-1)^jk_j}{2R}(x_j-x_j')^2]\right]e^{-\frac{1}{2}D_4} \tag{14}$$

where $\tilde{V}_4$ is defined as

$$\tilde{V}_4(\mathfrak{L}_1',\mathfrak{L}_2',\mathfrak{L}_3',\mathfrak{L}_4') = \langle [\int (k_1\mu(\mathfrak{L}_1',s') - k_2\mu(\mathfrak{L}_2',s') + k_3\mu(\mathfrak{L}_3',s') - k_4\mu(\mathfrak{L}_4',s'))ds']^2 \rangle$$

$$= \left(\frac{k_1-k_2+k_3-k_4}{k_1+k_2+k_3+k_4}\right)^2\Phi^2 + \sum_{i<j}^{4} (-1)^{i+j} k_i k_j D_\mu(\mathfrak{L}_i - \mathfrak{L}_j) \tag{15}$$

It is convenient to transform the co-ordinates of the observation plane to

$$\begin{bmatrix} \vec{\alpha} \\ \vec{\beta} \\ \vec{\gamma} \\ \vec{\delta} \end{bmatrix} = \frac{1}{2} \begin{bmatrix} 1 & 1 & 1 & 1 \\ 1 & 1 & -1 & -1 \\ 1 & -1 & -1 & 1 \\ 1 & -1 & 1 & -1 \end{bmatrix} \begin{bmatrix} \mathfrak{L}_1 \\ \mathfrak{L}_2 \\ \mathfrak{L}_3 \\ \mathfrak{L}_4 \end{bmatrix} \tag{16}$$

(similarly for the primed co-ordinates of the screen), and express combinations of the wavenumber variables as

$$\begin{bmatrix} \bar{k} \\ \delta k/2 \\ \tilde{k} \\ \Delta k \end{bmatrix} = \frac{1}{4} \begin{bmatrix} 1 & 1 & 1 & 1 \\ 1 & 1 & -1 & -1 \\ 1 & -1 & -1 & 1 \\ 1 & -1 & 1 & -1 \end{bmatrix} \begin{bmatrix} k_1 \\ k_2 \\ k_3 \\ k_4 \end{bmatrix} \tag{17}$$

In terms of these variables the full fourth moment is

$$\Gamma_4(\vec{\alpha},\vec{\beta},\vec{\gamma},\vec{\delta};R,k_1,k_2,k_3,k_4) = \frac{(k_1k_2k_3k_4)}{(2\pi R)^4} \int\int\int\int d^2\alpha' d^2\beta' d^2\gamma' d^2\delta' e^{-\frac{1}{2}\tilde{V}_4} \tag{18}$$

$$\exp\left[\frac{\tilde{k}}{R}[(\vec{\alpha}-\vec{\alpha}')\cdot(\vec{\beta}-\vec{\beta}')+(\vec{\gamma}-\vec{\gamma}')\cdot(\vec{\delta}-\vec{\delta}')] + i\frac{\Delta k}{R}[(\vec{\alpha}-\vec{\alpha}')^2+(\vec{\beta}-\vec{\beta}')^2+(\vec{\gamma}-\vec{\gamma}')^2+(\vec{\delta}-\vec{\delta}')^2]\right]$$

$$\exp\left[\frac{\bar{k}}{R}[(\vec{\alpha}-\vec{\alpha}')\cdot(\vec{\delta}-\vec{\delta}')+(\vec{\beta}-\vec{\beta}')\cdot(\vec{\gamma}-\vec{\gamma}')] + i\frac{\delta k}{2R}[(\vec{\alpha}-\vec{\alpha}')\cdot(\vec{\gamma}-\vec{\gamma}')+(\vec{\beta}-\vec{\beta}')\cdot(\vec{\delta}-\vec{\delta}')]\right]$$

The integration over the centroid, α' is immediate since the D_μ functions depend only on co-ordinate differences. The resulting expression is relevant for calculations of quantities like pulse jitter. The quantity we are concerned with for frequency decorrelation is a special case of the fourth moment - the two-point, two-frequency intensity correlation function

$$C_I(\vec{\rho}_1,\vec{\rho}_2,R;k_1,k_2) \equiv \langle I(\vec{\rho}_1,R;k_1)I(\vec{\rho}_2,R;k_2)\rangle = \Gamma_4(\vec{\rho}_1,\vec{\rho}_1,\vec{\rho}_2,\vec{\rho}_2,R;k_1,k_1,k_2,k_2) \qquad (19)$$

Because of translation invariance, C_I is a function only of the difference variable $\vec{\beta}=\vec{\rho}_1-\vec{\rho}_2$. In terms of the transformed variables in (16-17), we find that $\vec{\gamma}=\vec{\delta}=\Delta k=\tilde{k}=0$ so that, for the intensity correlation, (18) reduces (after integrating over the α' variable) to

$$C_I(\vec{\beta},R;k_1,k_2)=\left(\frac{k_1k_2}{2\pi\bar{k}R}\right)^2\int\int_{-\infty}^{\infty}\int e^{-\frac{1}{2}V_4}\,\delta\left(\vec{\delta}'+\frac{\delta k}{\bar{k}}\vec{\gamma}'\right) \qquad (20)$$

$$\exp\left[-i\frac{\bar{k}}{R}\vec{\gamma}'\cdot(\vec{\beta}-\vec{\beta}')\right]\exp\left[-i\frac{\delta k}{2R}\vec{\delta}'\cdot(\vec{\beta}-\vec{\beta}')\right]d^2\beta'd^2\gamma'd^2\delta'$$

where $\bar{k}=(k_1+k_2)/2$, $\delta k=k_1-k_2$, and V_4 is the reduced form of (15)

$$V_4(\vec{\beta}',\vec{\gamma}',\vec{\delta}')=k_1^2\,D_\mu(\vec{\gamma}'+\vec{\delta}')+k_2^2D_\mu(\vec{\gamma}'-\vec{\delta}') \qquad (21)$$

$$-k_1k_2[D_\mu(\vec{\beta}'+\vec{\gamma}')+D_\mu(\vec{\beta}'-\vec{\gamma}')-D_\mu(\vec{\beta}'+\vec{\delta}')-D_\mu(\vec{\beta}'-\vec{\delta}')]$$

The intensity cross spectrum, Φ_I, is given by the $\vec{\beta}$ Fourier transform of (20). Before proceeding to evaluate the cross-spectrum we will discuss the "saturated scintillations" approximation to it.

3. Fully Saturated Approximation for Intensity Correlations

If the field is a zero-mean Gaussian random process then the intensity correlation function can be expressed as

$$C_{I\,\text{saturated}}(\vec{\rho}_1,\vec{\rho}_2,R;k_1,k_2)=\langle I(\vec{\rho}_1,R;k_1)\rangle\langle I(\vec{\rho}_2,R;k_2)\rangle+|\Gamma_2(\vec{\rho}_1,\vec{\rho}_2,R;k_1,k_2)|^2 \qquad (22)$$

In the thin screen model where we are considering an incident plane wave, the mean intensities in the first term are independent of position. The second term is only a function of $\vec{\beta}=\vec{\rho}_1-\vec{\rho}_2$ as noted above. Inserting Γ_2 from (12) and transforming over $\vec{\beta}$ yields the saturated approximation to the intensity cross-spectrum

$$\Phi_{I\,saturated}(\vec{\ell},R;k_1,k_3)=\langle I_1\rangle\langle I_3\rangle\,\delta(\vec{\ell}) + \exp\left[-\left(\frac{\delta k}{\bar{k}}\right)^2\Phi^2\right]\int\int e^{-\frac{k_1k_3}{2}[D_\mu(\vec{\beta}_1)+D_\mu(\vec{\beta}_2)]}$$

$$\exp\left[\frac{ik_1k_3}{2\delta k\,R}[(\vec{\beta}_1)^2-(\vec{\beta}_2)^2]\right]\delta(\vec{\beta}_1-\vec{\beta}_2+\frac{R\delta k}{k_1k_3}\vec{\ell})\,d^2\beta_1 d^2\beta_2 \qquad (23)$$

Changing integration variables to

$$\vec{\Omega}=\frac{\vec{\beta}_1+\vec{\beta}_2}{2}\quad,\quad \vec{\Psi}=\vec{\beta}_1-\vec{\beta}_2 \qquad (24)$$

and defining

$$R_F^2=\frac{\bar{k}R}{k_1k_3} \qquad (25)$$

we secure

$$\Phi_{I\,saturated}(\vec{\ell},R;k_1,k_3)=\langle I_1\rangle\langle I_3\rangle\,\delta(\vec{\ell}) + \exp\left[-\left(\frac{\delta k}{\bar{k}}\right)^2\Phi^2\right]\int e^{-i\vec{\Omega}\cdot\vec{\ell}}$$

$$\exp\left[-\frac{k_1k_3}{2}[D_\mu(\vec{\Omega}+\frac{\delta k}{2\bar{k}}R_F{}^2\vec{\ell})+D_\mu(\vec{\Omega}-\frac{\delta k}{2\bar{k}}R_F{}^2\vec{\ell})]\right]d^2 \qquad (26)$$

There are two problems with the saturated approximation: the mean-square phase shift factor and the low spatial frequency behaviour. In order to see where the difficulties arise, consider a pure power-law structure function

$$D(\vec{s})=\left[\frac{s}{s_0}\right]^p \qquad (27)$$

where s_0 is the coherence length of the medium ($D(s_0)=1$). Define the size of the illuminated spot (scattering disk) as

$$R_s\equiv\vartheta_s R=\frac{R\bar{\beta}}{s_0} \qquad (28)$$

where ϑ_s is the width of the angular spectrum, and a measure of the "strength of scattering"

$$D(R_s)=\left[\frac{R_s}{s_0}\right]^p \qquad (29)$$

The other quantity of interest is the outer scale, L_{outer}, of the spectrum of phase irregularities where

$$D(\mathbf{s})=\phi^2 \qquad s>L_{outer} \tag{30}$$

In most cases of practical interest, the outer scale is much larger than the size of the scattering disk. In terms of R_e the saturated approximation to the intnsity cross-spectrum is written as

$$\Phi_{I,saturated}(\boldsymbol{\kappa},R;k_1,k_3)=\langle I_1\rangle\langle I_3\rangle\,\delta(\boldsymbol{\kappa}) + \exp\left[-\left(\frac{\delta k}{\bar{k}}\right)^2\phi^2\right]\int_{-\infty}^{\infty} e^{-i\boldsymbol{\kappa}\cdot\boldsymbol{\alpha}}$$
$$\exp\left[-\frac{k_1k_3}{2}\left[D_\mu\left(\boldsymbol{\alpha}+\frac{\delta k}{2\bar{k}}R_e\,s_0\boldsymbol{\kappa}\right)+D_\mu\left(\boldsymbol{\alpha}-\frac{\delta k}{2\bar{k}}R_e\,s_0\boldsymbol{\kappa}\right)\right]\right]d^2 \tag{31}$$

The cross-spectrum is negligible for wavenumbers greater than the inverse of the coherence scale so that the combination $s_0\kappa$ appearing in (31) is smaller than unity in the region of interest.

The argument for the field to be a zero-mean Gaussian random process begins by assuming that the coherence length, s_0 is small compared to the size of the illuminated spot. This implies that the field at the observation point is the sum of very many *independent* contributions from the scattering disk. By the central limit theorem the fields appear to obey Gaussian statistics and the intensity follows a Rayleigh distribution. However, when the outer scale is larger than the scattering disk, there are large-scale phase fluctuations which lead to coherent contributions of the fields from different regions of the illuminated spot, so that the fields don't behave as Gaussian processes. One immediate consequence of this picture is that there are intensity fluctuations over regions larger than the scattering disk. This effect will modify the cross-spectrum at wavenumbers $\kappa \leq 1/R_e$ and is described by geometrical optics at small enough wavenumber. How this modification occurs from a fourth-moment calculation is considered in the next section.

The randomness induced by the phase fluctuations much smaller than R_s are consistent with the field being a Gaussian process. Thus the "saturated approximation" is roughly correct if we replace ϕ^2 in (26) by $D(R_s)$ of (29). In the next section we show how this procedure leads to a good approximation for the large κ behaviour of the cross-spectrum.

4. Intensity Cross-spectrum

The intensity cross spectrum is given by the $\vec{\beta}$ Fourier transform of (20), which just produces the delta function, $\delta(\vec{\kappa}-(\bar{k}\vec{\gamma}'-\frac{\delta k}{2}\vec{\delta}')/R)$, where $\vec{\kappa}$ is the transform variable. With this delta function, (20) reduces to

$$\Phi_I(\vec{\kappa},R;k_1,k_3) = \int_{-\infty}^{\infty} e^{i\vec{\kappa}\cdot\vec{\beta}'} e^{-\frac{1}{2}V_4} d^2\beta' \tag{32}$$

with

$$V_4 \equiv V_4(\vec{\beta}',\vec{\gamma}'=R_s s_0\vec{\kappa},\vec{\delta}'=\frac{\delta k}{2\bar{k}}R_s s_0\vec{\kappa}) \tag{33}$$

$$= k_1^2 D_\mu(R_s s_0\vec{\kappa}(1+\frac{\delta k}{2\bar{k}})) + k_3^2 D_\mu(R_s s_0\vec{\kappa}(1-\frac{\delta k}{2\bar{k}}))$$

$$-k_1k_3[D_\mu(\vec{\beta}'+R_s s_0\vec{\kappa})+D_\mu(\vec{\beta}'-R_s s_0\vec{\kappa})-D_\mu(\vec{\beta}'+\frac{\delta k}{2\bar{k}}R_s s_0\vec{\kappa})-D_\mu(\vec{\beta}'-\frac{\delta k}{2\bar{k}}R_s s_0\vec{\kappa})]$$

Unfortunately, the final integral in (32) cannot be done exactly. Our approach is to find two separate approximations for high and low spatial frequency. First we consider high spatial frequencies because this is the region where the mean-square phase shift term in (31) appears.

In the monochromatic case at high spatial frequencies and strong scattering, the terms in V_4 that dominate the integral for the cross-spectrum are $D_\mu(\vec{\beta}'+\vec{\delta}')+D_\mu(\vec{\beta}'-\vec{\delta}')$ [Gochelashvily & Shishov, 1975; Rumsey, 1975]. Separate V_4 into $V_4 \equiv V_4^0 + V_4^R$, with

$$V_4^0(\vec{\beta}',\vec{\delta}') = k_1 k_3 [D_\mu(\vec{\beta}'+\vec{\delta}') + D_\mu(\vec{\beta}'-\vec{\delta}')] \tag{34a}$$

and

$$V_4^R = k_1^2 D_\mu(\vec{\gamma}'+\vec{\delta}') + k_3^2 D_\mu(\vec{\gamma}'-\vec{\delta}') - k_1 k_3 [D_\mu(\vec{\beta}'+\vec{\gamma}') + D_\mu(\vec{\beta}'-\vec{\gamma}')] \tag{34b}$$

where we set $\vec{\gamma}' = R_s s_0 \vec{\kappa}$ and $\vec{\delta}' = (\delta k / 2\bar{k}) R_s s_0 \vec{\kappa}$. For the monochromatic case ($\delta k = 0$), Rumsey showed that, over the important region of integration, the β' dependence of V_4^R is negligible compared to that of V_4^0, giving the intensity spectrum as the Fourier transform of $\exp[-k_1 k_3 D_\mu(\vec{\beta}')]$. This is because the quantity $s_0 \kappa$ is of the order of unity while the important region of integration is β' smaller than the scattering disk. When δk is not zero (but small), the high frequency behaviour of the cross-spectrum is still controlled by V_4^0 for the same reasons. It is important to realize that these terms do *not* dominate the behaviour of V_4 for all $\vec{\beta}'$ and $\vec{\kappa}$, but only for $\gamma' = R_s s_0 \kappa \gg \beta'$. Unlike the monochromatic case, when β' is zero V_4 is non-zero. However V_4 still increases with increasing β', so that the Fourier transform integrand, $e^{-V_4/2}$, is largest when β' is small. The approximate domain of $\vec{\beta}'$, in which the Fourier integrand is large, is where $\beta' \leq s_0$. In this regime V_4^R is roughly independent of β', so that the integrand is dominated by the V_4^0. The limiting value, $\beta' \approx s_0$, leads to the requirement

$$\kappa \gg R_s^{-1} \tag{35}$$

wherein we expect the β' behaviour of $e^{-V_4/2}$ to be controlled by the $D_\mu(\vec{\beta}'+\vec{\delta}') + D_\mu(\vec{\beta}'-\vec{\delta}')$ terms. This is verified explicitly in Appendix 1.

We proceed in our analysis by rewriting $V_4^R = V_4^{R0} + V_4^{R1}$, where

$$V_4^{R0}(\vec{\gamma}',\vec{\delta}') = V_4^R(\vec{\beta}'=0) \tag{36a}$$

$$= k_1^2 D_\mu(\vec{\gamma}'+\vec{\delta}') + k_3^2 D_\mu(\vec{\gamma}'-\vec{\delta}') - 2k_1 k_3 D_\mu(\vec{\gamma}')$$

and

$$V_4^{R1}(\vec{\beta}',\vec{\gamma}') = V_4^R - V_4^{R0} \tag{36b}$$

$$= k_1 k_3 [2D_\mu(\vec{\rho}') - D_\mu(\vec{\beta}' + \vec{\rho}') - D_\mu(\vec{\beta}' - \vec{\rho}')]$$

The exact expression for the cross-spectrum is then

$$\Phi_I(\vec{\kappa}, R; k_1, k_3) = \exp\left[-\frac{1}{2} V_4^{R0}(\vec{\rho}' = R_e s_0 \vec{\kappa}, \vec{\delta}' = \frac{\delta k}{2\bar{k}} R_e s_0 \vec{\kappa})\right] \int_{-\infty}^{\infty} e^{i2\vec{\kappa}\cdot\vec{\beta}'} \tag{37}$$

$$\exp\left[-\frac{1}{2} V_4^0(\vec{\beta}', \vec{\delta}' = \frac{\delta k}{2\bar{k}} R_e s_0 \vec{\kappa})\right] e^{-\frac{1}{2} V_4^{R1}(\vec{\beta}', \vec{\rho}' = R_e s_0 \vec{\kappa})} d^2\beta'$$

But V_4^{R1} is small compared to V_4^0 allowing us to expand the final exponential in a Taylor series yielding a corresponding series for the intensity cross-spectrum

$$\Phi_I(\vec{\kappa}, R; \bar{k}, \delta k) = \sum_{n=0}^{\infty} \Phi_{I_{RF}}^{\{n\}}(\vec{\kappa}, R; \bar{k}, \delta k) \tag{38}$$

Truncating this series after a few terms we will call the high frequency approximation since in the monochromatic case the corresponding series converges quickly for strong scattering and high spatial frequencies. The leading term is

$$\Phi_{I_{RF}}^{\{0\}}(\vec{\kappa}, R; k_1, k_3) = e^{-V_4^{R0}} \int_{-\infty}^{\infty} e^{i2\vec{\kappa}\cdot\vec{\beta}'} \tag{39}$$

$$\exp\left[-\frac{k_1 k_3}{2}[D_\mu(\vec{\beta}' + \frac{\delta k}{2\bar{k}} R_e s_0 \vec{\kappa}) + D_\mu(\vec{\beta}' - \frac{\delta k}{2\bar{k}} R_e s_0 \vec{\kappa})]\right] d^2\beta'$$

where V_4^{R0} is explicitly

$$V_4^{R0} = k_1^2 D_\mu(R_e s_0 \vec{\kappa}(1 + \frac{\delta k}{2\bar{k}})) + k_3^2 D_\mu(R_e s_0 \vec{\kappa}(1 - \frac{\delta k}{2\bar{k}})) - 2k_1 k_3 D_\mu(R_e s_0 \vec{\kappa}) \tag{40}$$

We are now in a position to compare this leading term with the "fully saturated" approximation, (31). Since the phase structure functions saturates to Φ^2 for scales larger than the outer scale (39) gives the same result as (31) only for spatial frequencies such that $\kappa > (l_{outer} / R_e) s_0^{-1}$. The only non-negligible portion of the spectrum is for $\kappa < 1/s_0$, leading to the conclusion that the saturated approximation is only valid for a significant portion of the spectrum when the outer scale, l_{outer}, is small compared to the size of the scattering disk.

However, in virtually every case of practical interest, the scattering disk is *small* relative to any estimates of an outer scale. In these cases, the saturated approximation becomes valid only after the cross-spectrum has dropped to a negligible value.

A common approach for dealing with the intensity cross-spectrum has been to use (31) but drop the phase shift factor, $e^{-(\delta k/\bar{k})^2\varphi^2}$.

$$\Phi_{I\,\text{saturated}}(\vec{\ell},R;k_1,k_3) \approx \int_{-\infty}^{\infty} e^{i\vec{\ell}\cdot\vec{u}} \exp\left[-\frac{k_1k_3}{2}\left[D_\mu\left(\vec{u}+\frac{\delta k}{2\bar{k}}R_e\,s_0{}^2\vec{\ell}\right)+D_\mu\left(\vec{u}-\frac{\delta k}{2\bar{k}}R_e\,s_0{}^2\vec{\ell}\right)\right]\right] d^2u$$

This expression can be compared with (39) and is roughly equivalent for a significant portion of the spectrum when V_4^{R0} is approximately zero. Using the largest significant κ value (s_0) leads to the requirement

$$k_1^2\,D_\mu\left(R_e\left(1+\frac{\delta k}{2\bar{k}}\right)\right)+k_3^2\,D_\mu\left(R_e\left(1-\frac{\delta k}{2\bar{k}}\right)\right)-2k_1k_3D_\mu(R_e)\ll 1 \qquad (42)$$

For a power law structure function this expression can be simplified by performing a small δk expansion (valid for $\delta k<2\bar{k}$) leading to

$$\frac{\delta k}{2\bar{k}}D(R_e)\ll 1 \qquad (43)$$

These points may be summarized by saying that the fully saturated approximation should *never* be used for estimates of the intensity decorrelation and (41) should only be used when $(\delta k/2\bar{k})D(R_e)\ll 1$. In fact, since using (39) is as easy as using (41), the leading order approximation (39) is the high spatial frequency approximation of choice.

We now consider the next-to-leading term in (38). Writing the phase structure function (for the mean wave number) in terms of the phase spectrum

$$D(\vec{s}) = 2\int_{-\infty}^{\infty}\Phi_\theta(\vec{\kappa}')\left[1-e^{i\vec{\kappa}'\cdot\vec{s}}\right]d^2\kappa' \qquad (44)$$

with Φ_θ as the power spectrum of phase shift through the screen, the second

term in the series expansion of $\exp[-\frac{1}{2}V_4^{R1}]$ is

$$-\frac{1}{2}V_4^{R1} = -4\frac{k_1k_3}{k^2}\int_{-\infty}^{\infty}\Phi_0(\vec{\kappa}')e^{i\vec{R}\cdot\vec{\gamma}'}\sin^2\left[\frac{\vec{\kappa}'\cdot\vec{\beta}'}{2}\right]d^2\kappa' \tag{45}$$

This yields the first correction to the leading approximation, (39),

$$\Phi_{I_1I_3}^{(1)}(\vec{\kappa},R;k_1,k_3) = -4\frac{k_1k_3}{k^2}e^{-V_4^{R0}}\int\int_{-\infty}^{\infty}\Phi_0(\vec{\kappa})e^{i\vec{R}\cdot(\vec{\beta}'+R_0s_0\vec{\kappa}')} \tag{46}$$

$$\exp\left[-\frac{k_1k_3}{2}[D_\mu(\vec{\beta}'+\frac{\delta k}{2\bar{k}}R_0s_0\vec{\kappa})+D_\mu(\vec{\beta}'-\frac{\delta k}{2\bar{k}}R_0s_0\vec{\kappa})]\right]\sin^2\left[\frac{\vec{\kappa}'\cdot\vec{\beta}'}{2}\right]d^2\beta'd^2\kappa'$$

where V_4^{R0} is given in (40).

We now turn our attention to the low spatial frequencies. When $\kappa \ll 1/R_0$, the $\vec{\beta}'$ Fourier transform has substantial contributions from everywhere in the integration plane, and over most of this region, $\beta' \gg R_0 s_0 \kappa$. When this is the case, it can be seen from (32), that V_4 will be dominated by the first two terms on the right hand side of that equation since the β' dependent terms nearly cancel. Unlike the high frequency approximation, however, the dominant behaviour is $\vec{\beta}'$ independent, which is the source of the delta function in the saturated approximation, (31). By construction, $\langle I_1\rangle=\langle I_3\rangle=1$ since we set the input amplitude to unity. Since the $\vec{\beta}'$ dependent terms in V_4 are small, the exponent may be expanded in a Taylor series

$$e^{-\frac{1}{2}V_4(\vec{\beta}',\vec{\gamma}',\vec{\delta}')}=\exp\left[\frac{1}{2}[k_1^2D_\mu(\vec{\gamma}'+\vec{\delta}')+k_3^2D_\mu(\vec{\gamma}'-\vec{\delta}')]\right] \tag{47}$$

$$\sum_{n=0}^{\infty}\frac{1}{n!}(k_1k_3)^n\left[D_\mu(\vec{\beta}'+\vec{\gamma}')+D_\mu(\vec{\beta}'-\vec{\gamma}')-D_\mu(\vec{\beta}'+\vec{\delta}')-D_\mu(\vec{\beta}'-\vec{\delta}')\right]^n$$

yielding the low frequency series for the cross-spectrum

$$\Phi_I(\vec{\kappa},R;k_1,k_3)=\sum_{n=0}^{\infty}\Phi_{I_1I_3}^{(n)}(\vec{\kappa},R;\bar{k},\delta k) \tag{48}$$

Inserting the above expansion into (31) yields explicit expressions for the terms in the low-frequency series. Using (44) to express the structure functions of (47) in terms of the phase spectrum, we find that the two leading terms in the low-frequency series are

$$\Phi_I^{(0)}(\vec{\kappa},R;k_1,k_3)=\delta(\vec{\kappa}) \tag{49}$$

and

$$\Phi_I^{(1)}(\vec{\kappa},R;\bar{k},\delta k)=\frac{4k_1k_3}{\bar{k}^2}\exp\left[-\frac{1}{2}[k_1^2D_\mu((1+\frac{\delta k}{2\bar{k}})R_e s_0\vec{\kappa})+k_3^2D_\mu((1-\frac{\delta k}{2\bar{k}})R_e s_0\vec{\kappa})]\right] \tag{50}$$

$$\Phi_\theta(\vec{\kappa})\left[\sin^2(R_e s_0\kappa^2/2)-\sin^2(\frac{\delta k}{\bar{k}}R_e s_0\kappa^2/4)\right]$$

As mentioned earlier, the delta function is the same as in the saturated approximation, but the behaviour for $0<\kappa<<1/R_e$ is very different.

5. Summary

References

Budden, K. G., F. R. S. and B. J. Uscinski, The scintillation of extended radio sources when the receiver has a finite bandwidth, Proc. Roy. Soc. Lond. A. 316, 315-339, 1970.

Codona, J.L., D.B. Creamer, S.M. Flatté , R.G. Frehlich, and F. Henyey, Solution for the fourth moment of waves propagating in random media, submitted to Radio Science, 1985.

Fante, Ronald L., Effect of source bandwidth and receiver response time on the scintillation index in random medium, Radio Sci. 12, 223-229, 1977.

Flatté , S.M., Wave propagtion through random media: Contributions from ocean acoustics, Proc. IEEE, 71, 1267-1294, 1983.

Gochelashvily, K.S., and V.I. Shishov, Saturation of laser irradiance fluctuations beyond a turbulent layer, Optical and Quantum Electronics, 7, 524-536, 1975.

Lee, L. C., Strong scintillations in astrophysics. IV. Cross-correlation between different frequencies and finite bandwidth effects, Ap. J. 206, 744-752, 1976.

Liu, C. H. and K. C. Yeh, Pulse spreading and wandering in random media, Radio Sci. 14, 925-931, 1971.

Rumsey, V.H., Scintillations due to a concentrated layer with a power-law turbulence spectrum, Radio Science, 14, 107-114, 1975.

Shishov, V. I., Frequency correlation of scintillations, Izv. Vysh. Ucheb. Zaved. Radiofiz. 16, 423-433 (1973). English, Radiophysics and Quantum Electronics 16, 319-327, 1973.

Tatarski, V. I., The effects of the Turbulent Atmosphere on Wave Propagation, National Technical Information Service, Springfield, Va., 1971.

Appendix

In this appendix we show that $\vec{\beta}'$ dependence of V_4^R is negligible compared to that of V_4^0 where, from (27),

$$V_4^0(\vec{\beta}',\vec{\delta}')k_1k_3[D_\mu(\vec{\beta}'+\vec{\delta}')+D_\mu(\vec{\beta}'-\vec{\delta}')] \tag{A1a}$$

and

$$V_4^R(\vec{\beta}',\vec{\delta}',\vec{\gamma}')=k_1^2D_\mu(\vec{\gamma}'+\vec{\delta}')+k_3^2D_\mu(\vec{\gamma}'-\vec{\delta}')+k_1k_3[D_\mu(\vec{\beta}'+\vec{\gamma}')+D_\mu(\vec{\beta}'-\vec{\gamma}')] \tag{A1b}$$

We have argued in section 4 that the dominant region of integration is for small $\beta' \ll R_e s_0 \kappa$. In that case, the two terms in the brackets in (A1b) may be expanded as

$$D_\mu(R_e s_0\hat{k}+\vec{\beta}')+D_\mu(R_e s_0\hat{k}-\vec{\beta}')=2D_\mu(R_e s_0\hat{k})+\left[\vec{\beta}'\cdot\frac{\partial}{\partial\vec{s}}\right]^2 D_\mu(\vec{s})|_{\vec{s}=R_e s_0\kappa}+\cdots \tag{A2}$$

The second term may be bounded by

$$\left|\left[\vec{\beta}'\cdot\frac{\partial}{\partial\vec{s}}\right]^2 D_\mu(\vec{s})|_{\vec{s}=R_e s_0\kappa}\right| \le \beta'^2 |D_\mu''(R_e s_0\kappa)| \tag{A3}$$

giving the leading $\vec{\beta}'$ dependence of V_4^R as

$$V_4^R \sim k_1k_3\beta'^2 D_\mu''(R_e s_0\kappa) \tag{A4}$$

In verifying that V_4^0 controls the $\vec{\beta}'$ dependence we will examine three cases

$$\begin{aligned} &\text{Case 1: } \frac{\delta k}{2\bar{k}}R_e s_0\kappa \ll \beta' \\ &\text{Case 2: } \beta' \ll \frac{\delta k}{2\bar{k}}R_e s_0\kappa \\ &\text{Case 3: } \frac{\delta k}{2\bar{k}}R_e s_0\kappa \approx \beta' \end{aligned} \tag{A5}$$

In the first case, β is large compared to $\delta k R_e s_0\kappa/2\bar{k}$ giving the leading dependence of V_4^0 as

$$V_4^0 \sim 2k_1k_3D_\mu(\beta') \tag{A6}$$

so that we require

$$\beta'^2 D_\mu''(R_e s_0 \kappa) \ll D_\mu(\beta') \tag{A7}$$

Using a model power-law structure function as in (30) this requirement becomes

$$\left[\frac{\beta'}{s_0}\right]^{2-p} \left[R_e \kappa\right]^{p-2} \ll \frac{2}{p(p-1)} \tag{A8}$$

Since p is typically in the range $0<p\leq 2$, we find an upper bound for the left-hand side by setting $\beta'=s_0$ and $\kappa=s_0^{-1}$ resulting in the requirement

$$\frac{p(p-1)}{2} \ll D(R_e)^{(2-p)/p} \tag{A9}$$

Therefore, the V_4^0 term controls the $\hat{\beta}$ dependence when the strength of scattering parameter, D(R sub s), is large. When p is 1 or 2, our argument breaks down. For $p=1$ the approximation still holds by another argument, while for $p=2$, there are no scintillattions.

In the second case, β' is small compared to $\delta k R_e s_0 \kappa / 2\bar{k}$, so that a Taylor expansion of the V_4^0 term yields the leading β' dependence

$$V_4^0 \sim k_1 k_3 \beta'^2 D_\mu''\left(\frac{\delta k}{2\bar{k}} R_e s_0 \kappa\right) \tag{A10}$$

This leads to the requirement

$$D_\mu''(R_e s_0 \kappa) \ll D_\mu''\left(\frac{\delta k}{2\bar{k}} R_e s_0 \kappa\right) \tag{A11}$$

which for a power-law structure function is equivalent to

$$1 \ll \left[\frac{\delta k}{2\bar{k}}\right]^{p-2} \tag{A12}$$

Since p is less than 2, this implies that δk is small compared to twice the mean of the wavenumbers.

Finally, in the third case, β' is about the same size as $\delta k R_e s_0 \kappa / 2\bar{k}$ so that

the requirement for neglecting the β' dependence of V_q^R becomes

$$\left[\frac{\delta k}{2\bar{k}} R_0 s_0 \kappa\right]^2 D_\mu'' \ll D_\mu\left(\frac{\delta k}{\bar{k}} R_0 s_0 \kappa\right) \tag{A13}$$

which, for a power-law structure function leads to

$$(\delta k / \bar{k})^{2-p} \ll \frac{4}{p(p-1)} \tag{A14}$$

and is easily satisfied for small wavenumber differences.

In all three case considered above, the combination of structure functions in V_q^0 dominate the β' dependence if $D(R_0 s_0)$ is large and $\delta k / 2\bar{k}$ is small.

V. ECLIPSE SHADOW BANDS

The following is an unfinished draft paper on eclipse shadow bands, by J. Codona.

The Scintillation Theory of Eclipse Shadow Bands

by

Johanan L. Codona *

Abstract. The results of a theoretical investigation of solar eclipse shadow bands are presented. The study provides both quantitative and qualitative insight into the factors governing the visibility of shadow bands. Without making use of auxiliary hypotheses such as solar limb darkening or turbulence enhancements caused by the passage of the lunar shadow, all of the salient features of the shadow bands are explained by standard scintillation theory. The contrast is found to be greater for shorter wavelengths and the band spacing to scale like the square-root of the wavelength very near totality. For times greater than about 10 seconds before (or after) totality the band spacing becomes frequency independent and the scintillations are dominated by turbulence near the ground. The turbulence mainly responsible for shadow bands is found to be below two kilometers in altitude. Turbulence at the tropopause is found to have no impact on shadow bands until 2-3 seconds from totality. Longer eclipses are expected to show bands with greater contrast and linearity. Intensity correlation scales are typically less than 10 cm within 30 seconds of totality. The scintillation theory predictions for shadow band structure, motion, and evolution are found to be in remarkable agreement with both visual and photoelectric observations.

1. Introduction.

In the minutes just preceding and just following totality during solar eclipses, faint shadowy patterns have sometimes been seen to appear projected on the ground [1]. These "shadow bands" are initially seen to be random and wavy, becoming more linear and aligned with the edge of the lunar shadow as totality approaches. At the same time the band spacing decreases and the

* La Jolla Institute
Center for Studies of Nonlinear Dynamics
8950 Villa La Jolla Drive Suite 2150
La Jolla, CA 92037
and
Interplanetary Scintillations Laboratory
Department of Electrical Engineering and Computer Science
C-014
University of California, San Diego
La Jolla, CA 92093

contrast increases. The bands appear to move in a drection perpendicular to their elongation [1]. Photoelectric studies have shown that the bands' contrast is greater at shorter wavelengths while, near totality, the typical width of the bands increases with wavelength [2]. The phenomena appear to reverse their general trends after totality with the exception of the band motion, which appears to be unrelated to the location of the lunar shadow.

It has long been suggested that shadow bands are most likely a scintillation phenomenon caused by the Earth's atmosphere [3]. However, details such as whether or not shadow bands will be seen and how well, the wavelength dependence of the bands, and the nature of the atmospheric irregularities have not been well understood. The wavelength dependence has been attributed to solar limb darkening [4] and the turbulence to possibly have been enhanced by the thermal effects of the moon's shadow [5]. In this paper it will be shown that all of the effects of shadow bands can be explained with standard scintillation theory, without the use of limb darkening or enhanced turbulence.

In the next section, the problem of a general, extended, incoherent light source at infinity illuminating a thin phase screen will be considered. A model for the two point intensity correlation will be found as well as the normalized intensity variance (the scintillation index). In section 3 the specific case of crescent source distributions will be presented. Section 4 will utilize the thin screen model to find the shadow bands' intensity variance and wavelength dependence. In section 5 the morphology and scales of the thin screen shadow bands will be discussed. The intensity fluctuations' dependence on time and wavelength will be calculated. In section 6 the theory will be generalized to consider extended atmospheric turbulence. The implications of the extended atmospheric turbulence model for the shadow bands' wavelength dependence, contrast, and structure will be shown. Section 7 will summarize the results of the theory and make comparisons to data.

2. The Phase Screen Model

The shadows on the ground can be described as a random intensity pattern, $I(\underline{\rho})$, at any given moment. Here, $\underline{\rho}$ is a position vector in the observation plane.

The intensity patterns result from temperature and density fluctuations in the atmosphere and change in a semi-random fashion as the irregularities evolve and are convected by the wind. We will treat the light as being essentially monochromatic. This will be a good approximation if the intensity is detected through narrow-band filters. A study of the two-point intensity correlation, $C_I(\vec{s}) = \langle I(\vec{x})I(\vec{x}+\vec{s})\rangle$, will lend a great deal of insight to the nature of the shadow bands. The angle brackets denote ensemble averaging over fluctuations in the atmosphere. The intensity correlation function allows us to discuss how the correlation scales vary in time as well as the variance in the intensity. The variance is $\langle (I-\langle I\rangle)^2\rangle = C_I(0) - C_I(\infty)$. The "scintillation index" is the normalized rms fluctuations in intensity, $m = \langle (I-\langle I\rangle)^2\rangle^{1/2} / \langle I\rangle$. Therefore,

$$m^2 = \frac{C_I(0) - C_I(\infty)}{C_I(\infty)} \tag{2.1}$$

In this section we derive $C_I(\vec{x})$ for a weakly scattering layer of turbulent atmosphere at height z (a thin "phase changing screen"). Below this layer the index of refraction is constant. Without loss of generality, the sun will be considered to be at the zenith (figure[]). The index of refraction fluctuations, $n(\vec{r})$, are assumed to arise from a turbulent process in the air. The "turbulence spectrum" is defined as

$$\Phi_n(\vec{q}) = \frac{1}{(2\pi)^3}\int_{-\infty}^{\infty} B_n(\vec{r})e^{-i\vec{q}\cdot\vec{r}}\,d^3r \tag{2.2}$$

where $\vec{q}$ is the three dimensional wave vector and the index of refraction autocovariance, $B_n(\vec{r}) = \langle n(\vec{r}_0)n(\vec{r}_0+\vec{r})\rangle$, is assumed to be homogeneous and isotropic within the turbulent region. For spatial frequencies important to scintillations, we can treat the turbulence spectrum as a power-law with spectral index α [6].

$$\Phi_n(\vec{q}) = 0.033C_n^2 q^{-\alpha} \tag{2.3}$$

where C_n^2 is the turbulence structure constant and $\alpha = 11/3$ for the case of Kolmogorov turbulence [6].

Propagation of light through the turbulent layer and to the ground can be treated as narrow angle forward scattering. In situations where the radiation is

scattered into a narrow cone about the incoming direction and the fluctuations in the index of refraction are much less than unity, the Helmholtz wave equation reduces to the "parabolic wave equation"

$$\frac{\partial E}{\partial z} = \frac{i}{2k}\nabla^2 E - ikn(\underline{x},z)E \tag{2.4}$$

where $\mathcal{E}=\mathrm{Re}\{Ee^{i(kz-\omega t)}\}$ is the scalar electric field, z is the coordinate in the direction of propagation, $\underline{x}$ is a vector perpendicular to the z axis, $k=2\pi/\lambda$ is the wavenumber, λ is the wavelength, and $\nabla^2=\partial^2/\partial x^2+\partial^2/\partial y^2$ is the transverse Laplacian [6]. In the region between the screen and the ground $n=0$. Setting $n=0$ in (2.4) and Fourier transforming with respect to $\underline{x}$ yields

$$\frac{\partial \tilde{E}}{\partial z} = -\frac{i\kappa^2}{2k}\tilde{E} \tag{2.5}$$

where

$$\tilde{E}(\underline{\kappa},z) = \frac{1}{(2\pi)^2}\int_{-\infty}^{\infty} E(\underline{x},z)e^{-i\underline{\kappa}\cdot\underline{x}}d^2x \tag{2.6a}$$

$$E(\underline{x},z) = \int_{-\infty}^{\infty} \tilde{E}(\underline{\kappa},z)e^{i\underline{\kappa}\cdot\underline{x}}d^2\kappa \tag{2.6b}$$

and $\underline{\kappa}$ is the two dimensional spatial frequency. Equation (2.5) implies

$$\tilde{E}(\underline{\kappa},z) = \exp\left\{-\frac{i\kappa^2 z}{2k}\right\}\tilde{E}(\underline{\kappa},0)$$

where $\tilde{E}(\underline{\kappa},0)$ is the Fourier transform of the field just under the turbulent layer ($z=0^+$). This allows us to write the field on the ground as

$$E(\underline{x},z) = \int_{-\infty}^{\infty} \tilde{E}(\underline{\kappa},0)\exp\left\{i\underline{\kappa}\cdot\underline{x}-\frac{i\kappa^2 z}{2k}\right\}d^2\kappa \tag{2.7}$$

Define $E_0(\underline{x})$ to be the field at $z=0^+$ which would result from a plane wave impinging on the phase screen along the z axis. Since the screen is assumed to be thin, a wave that is incident on the screen with an angle $\vec{\theta}$ to the z axis will result in a field at $z=0^+$ of $E_0(\underline{x})\exp(-ik\vec{\theta}\cdot\underline{x})$. Using equation (2.7) and the Fourier shift theorem we write the field on the ground resulting from a unit

amplitude plane wave incident from an angle $\vec{\vartheta}$ as

$$E(\vec{x},z;\vec{\vartheta}) = \int_{-\infty}^{\infty} \tilde{E}_0(\vec{\kappa} - k\vec{\vartheta}) \exp\left\{i\vec{\kappa}\cdot\vec{x} - \frac{i\kappa^2 z}{2k}\right\} d^2\kappa \tag{2.8}$$

The corresponding intensity pattern is

$$I(\vec{x},z;\vec{\vartheta}) = E(\vec{x},z;\vec{\vartheta})E^*(\vec{x},z;\vec{\vartheta})$$

where the asterisk (*) denotes complex conjugation. Using equation (2.8), this is written in integral form as

$$I(\vec{x},z;\vec{\vartheta}) = \int_{-\infty}^{\infty}\int \exp\left\{i\vec{x}\cdot(\vec{\kappa}_1 - \vec{\kappa}_2) - i\frac{z}{2k}(\kappa_1^2 - \kappa_2^2)\right\} \tag{2.9}$$

$$\tilde{E}_0(\vec{\kappa}_1 - k\vec{\vartheta})\tilde{E}_0(\vec{\kappa}_2 - k\vec{\vartheta})\, d^2\kappa_1\, d^2\kappa_2$$

If we illuminate the screen by an incoherent, extended source with a brightness distribution, $B(\vec{\vartheta})$, the intensity pattern becomes

$$I(\vec{x},z) = \int_{-\infty}^{\infty} B(\vec{\vartheta}) I(\vec{x},z;\vec{\vartheta})\, d^2\vartheta \tag{2.10}$$

Since $B(\vec{\vartheta})$ is zero beyond the edge of the source, the limits of integration can be written as infinite without any difficulty. An examination of equation (2.9) shows that

$$I(\vec{x},z;\vec{\vartheta}) = I(\vec{x} + z\vec{\vartheta},z;\vec{\vartheta} = 0) \equiv I_{pt}(\vec{x} + z\vec{\vartheta}) \tag{2.11}$$

where the subscript, pt, refers to a point brightness distribution at $\vec{\vartheta} = 0$. Equation (2.11) is valid as long as the angle $\vec{\vartheta}$ is small compared to a radian. Combining equations (2.10) and (2.11) we write

$$I(\vec{x}) = \int_{-\infty}^{\infty} B(\vec{\vartheta}) I_{pt}(\vec{x} + z\vec{\vartheta})\, d^2\vartheta \tag{2.12}$$

leading to the intensity correlation

$$C_I(\vec{s}) = \int_{-\infty}^{\infty}\int B(\vec{\vartheta}_1)B(\vec{\vartheta}_2)C_{pt}(\vec{s} - z(\vec{\vartheta}_1 - \vec{\vartheta}_2))\, d^2\vartheta_1\, d^2\vartheta_2 \tag{2.13}$$

where $C_{pt}(\vec{s}) = \langle I_{pt}(\vec{x})I_{pt}(\vec{x} + \vec{s})\rangle$ and translational invariance has been

assumed. Note that $C_I(\vec{s})$ need not be isotropic if $B(\vec{\vartheta})$ is anisotropic. This is why the scintillations of stars and planets are isotropic [7] but the shadow bands are not. The intensity spectrum is defined by

$$\Phi_I(\vec{\kappa}) = \frac{1}{(2\pi)^2}\int_{-\infty}^{\infty} C_I(\vec{s})\, e^{-i\vec{\kappa}\cdot\vec{s}}\, d^2s \tag{2.14}$$

Therefore, equation (2.13) leads to

$$\Phi_I(\vec{\kappa}) = (2\pi)^4 |\tilde{B}(z\vec{\kappa})|^2\, \Phi_{pt}(\vec{\kappa}) \tag{2.15}$$

where $\tilde{B}(z\vec{\kappa})$ is the Fourier transform of the brightness distribution with respect to $\vec{\vartheta}$ and $\Phi_{pt}(\vec{\kappa})$ is the Fourier transform of $C_{pt}(\vec{s})$. This is the Cohen-Salpeter formula for the intensity spectrum of an extended, incoherent source [8].

The intensity spectrum in equation (2.15) consists of two factors. There is the intensity spectrum of a point source, $\Phi_{pt}(\vec{\kappa})$, and the source function, $|\tilde{B}(z\vec{\kappa})|^2$, which smoothes the intensity fluctuations. Examination of an intensity spectrum will reveal a delta function at the origin due to the mean intensity. The remainder of the spectrum is the Fourier transform of the intensity autocovariance and is a consequence of the intensity fluctuations. Writing the fluctuations in intensity as $I' = I - \langle I \rangle$ we note that

$$\Phi_I(\vec{\kappa}) = \langle I \rangle^2 \delta(\vec{\kappa}) + \Phi_{I'}(\vec{\kappa}) \tag{2.16}$$

where $\delta(\vec{\kappa})$ is the two dimensional Dirac delta function and $\Phi_{I'}(\vec{\kappa})$ is the intensity fluctuation spectrum. Combining equations (2.1) and (2.16), the scintillation index becomes

$$m^2 = \frac{\int_{-\infty}^{\infty} \Phi_{I'}(\vec{\kappa})\, d^2\kappa}{\langle I \rangle^2} \tag{2.17}$$

From equations (2.15) and (2.17) we can see why the scintillation strength varies with source size. A brightness distribution with a characteristic width ϑ_0 will have a Fourier transform with a characteristic width of order $2\pi/\vartheta_0$. Therefore, the brightness distribution acts as a low-pass filter in κ with a cutoff around $2\pi/(z\vartheta_0)$. As we increase the size of the source, ϑ_0, we decrease the cutoff

frequency in Φ_I. This diminishes the integral in equation (2.17) leading to a decrease in the scintillation index, m^2. This is the reason that stars twinkle so much more than planets. The situation for shadow bands is complicated by the fact that the brightness distribution for a solar crescent is so asymmetrical. In such a case, the filtering becomes a function of direction. This will be discussed in detail in the following sections.

In addition to the effect of the source on the scintillations, we must also consider the point source intensity spectrum, $\Phi_{pt}(\vec{\kappa})$. This function describes how a star would scintillate under the same conditions. To discuss this function, it is necessary to look at the fourth moment of the electric field. This approach is necessary because there is no completely correct propagation equation for the intensity correlation function. The fourth moment is defined

$$\Gamma(\vec{\rho}_1,\vec{\rho}_2,\vec{\rho}_3,\vec{\rho}_4,z) = \langle E(\vec{\rho}_1)E^*(\vec{\rho}_2)E(\vec{\rho}_3)E^*(\vec{\rho}_4)\rangle$$

where the $E(\vec{\rho}_n)$ factors are the electric field at the points $\vec{\rho}_n$ resulting from a plane wave impinging perpendicularly on the screen. The intensity correlation, $C_{pt}(\vec{s})$, is found from the fourth moment as

$$C_{pt}(\vec{s}) = \Gamma(\vec{\rho},\vec{\rho},\vec{\rho}+\vec{s},\vec{\rho}+\vec{s}) \quad (2.18)$$

The parabolic wave equation, equation (2.4), can be used to derive a propagation equation for the fourth moment, Γ [6]. In the region below the screen, where $n = 0$, this equation is

$$\frac{\partial \Gamma}{\partial z} = \frac{i}{2k}(\nabla_1^2 - \nabla_2^2 + \nabla_3^2 - \nabla_4^2)\Gamma(\vec{\rho}_1,\vec{\rho}_2,\vec{\rho}_3,\vec{\rho}_4,z) \quad (2.19)$$

where ∇_n^2 is the transverse Laplacian with respect to $\vec{\rho}_n$. Following Rumsey [9], we change variables to $\vec{\alpha}$, $\vec{\beta}$, $\vec{\gamma}$, and $\vec{\delta}$ according to the transformation

$$\begin{bmatrix}\vec{\alpha}\\ \vec{\beta}\\ \vec{\gamma}\\ \vec{\delta}\end{bmatrix} = \frac{1}{2}\begin{bmatrix}1 & 1 & 1 & 1\\ 1 & 1 & -1 & -1\\ 1 & -1 & -1 & 1\\ 1 & -1 & 1 & -1\end{bmatrix}\begin{bmatrix}\vec{\rho}_1\\ \vec{\rho}_2\\ \vec{\rho}_3\\ \vec{\rho}_4\end{bmatrix} \quad (2.20)$$

Since both the medium's statistical properties and the geometry of the problem are invariant under translations in $\vec{\rho}$, we can assume that Γ will be independent

of $\vec{\alpha}$. Thus, equation (2.19) becomes

$$\frac{\partial W}{\partial z} = \frac{i}{k}\nabla_\beta \cdot \nabla_\gamma W(\vec{\beta},\vec{\gamma},z) \tag{2.21}$$

where we have set $\vec{\alpha} = \vec{\delta} = 0$ without any loss of generality. This leaves the four points in a parallelogram with sides $\vec{\beta}$ and $\vec{\gamma}$. The intensity correlation will be found by setting $\vec{\gamma} = 0$. For convenience, a superscript $\vec{\beta}$ or $\vec{\gamma}$ will denote a Fourier transform with respect to that variable. The corresponding spatial frequency variable will be written as a subscripted $\vec{\kappa}$. Transforming equation (2.21) we get

$$\frac{\partial W^{\beta\gamma}}{\partial z} = -\frac{i}{k}\vec{\kappa}_\beta \cdot \vec{\kappa}_\gamma W^{\beta\gamma}$$

This implies that

$$W^{\beta\gamma}(\vec{\kappa}_\beta,\vec{\kappa}_\gamma,z) = \exp\left\{-\frac{iz}{k}\vec{\kappa}_\beta \cdot \vec{\kappa}_\gamma\right\} W^{\beta\gamma}(\vec{\kappa}_\beta,\vec{\kappa}_\gamma,z=0^+)$$

Inverse Fourier transforming with respect to $\vec{\kappa}_\gamma$, we find

$$W^{\beta}(\vec{\kappa},\vec{\gamma},z) = W_0^{\beta}(\vec{\kappa},\vec{\gamma}-\frac{\vec{\kappa}z}{k}) \tag{2.22}$$

where we have dropped the β subscript on $\vec{\kappa}$ and the subscript 0 on W refers to $z = 0^+$.

To find W_0, we assume that the screen contributes a random phase shift, $\varphi(\vec{\rho}) = -k\int_{-l}^{0} n(\vec{\rho},z)dz$, at the point $\vec{\rho}$ where l is the thickness of the screen. Since we are illuminating the screen with a normally incident plane wave, the electric field at $z = 0^+$ would be unity in the absence of the screen. With the screen, the field is $\exp[i\varphi(\vec{\rho})]$. Therefore, a realization for W_0 is $\exp[i(\varphi(\vec{\rho}_1) - \varphi(\vec{\rho}_2) + \varphi(\vec{\rho}_3) - \varphi(\vec{\rho}_4))]$. Assuming $\varphi(\vec{\rho})$ to be a zero mean Gaussian random variable, we write

$$W_0(\vec{\rho}_1,\vec{\rho}_2,\vec{\rho}_3,\vec{\rho}_4) = \exp\left[-\frac{1}{2}[D_{12} + D_{34} + D_{14} + D_{23} - D_{13} - D_{24}]\right] \tag{2.23}$$

where $D_{ij} = \langle(\varphi(\vec{\rho}_i) - \varphi(\vec{\rho}_j))^2\rangle$ is the phase structure function of the screen [6].

Changing variables in equation (2.23) according to equation (2.20) with $\vec{\alpha} = \vec{\delta} = 0$, we get

$$W_0(\vec{\beta},\vec{\gamma}) = \exp\left[- D(\vec{\beta}) - D(\vec{\gamma}) + \tfrac{1}{2}(D(\vec{\beta}+\vec{\gamma}) + D(\vec{\beta}-\vec{\gamma}))\right] \qquad (2.24)$$

Examination of the exponent in equation (2.24) shows that it is bounded between $-D(\vec{\gamma})$ and 0. In weak scattering, the exponential of the structure functions that depend on $\vec{\beta}$ in equation (2.24) can be Taylor expanded to give

$$W_0(\vec{\beta},\vec{\gamma}) \approx e^{-D(\vec{\gamma})}[1 - D(\vec{\beta}) + \tfrac{1}{2}(D(\vec{\beta}+\vec{\gamma}) + D(\vec{\beta}-\vec{\gamma})) + \cdots]$$

The $\exp[-D(\vec{\gamma})]$ factor may be ignored in weak scattering. Assuming that the screen is thicker than several index of refraction correlation scales, we write the phase structure function as

$$D(\vec{s}) = 4\pi k^2 l \int_{-\infty}^{\infty} \Phi_n(\vec{\kappa}, q_z = 0)[1 - e^{i\vec{\kappa}\cdot\vec{s}}]d^2\kappa \qquad (2.25)$$

where q_z is the vertical component of the wave vector $\vec{q}$. Substituting equation (2.25) in the expansion above, we find after some manipulation that

$$W_\delta(\vec{\kappa},\vec{\gamma}) = \delta(\vec{\kappa}) + 8\pi k^2 l \sin^2\left(\frac{\vec{\kappa}\cdot\vec{\gamma}}{2}\right)\Phi_n(\vec{\kappa})$$

Combining this result with equations (2.22) and (2.18) we see that

$$\Phi_{pt}(\vec{\kappa}) = \delta(\vec{\kappa}) + 8\pi k^2 l \sin^2\left(\frac{z\kappa^2}{2k}\right)\Phi_n(\vec{\kappa}) \qquad (2.26)$$

This is the weak scattering approximation to the intensity spectrum for a point source. The $\sin^2(z\kappa^2/2k)$ factor is called the "Fresnel filter." The general intensity spectrum is found by combining equations (2.26) and (2.15) to give

$$\Phi_I(\vec{\kappa}) = I_{total}^2\delta(\vec{\kappa}) + (2\pi)^4 8\pi k^2 l\, |\tilde{B}(z\vec{\kappa})|^2 \sin^2\left(\frac{z\kappa^2}{2k}\right)\Phi_n(\vec{\kappa}) \qquad (2.27)$$

where we have made use of the fact that $(2\pi)^2\tilde{B}(0) = I_{total}$, the total intensity of the extended source. The intensity fluctuation spectrum is the second term in (2.27).

We can now write down the intensity correlation on the ground and the scintillation index. From equations (2.27) and (2.16) we make the identification

$$\langle I \rangle = \int_{-\infty}^{\infty} B(\vec{\vartheta}) d^2\vartheta \equiv I_{total}$$

Therefore the intensity correlation is

$$C_I(\vec{s}) = I_{total}^2 + (2\pi)^4 8\pi k^2 l \int_{-\infty}^{\infty} e^{-i\vec{\kappa}\cdot\vec{s}} |\vec{B}'(z\vec{\kappa})|^2 \sin^2\left[\frac{z\kappa^2}{2k}\right] \Phi_n(\vec{\kappa}) d^2\kappa \qquad (2.28)$$

and the scintillation index is

$$m^2 = 8\pi k^2 l \int_{-\infty}^{\infty} \frac{|\vec{B}'(z\vec{\kappa})|^2}{|\vec{B}'(0)|^2} \sin^2\left[\frac{z\kappa^2}{2k}\right] \Phi_n(\vec{\kappa}) d^2\kappa \qquad (2.29)$$

Equations (2.28) and (2.29) are valid for essentially any broad source seen through a thin turbulent layer. The crescent source distribution is what makes the special case of shadow bands so unique. We look at this next.

3. Crescent Source Distributions.

The very thin solar crescent is what makes the common scintillation effects in shadow bands so remarkable. Its sheer brilliance sets it apart from other scintillating objects in that it may be observed by backscattering off the ground. The crescent also changes its shape and size rapidly as totality nears. The manner and rate at which this evolution takes place is governed by the relative sizes of the sun and moon, which change from one eclipse to the next. The crescent may even change its complete nature, as in annular eclipses, from a crescent to a ring. During some total eclipses, the moon may be very nearly the same apparent diameter as the sun. On other occasions, the moon may appear considerably larger than the sun. So that we may study the relationships between shadow bands with different eclipse geometries, we need to define some characterizing parameters. Let the angular radii of the sun and moon be R_S and R_M, respectively. Even though both of these radii may change from eclipse to eclipse, it is their ratio which defines the nature of the eclipse and has the greatest effect on shadow bands. Therefore, we define an 'eclipse parameter', ε,

as

$$\varepsilon = \frac{R_M - R_S}{R_S} = \frac{t_{III} - t_{II}}{t_{II} - t_I} \tag{3.1}$$

where the subscripted t is the time at the appropriate contact. The parameter ε is positive for total eclipses and negative for annular eclipses. A total eclipse where Baily's beads are prominent and seen over a large arc of the crescent will have an ε very near zero. A long total eclipse will have a larger value of ε. Another important parameter is the time away from totality. Define the angular velocity of the moon relative to the sun as Ω. The normalized time away from totality is defined

$$\tau = \frac{\Omega|t - t_{contact}|}{R_S} \tag{3.2}$$

where $t_{contact}$ is the time of either second or third contact, depending on whether we are in the waxing or waning phases of the eclipse. At both first and fourth contact, τ has a value of two. At second or third contact, τ is zero. As a benchmark number, we will use 60 minutes for the interval $t_{II} - t_I$. This gives approximate formulae for τ and ε as

$$\varepsilon \approx \frac{\text{duration of totality in minutes}}{60}$$

$$\tau \approx \frac{\text{time away from totality in minutes}}{30}$$

This gives typical values for ε as 0 to 0.12 for total eclipses. Shadow bands are usually seen for times less than two minutes away from totality. Therefore, the values of τ that we are interested in lie in the range 0 to about 0.1 .

A set of solar crescents is shown in figure 1. The most striking difference between eclipses with different values of ε are extent of the crescent's horns. Treating the moon and sun as circles whose centers are separated by an angle $R_S(\varepsilon + \tau)$ we write the horn angles from the center of the moon and the sun as

$$\begin{aligned} \cos(\varphi_M) &= \frac{(1+\varepsilon)^2 + (\varepsilon+\tau)^2 - 1}{2(\varepsilon+\tau)(1+\varepsilon)} \\ \cos(\varphi_S) &= \frac{(1+\varepsilon)^2 - (\varepsilon+\tau)^2 - 1}{2(\varepsilon+\tau)} \end{aligned} \tag{3.3}$$

These angles are shown in figure 2. Figure 3 shows the evolution of the solar horn angle, φ_S, with τ for various values of epsilon. Eclipses with smaller values of ε tend to keep their horns up to the last moments before totality while eclipses with larger values of epsilon lose their horns rapidly and display a lengthy "Diamond Ring" effect. Smaller crescent horn angles mean that the solar crescent is forming a better "slit." Thus, we might expect that eclipses with larger values of ε would make crisper shadow bands. This is true, but the horn angle will affect the observed structure of the bands more profoundly than the contrast. The other point that we need to consider is the mean intensity of the crescent. Relative to the sun's full disk intensity we write the cresent's intensity as

$$\frac{I_{total}(\varepsilon,\tau)}{\pi R_S^2 B_0} = \frac{1}{2\pi}(2\varphi_S - \sin(2\varphi_S)) - \frac{1}{2\pi}(2\varphi_M - \sin(2\varphi_M)) \qquad (3.4)$$

This normalized intensity is shown in figure 4. The larger horns in small ε eclipses keep the intensity up much higher than in eclipses with a larger value of ε.

The center of the crescent lies along the line between the apparent centers of the sun and moon. Therefore, if an observer is not on the center of the path of totality, the crescent's orientation will be a function of time. This effect is illustrated in figure 5. If the observer is not on the center-line, while ε is unchanged, τ will become a more complicated function of time than given in (3.2).

$$\tau = \begin{cases} (\tau_0^2 + 2\varepsilon\tau_0\sqrt{1-\rho^2} + \varepsilon^2)^{1/2} - \varepsilon & 0 \le \rho \le 1 \\ (\tau_0^2 + \rho^2\varepsilon^2)^{1/2} - \varepsilon & \rho > 1 \end{cases} \qquad (3.5)$$

where τ_0 is the value of τ that would be found by using (3.2) and ρ is a normalized "impact parameter" showing the observer's fractional distance from the center of the path of totality toward the edge. If $\rho>1$ the observer will not experience totality at all. In that case, τ_0 is calculated using (3.2) with $t_{contact}$ replaced with the time of greatest partial phase. Note that for $\rho>1$, τ never goes to zero (figure 6).

4. Shadow Band Intensity Variance Due to a Phase Screen.

Calculation of the intensity spectrum requires knowledge of the crescent's angular power spectrum, $|\tilde{B}(z\hat{\ell})|^2$. This is very difficult to calculate exactly. Fortunately, we can make two good approximations to $|\tilde{B}(z\hat{\ell})|^2$: one that is valid for large values of $z\hat{\ell}$ and one that is good for small values of $z\hat{\ell}$. Ignoring the effects of solar limb darkening, we can write the brightness distribution as

$$B(\vec{\vartheta}) = \begin{cases} B_0 & \text{if } \vec{\vartheta} \text{ is inside the crescent} \\ 0 & \text{otherwise} \end{cases}$$

The corresponding source spectrum is

$$\tilde{B}(z\hat{\ell}) = \frac{1}{(2\pi)^2}\int_{-\infty}^{\infty} B(\vec{\vartheta})e^{-iz\hat{\ell}\cdot\vec{\vartheta}}d^2\vartheta = \frac{B_0}{(2\pi)^2}\int_C e^{-iz\hat{\ell}\cdot\vec{\vartheta}}d^2\vartheta$$

where C denotes that the region of integration is over the crescent. Using a two dimensional form of the divergence theorem we arrive at

$$\tilde{B}(z\hat{\ell}) = \frac{iB_0}{(2\pi)^2 z\kappa^2}\int_{\partial C}\hat{n}(\vec{\vartheta})\cdot\hat{\ell}e^{-iz\hat{\ell}\cdot\vec{\vartheta}}d\vartheta \qquad (4.1)$$

where ∂C denotes the boundary of the crescent, $\hat{n}(\vec{\vartheta})$ is the unit outward-facing normal, and $d\vartheta$ is the differential angular path length along the edge of the crescent. Equation (4.1) lends itself to asymptotic analysis as $z\kappa R_S$ becomes large. Using the method of stationary phase and the fact that $\varepsilon^2 \ll 1$ we can write

$$|\tilde{B}(z\hat{\ell})|^2 \sim \frac{8\pi B_0^2 R_S^4(1+\varepsilon)^{1/2}}{(2\pi)^4(z\kappa R_S)^3}\sin^2\left[\frac{z\kappa R_S}{2}(\varepsilon - (\varepsilon+\tau)\cos(\psi))\right] \qquad (4.2)$$

$$\text{for } z\kappa R_S \gg 1 \text{ and } |\psi| < \varphi_M$$

where ψ is the angle between $\hat{\ell}$ and the axis perpendicular to the crescent (figure 2). For $\psi > \varphi_S$, $|\tilde{B}(z\hat{\ell})|^2$ is essentially zero. The region $\varphi_S < \psi < \varphi_M$ has a different asymptotic behavior but may be neglected in practice. When we use (4.2) in (2.29) to get the scintillation index, we will be integrating over ψ. If $\varphi_S < \frac{\pi}{2}$, the result of this integration is given asymptotically as

$$\int_0^{2\pi} |\tilde{B}(z\hat{\ell})|^2 d\psi \sim \frac{16\pi B_0^2 R_S^4(1+\varepsilon)^{1/2}}{(2\pi)^4(z\kappa R_S)^3}\left|\varphi_S - \frac{\cos(z\kappa R_S\tau + \frac{\pi}{4})}{(\frac{2}{\pi}z\kappa R_S(\varepsilon+\tau))^{1/2}}\right| \qquad (4.3)$$

for $z\kappa R_S \gg 1$. An approximate form for for the crescent's power spectrum along the $\psi = 0$ axis is given by

$$
\begin{aligned}
|\vec{B}(z\vec{\kappa})|^2 &\approx \frac{I_{total}^2(\varepsilon,\tau)}{(2\pi)^4}\exp\left\{a_3\left(\exp\left\{\frac{-a_2u^2 + a_1u}{a_3}\right\} - 1\right) - a_1u\right\} \\
u &= z\kappa R_S\tau \\
a_1 &= 0.9 \\
a_2 &= \exp(.027\ln^2(\varepsilon+\tau) - 1.78\ln(\varepsilon+\tau) - 2.63) \\
a_3 &= 3\exp(-11.0(\varepsilon+\tau))
\end{aligned}
\tag{4.4}
$$

Equation (4.4) is the result of numerical curve fitting and is good for $z\kappa R_S\tau$ between zero and about 3 or 4. Numerical calculations show that (4.2) and (4.4) form an approximation that is good for the entire range of κ for $\psi = 0$ (figure 7). The ψ integration will be approximated by multiplying (4.4) by the factor $4\varphi_S$.

We now have all of the information necessary to find the scintillation index due to a thin screen. We need only to pick the wavelength, λ, the distance to the screen, z, the strength of turbulence, C_n^2, and the parameters ε and τ. To see which altitudes are most efficient at generating intensity fluctuations, we define a "scintillation efficiency"

$$\eta_{m^2}(z,\lambda,\varepsilon,\tau) \equiv \frac{m^2}{lC_n^2}. \tag{4.5}$$

where m^2 is the result of integrating (2.29). Larger values of η_{m^2} imply that more intensity variance will be generated for a given level of turbulence. Figure 8 shows η_{m^2} vs. z for different values of λ, ε, and τ. At larger values of z, the source spectrum limits the integral in (2.29). This "source averaging" reduces the scintillations by smearing the pattern on the ground. When the source width is much broader than $\sqrt{\lambda/z}$, the sine-squared factor may be approximated as $(z\kappa^2/2k)^2$. This provides a factor which cancels the k^2 in front of the integral. Therefore, when the turbulence is sufficiently distant from the observer or the source sufficiently broad, the scintillations will not have a wavelength dependence. At lower altitudes, when the source does not provide a cutoff, the intensity variance will be greater for shorter wavelengths. This is because the Fresnel frequency is proportional to $\sqrt{\lambda}$ and the Fresnel filter gives a larger contribution to (2.29) for shorter wavelengths. The transition altitude between wavelength

dependent and wavelength independent scintillations depends on the width of the crescent and is proportional to λ/τ^2. The eclipse parameter, ε, also has an effect on the scintillation efficiency. While not as important as source averaging, a smaller value of ε will degrade the scintillation efficiency at all altitudes. For two eclipses with identical viewing situations and weather, an eclipse with $\varepsilon = .01$ will have rms intensity fluctuations that are 20% less than an eclipse with $\varepsilon = .10$. Because shadow bands are usually near the limit of the eye's ability to detect contrast and eclipses with smaller values of ε are brighter, the ε dependence could mean the difference between whether the bands are seen or not.

The scintillation efficiency of a star is never limited by its source distribution. It is given by

$$\eta_{m^2,*} = 2.2k^{7/6}z^{5/6}$$

which increases monotonically with z. It is because distant turbulence is more effective than nearby turbulence that stellar scintillations are commonly said to arise in the tropopause at an altitude of 10 - 12 km. However, lower altitude turbulence, which is more responsible for the related phenomenon of "seeing," can contribute substantially to a star's scintillations. Young [7] noted that planetary scintillation intensity spectra could not be well modeled by considering only a thin screen at the tropopause. A finite diameter source may be more sensitive to high level or low level turbulence or both depending on the scintillation efficiency profile. Shadow bands are unique in that their scintillation efficiency evolves rapidly and dramatically with time. For larger values of τ, shadow bands are more sensitive to turbulence near the ground. As totality nears, turbulence at higher altitudes begins to play a more important role. This will change the shadow bands' wavelength dependence as well as their morphology as time progresses. This behavior is included with a model for the distributed atmospheric turbulence in section 6.

5. Phase Screen Shadow Band Structure.

Features of shadow bands such as their orientation, spacing, motion, and linearity are all able to be discussed in terms of the spatial intensity fluctuation

spectrum (2.27). This spectrum is an ensemble average of the instantaneous spatial spectra and is ergodically related to a spatial average, *not* a temporal average. Since the spectrum evolves very rapidly near totality, temporal statistics are at best confused and at worst meaningless. However, the evolving morphology of the bands may be understood as snap-shot realizations of the spatial spectrum calculated for the appropriate time. The simplest such insight is the orientation of the bands with time. As mentioned in section 3, the crescent's orientation is a function of time if the observer is not on the center of the path of totality. The source power spectrum, $|\tilde{B}'(z\hat{\xi})|^2$, rotates with the source. Therefore, since $|\tilde{B}'(z\hat{\xi})|^2$ is the only source of anisotropy in $\Phi_I(\hat{\xi})$, the shadow bands will rotate with the source. A possible caveat is when there is some anisotropy in the turbulence spectrum not included in the standard Kolmogorov turbulence model. Such an anisotropy might be due to atmospheric gravity waves propagating through the background turbulence. Although the medium's anisotropy is a possibility, it is unlikely to be an important effect.

In our phase screen model, moving the screen perpendicular to the line of sight *moves* the intensity pattern with it. Therefore, wind convecting the turbulent eddys through the atmosphere shift the pattern on the ground. This idea is complicated by the fact that the turbulent eddys are themselves rearranging in time and that the atmosphere is not a phase screen. Both of these effects will reduce the correlation between two intensity detectors on the ground. When the pattern has a large axial ratio, only the wind velocity component perpendicular to the bands will be evident in the observed motion. If the wind is parallel with the bands, they may be very difficult to see even if the intensity fluctuations are relatively strong. Under such circumstances, the dominant effect would be due to turbulent rearrangement. This would lead to a "shimmering" effect that might not catch the eye as well as moving bands. Combining this effect with the changing orientation of the crescent could explain why shadow bands are sometimes seen on one side of totality but not the other. Annular eclipses and eclipses with small values of ε have much less of an anisotropy in $|\tilde{B}'(z\hat{\xi})|^2$. In these cases the wind has a much higher probability of blowing in a direction parallel to the crescent. This is one of the reasons why small ε eclipses are not likely to generate profound shadow band events.

The characteristic length scale parallel to the bands is roughly $L_{parallel} \approx z R_S \sin(\varphi_S)$. The characteristic length scale perpendicular to the bands is not as straightforward to calculate. The intensity spectrum perpendicular to the crescent for a screen at a given altitude has three characteristic scales (figure 9). The largest scale is

$$L_{peak} \approx 2\pi z R_S \tau \sqrt{6\alpha_2(\varepsilon,\tau)} \tag{5.1}$$

which corresponds to the low frequency peak in the spectrum. The parameter $\alpha_2(\varepsilon,\tau)$ is given in eqn. (4.4). The next scale is where the source spectrum's asymptotic form has its first null.

$$L_{source} = z R_S \tau \tag{5.2}$$

The third scale is the length corresponding to the first non-trivial zero of the Fresnel filter.

$$L_{Fresnel} = \sqrt{\lambda z} \tag{5.3}$$

Which of the above lengths will be the dominant shadow band scale will depend on the distance of the screen from the observer and the time to totality, τ. The eye's response to moving intensity patterns is a strong function of the pattern's observed angular velocity [10]. Visual sensitivity also drops off precipitously at both low and high spatial frequencies. For common shadow band contrast levels of 2 to 3% the lowest visible frequency differs from the highest by less than a factor of 50, bandwidth decreasing with increasing pattern speed. This implies that if an observer can see scales on the order of a few centimeters, scales larger than 1 to 2 meters would be invisible. Therefore, even though there is a great deal more variance at L_{peak} than in the vicinity of L_{source} or $L_{Fresnel}$, these scales will be much more visible. The only exception is when the screen is very near the observer, say 100 meters or less. In such a case the Fresnel filter and the source spectrum combine to form a high-pass spatial filter in one direction. This will cause an effect similar to a crude Schlieren camera about the mean intensity. The effect would be to create intensity fluctuations on the ground that are like refractive "shadows" of the turbulent irregularities. These patterns would appear more like "smoky wisps" than shadow bands. The broad source in

the direction parallel to the crescent will limit the refractive resolution of the irregularities to $L_{parallel}$. Thus the "smoky wisps" would have a characteristic width L_{peak} and a longitudinal scale of roughly $L_{parallel}$. At longitudinal distances greater than $L_{parallel}$ the pattern would appear to lose linearity and wander randomly. When the screen is 1000 meters or more away from the observer, the fluctuations with scale L_{peak} will be too large to see until very near totality. The scales of interest are now L_{source} and $L_{Fresnel}$. Two minutes away from totality, a screen at 1000 meters will have a value of L_{source} of about 30 cm. As totality nears, L_{source} will decrease linearly with τ. A screen at 1000 meters will have a Fresnel length scale of about 2.5 cm. As L_{source} drops toward $L_{Fresnel}$ the power in the intensity spectrum will increase in the vicinity of $L_{Fresnel}$. When this occurs, the pattern will develop structures with a characteristic scale $L_{Fresnel}$. When L_{source} is smaller than $L_{Fresnel}$ the larger scale will remain dominant. Whenever structures at the Fresnel scale are visible, the spacing will be wavelength dependent since $L_{Fresnel} \propto \sqrt{\lambda}$. Also, the intensity variance in the structure will be greater with smaller wavelength. From the time when $L_{source} = L_{Fresnel}$ to totality, the pattern will remain wavelength dependent with scale $L_{Fresnel}$ and the contrast will continue to increase. In the last few moments before totality, L_{peak} will drop into the visible range and provide some larger scale contrast patterns superimposed on the smaller, wavelength dependent shadow bands. A screen at an altitude of 10 km would have the same behavior as given above except for the fact that source averaging will keep the pattern's contrast low until relatively near totality. For a high altitude screen, it is only within a few seconds of totality that sufficient scintillation power is present to make the patterns visible.

How well the shadow bands display frequency dependent structures depends on ε. While the asymptotic form of $|\tilde{B}(z\hat{x})|^2$ depends only weakly on ε, the total intensity, I_{total}, depends strongly on ε. Since I_{total} is much larger for small ε eclipses, the *relative contrast* in the asymptotic region will be smaller. This means that eclipses with larger values of ε will be better at making the narrow, high axial-ratio patterns usually associated with shadow bands. Nevertheless, small ε eclipses would still display the features associated with L_{peak}. Since L_{peak} effects are only visible when the screen is close to the observer, we expect that small ε eclipses or annular eclipses will predominantly display the random,

smoky patterns caused by low level Schlieren effects.

The last point to consider is how an intensity detector's time series is related to what we have calculated. Unfortunately, shadow band time series are very complicated and require a great deal of information in order to analyze. The simplest approach is to assume that the turbulence is "frozen" and does not rearrange as the wind moves it past (Taylor's hypothesis). As such, the intensity pattern moves at a velocity equal to the wind component perpendicular to the line of sight. For the moment, we will ignore the fact that the source is changing rapidly in time. The wind velocity vector perpendicular to the line of sight is $\vec{v}$. Using Taylor's hypothesis we see that

$$I(\vec{x},t_0) = I(\vec{x}-\vec{v}t,t_0+t)$$

which leads us to the temporal intensity correlation as

$$C_{I,temporal}(t) = C_I(\vec{v}t) \tag{5.4}$$

Transforming (5.4) with respect to t to find the temporal intensity power spectrum we see that

$$\Phi_{I,temporal}(f) = \frac{2\pi}{v}\int_{-\infty}^{\infty}\Phi_I(\kappa_\perp,\kappa_\parallel=\frac{2\pi f}{v})d\kappa_\perp \tag{5.5}$$

where $\kappa_\parallel$ and $\kappa_\perp$ are the components of $\vec{\kappa}$ parallel and perpendicular to the wind vector, $\vec{v}$, and f is the temporal frequency in cycles per second. We may include the effect of the finite detector aperture by multiplying the right hand side of eqn. (2.27) by $(2\pi)^4|\tilde{A}(\vec{\kappa})|^2$ where $\tilde{A}(\vec{\kappa})$ is the Fourier transform of the detector's aperture distribution. The difficulty in the analysis comes from the fact that the wind vector typically lies along some direction other than the perpendicular to the crescent. This leads to a rather complicated integral. The "strip integration" in (5.5) washes out most of the oscillatory structure in the source spectrum and the Fresnel filter allowing us to find approximate scaling laws for eqn. (5.5) when the wind is perpendicular to the shadow bands. For temporal frequencies greater than $v/L_{aperture}$, where $L_{aperture}$ is the size of the detector aperture, there is essentially no power. If $v/L_{Fresnel} \ll f \ll v/L_{aperture}$ and the apparent wind is at angle less than $\frac{\pi}{2}-\varphi_s$ to the $\psi=0$ axis, the temporal intensity

spectrum will scale approximately as $f^{-17/3}$. In the frequency range $v/L_{source} \ll f \ll v/L_{Fresnel}$ the scaling will be roughly $f^{-8/3}$. For $v/L_{peak} \ll f \ll v/L_{source}$ or when $L_{Fresnel} > L_{source}$, the spectrum will depend strongly on the details of the source spectrum and the wind direction. For very low temporal frequencies, $f \ll v/L_{peak}$, the spectral power will scale approximately as $f^{4/3}$. If the apparent wind is at an angle greater than $\frac{\pi}{2} - \varphi_s$ the lower temporal frequencies are greatly enhanced. For this case, the analysis of the temporal spectrum's shape would require detailed numerical calculations specific to the observation geometry and the wind direction.

The inherent difficulties in shadow band time series analysis are compounded by the dynamic character of the source distribution. Estimates of the temporal intensity spectrum must be done on time series whose length is sufficiently short that the source distribution may be considered unchanging. From this perspective it may be preferred to examine time series taken relatively far from totality. Unfortunately, this does not permit making use of the stronger fluctuations near totality. The other option would be to use shorter time series. However, this approach would lead to prohibitive spectral estimation error unless the wind speed was quite high. These problems are particularly difficult if we try to observe the low-frequency spectral behavior for $f \ll v/L_{peak}$.

6. The Effects of Extended Atmospheric Turbulence.

Atmospheric turbulence is not confined to a thin layer. It is present everywhere from the ground to tens of kilometers in altitude. The models described in the previous sections need to be modified to take this into account. As long as the scattering is weak, the intensity fluctuation spectrum is the linear superposition of the thin screen results. It is given by

$$\Phi_I(\vec{\kappa}) = (2\pi)^4 8\pi k^2 \int_0^{\infty} \Phi_n(\vec{\kappa};z)\,|\vec{B}(z\vec{\kappa})|^2 \sin^2\left(\frac{z\kappa^2}{2k}\right) dz$$

where $\Phi_n(\vec{\kappa};z)$ is the turbulence spectrum at a distance z from the observer. If the sun is *not* at the zenith, the altitude is given by $z\cos(\zeta)$ where ζ is the sun's

zenith angle. The resulting formula for the intensity spectrum becomes

$$\Phi_I(\vec{\kappa}) = I_{total}^2 \delta(\vec{\kappa}) + (2\pi)^3(0.132)\kappa^{-\alpha}\int_0^\infty |B(z\vec{\kappa})|^2 C_n^2(z\cos(\zeta))\sin^2\left(\frac{z\kappa^2}{2k}\right)dz \qquad (6.1)$$

where $C_n^2(h)$ is the turbulence structure constant at altitude h. Combining eqs. (6.1), (4.5), and (2.17) gives the total scintillation index as

$$m^2(\lambda,\varepsilon,\tau,\zeta) = \int_0^\infty C_n^2(z\cos(\zeta))\eta_{m^2}(z,\lambda,\varepsilon,\tau)dz \qquad (6.2)$$

The integrand in (6.2) shows the relative importance of each distance to the total intensity fluctuation spectrum. Given the turbulence strength profile, $C_n^2(h)$, we can see which altitudes are contributing most to the shadow bands. $C_n^2(h)$ is known to vary with time of day, season, geographical position, humidity, wind speed, and surface texture [11]. For our purposes, we will use a combination of models to generate a generic turbulence profile. Our profile will be a form of the Hufnagel model [12], modified to account for the strong turbulence at low altitudes, given by

$$C_n^2(h) \cong C_n^2(1)h^{-4/3}e^{-h/1000} + (2.7\times10^{-16})e^{-h/1500} \qquad (6.3)$$

$$+ (8.1\times10^{-16})\langle v^2\rangle\left[\frac{h}{10000}\right]^{10}e^{-h/1000}$$

where h is the altitude in meters, $C_n^2(1)$ is the turbulence structure constant at 1 meter, and $\langle v^2\rangle$ is the mean-square wind speed at high altitudes. For the calculations that follow, we assume "typical" values for the constants in (6.3): $C_n^2(1) \approx 6\times10^{-13}m^{-2/3}$ and $\langle v^2\rangle \approx 850m^2/s^2$. The resulting turbulence profile is shown in figure 10. The peak at 10000 m is the enhanced turbulence at the tropopause. The resulting contribution to the total scintillation index for various altitudes is shown in figure 11. Figure 11a shows the temporal evolution of the m^2 profile for a typical eclipse. At about two minutes before totality, only turbulence very near the ground is making substantial contributions to the intensity fluctuations. Even by 20 seconds before totality, the turbulence within the bottom two kilometers is responsible for essentially all of the scintillations. Only within 5 to 10 seconds of totality does the high altitude turbulence make a

noticeable effect. However, even at this late time, the turbulence within two kilometers of the ground is much more important than the turbulence at the tropopause. Figure 11b shows the dependence of the scintillation profile on wavelength. At twenty seconds before totality, the wavelength dependence is confined to within a few hundred meters of the ground. By ten seconds away from totality, the wavelength dependence has spread to include all of the lower altitude turbulence while the scintillations from the tropopause are still wavelength independent. Only within a few seconds of totality does the tropopause produce wavelength dependent scintillations. Figure 11c shows that the scintillation contribution is degraded at all altitudes equally for smaller ε eclipses. Figure 11d shows the effect of zenith angle on the scintillation profile. Note that not only are the scintillations stronger, they are the result of more distant turbulence. The total scintillation index is shown in figure 12. An observer's estimate of the intensity variance would depend on the scales observed. The calculations shown in figure 12 include *all* scales. The wavelength dependence shown in figure 12a would be much more pronounced if the large-scale, wavelength independent scintillations were ignored. The same point is true of figure 12b which would show a much greater decrease in m^2 for smaller values of ε if the large-scale irregularities were left out. The dependence of m^2 on zenith angle is shown in figure 13. As long as the turbulence in the bottom few kilometers dominates the scintillations, we may treat C_n^2 as being proportional to $h^{-4/3}$. This leads to an approximate scaling formula for m^2 with zenith angle as

$$m^2(\zeta) = (\sec(\zeta))^{4/3} m^2(\zeta = 0) \tag{6.4}$$

The m^2 profile allows us to define a "typical" scattering distance which is the centroid of the scintillation contributions. We define the n-th moment of the m^2 profile as

$$\bar{z}^n = \frac{\int_0^\infty z^n C_n^2(z\cos(\zeta))\eta_{m^2}(z)dz}{\int_0^\infty C_n^2(z\cos(\zeta))\eta_{m^2}(z)dz} \tag{6.5}$$

The typical scattering distance is $\bar{z}$ and the typical width of the scattering region is

$$w = \sqrt{\overline{z^2} - \bar{z}^2}$$

A more meaningful estimate of the typical scattering distances is achieved by treating the low altitude and the tropopause turbulence contributions separately. In our turbulence profile model, eq. (6.3), the tropopause turbulence is described by the last term. Using the moments of these terms separately, two typical scattering distances are found, figure 14. Note that the typical scattering distance of the low altitude turbulence is rather insensitive to zenith angle while the tropopause distance increases with ζ.

The structure of shadow bands in the extended turbulence model is a combination of thin screen model structures from all of the contributing distances. A good picture of the evolving scales may be found, without making a detailed spectrum calculation, by using the thin screen model appropriate for the typical scattering distance. The structure is found by using eqs. (5.1), (5.2), and (5.3) with z replaced by $\bar{z}$. The effect of the actual, distributed turbulence will be to make the thin screen scales less distinct, rather than to introduce any new scales. The thin screen scales are shown in figure 15. Features much larger than 1 meter are not visible and are not shown although they contribute to m^2. When the scintillations first become visible, they present wavelength independent structures with scale L_{peak} from turbulence very near the ground. As totality nears, the typical scattering distance goes up and the prominent scale becomes L_{source} from the low altitude turbulence. The scintillations from the tropopause are still suffering from source averaging and are too faint to be seen. As the crescent narrows, the axial ratio of the pattern increases and the patterns become true "shadow bands." The very low pattern contrasts will lead to the observation that the bands are narrow dark strips separated by larger bright regions due to the logarithmic sensitivity of the eyes [13]. As the contrast increases, the pattern will appear to have roughly equal strips of light and dark. Finally, the structures at scale L_{source} merge with structures at scale $L_{Fresnel}$ and become wavelength dependent. Once $L_{Fresnel}$ is the dominant scale, the pattern spacing will slowly increase as the typical scattering distance

continues to increase. Meanwhile, scintillation structures with scale L_{peak} will have returned to a visible size, displaying small axial-ratio, wavelength independent patterns superimposed on the shadow bands. In the last few seconds from totality, the tropopause finally makes a visible effect, with patterns at scale L_{source} rapidly merging with the tropopause's $L_{fresnel}$. If the eclipse has a small value of ε, the axial ratio is never as great as in longer eclipses. In addition, the mean intensity is greater causing a diminished contrast at all scales except L_{peak}. Therefore, small ε eclipses and annular eclipses will predominantly generate the random, smoky patterns associated with L_{peak}. Figure 15b shows the effect of zenith angle on the characteristic scales. While the low altitude structures are relatively unaffected, the turbulence at the tropopause remains heavily source averaged until even closer to totality.

Since the wind velocity is often a function of altitude, the shadow band motion may change as the typical scattering distance moves to greater altitudes. If a wind-shear layer is present, distinct shadow band patterns may be seen superimposed on each other, moving with different speeds. If the observer is not on the center-line of the path of totality, the band motion will be even more complex: the wind velocity component perpendicular to the bands changing as the crescent rotates. The complications caused by wind speed variations are yet another insurmountable problem in shadow-band time series analysis. The most reasonable approach would be to treat the scintillations as if they arose from a thin screen located at the typical scattering distance and ignore changes in the shadow band speed during the observation. Nevertheless, the error analysis should seriously take such factors into account.

The generic turbulence profile, eq. (6.3), has given us a perspective on the evolution of a typical shadow band event. However, the actual turbulence profile present at an observation site may differ greatly from the model. In addition to large-scale turbulence distributions, an actual C_n^2 profile is *not* smooth; it is layered and patchy[14]. One general principle may be inferred from the generic profile: shadow band visibility is largely controlled by the level of turbulence within the bottom 2-3 kilometers of the atmosphere. Therefore, any situation in which the lower altitude turbulence is diminished will not present a strong shadow band display. Such cases would include sites with very good "seeing" or

places with high humidity, such as near lakes or on the ocean. Observations made under very windy conditions should not make good visual shadow band events due to the response time of the eye. However, properly sampled photoelectric observations obtained under similar circumstances and would lead to better temporal spectrum estimates. Sites where the eclipse is seen further from the zenith will show stronger shadow bands.

7. Summary and Comparison with Experiments.

In the preceding sections, we have seen how weak scattering scintillation theory can be used to explain all of the salient features of eclipse shadow bands. The unknown turbulence and wind speed profiles are the only reasons why explicit shadow band predictions are not possible. However, with reasonable assumptions about the meteorology, many features of the shadow bands may be understood. The band motion is driven by the wind velocity component at various contributing altitudes perpendicular to the bands. The band orientation is parallel with the crescent which is a function of time if the observer is not on the center of the path of totality. The bands will be perpendicular to the lunar shadow's path far from totality and parallel with edge of the shadow near totality. The band spacing is a complicated interplay of three intensity spectrum scales and a changing scattering altitude. The patterns start out random and disorganized, becoming more linear and organized as the crescent narrows and the scattering height increases. The band spacing decreases as totality nears and finally becomes wavelength dependent with a spacing proportional to $\sqrt{\lambda}$. The pattern contrast is wavelength dependent as diffraction effects become more important near totality, shorter wavelengths exhibiting higher contrast patterns. Both pattern contrast and spacing increase with increasing zenith angle. The scintillation theory provides no means for polarization effects and none are expected. Shorter eclipses and annular eclipses are not efficient at generating high axial-ratio shadow bands; only random, smoky patterns. Shadow bands are related to the same turbulence responsible for "seeing": good seeing implies poorer shadow band contrast. All shadow band phenomena are statistically symmetric before and after totality, except for motion. The temporal structure of the intensity fluctuations is strongly dependent on the direction and altitude

distribution of the wind.

Several experimental studies of the shadow band phenomena have been performed. Unfortunately, published experiments with sufficient information and quality to make useful theoretical comparisons are rare. Three of the best are Hults *et al* [15], Quann and Daly [4], and Marschall *et al* [16]. Hults *et al* made a study of the band orientation within the path of totality. They note a "curious rotation" of the bands when the observer was not on the center-line of the path of totality. Quann and Daly noted the same rotation but correctly attributed it to the apparent rotation of the solar crescent. Their position was just outside of the path of totality and hence would have observed the solar crescent rotate by nearly 180°. They reported data from a rawinsonde, launched prior to the eclipse, which showed the wind to be roughly parallel with the path of totality. They also made a detailed photoelectric survey to study polarization and wavelength effects. They found no polarization effects and their aggregate power spectra have widths which scale roughly as $\sqrt{\lambda}$. Unfortunately, they apparently averaged *all* times into their spectra and no real conclusions may be drawn. In the blue and ultraviolet, they observed the bands to slow down and become invisible near maximum partial eclipse. This was not seen in the green-yellow observations. During the time of this "cutoff," the wind was roughly parallel to the bands and the wavelengths affected would have had the greatest axial ratio. Additionally, the actual effect of solar limb darkening would be to reduce the mean intensity of the solar crescent in blue and ultraviolet near totality. Therefore, the observed cutoff may have been due to insufficient mean intensity at those wavelengths. The best intensity fluctuation spectrum measurements to date were made by Marschall, Mahon, and Henry [16]. Their two published spectra were taken sufficiently far from totality that the source evolution could be ignored. The noise in the pre-totality spectrum appears more pronounced than in the post-totality spectrum, suggesting that the wind was more nearly perpendicular to the bands after totality. Assuming $v / L_{Fresnel}$ to be about 30 Hz, the approximate scaling form of the power spectrum may be fit to the post-totality spectrum (figure 16). The thin screen spectrum is too steep above $v / L_{Fresnel}$. This is doubtless due to the distributed nature of the turbulence, lower altitudes providing higher frequency intensity fluctuations.

Despite the high quality of the power spectrum obtained by Marschall *et al*, the uncertainties involved in the time dependence and the wind direction make an exact comparison with the theory difficult. Two dimensional observations that did not depend on pattern drift would be far better. Perhaps with the advent of higher quality video cameras and photographic film, better comparisons will be possible in the future.

Acknowledgements.

It is a pleasure to acknowledge Stanley Flatte 'and the La Jolla Institute, Center for Studies of Nonlinear Dynamics, for support and encouraging me to pursue this application of scintillation theory to the end. I would also like to thank Rod Frehlich for technical feedback, Bernie Jackson for enthusiasm, and Rhea Eskew for a very beneficial discussion of vision and references 10 and 13.

References.

1. L. A. Marschall, "Shadow Bands – Solar Eclipse Phantoms," Sky Telesc. 67, 116 (1984).
2. A. T. Young, "Shadow Bands and the March Solar Eclipse - II," Sky Telesc. 39, 212 (1970).
3. M. Minnaert, *The Nature of Light and Color in the Open Air* (Dover, New York, 1954).
4. J. J. Quann and C. J. Daly, "The Shadow Band Phenomena," J. Atmos. Terr. Phys. 34, 577 (1972).
5. A. T. Young, "Shadow Bands and the March Solar Eclipse - I," Sky Telesc. 39, 176 (1970).
6. V. I. Tatarskii, *The Effects of the Turbulent Atmosphere on Wave Propagation* (National Technical Information Service, Springfield, VA., 1971).
7. A. T. Young, "Photometric Error Analysis. 8: The Temporal Power Spectrum of Scintillation," Appl. Opt. 8, 869 (1969).
8. E. E. Salpeter, "Interplanetary Scintillations. 1. Theory," Astrophys. J. 147, 443 (1967).
9. V. H. Rumsey, "Scintillations due to a concentrated layer with a power law turbulence spectrum," Radio Sci. 10, 107 (1975).
10. D. H. Kelly, "Motion and vision. II. Stabilized spatio-temporal threshold surface," J. Opt. Soc. Am., 69, 1340 (1979).
11. R. L. Fante, "Electromagnetic Beam Propagation in Turbulent Media: An Update," Proc. IEEE 68, 1424 (1980).
12. R. Hufnagel, "Variations of atmospheric turbulence," in *Dig. Tech. Papers, Topical Meet. Optical Propagation Through Turbulence*, pp. Wa 1-1 to Wa 1-4 (Optical Society of America, Washington, DC, 1974).
13. T. N. Cornsweet, *Visual Perception*, (Academic Press Inc., New York, N.Y., 1970).
14. J. L. Bufton, P. O. Minott, M. W. Fitzmaurice, and P. J. Titterton, "Measurements of Turbulence Profiles in the Troposphere," J. Opt. Soc. Am., 62, 1068 (1972).

Figure Captions

1. Geometry for the thin screen model.
2. Evolution of solar crescents for an observer on the center of the path of totality. Crescents are shown at τ intervals of 0.01 and ε is (a) 0.01, (b) 0.05, and (c) 0.10.
3. Definitions of crescent angles and lengths.
4. Evolution of crescent horn angles for ε = 0.001, 0.01, 0.05, and 0.1.
5. Mean intensity of solar crescent for ε = 0.001, 0.01, 0.05, and 0.1. Intensity has been normalized to the full disk intensity.
6. Evolution of solar crescents for an observer not on the center of the path of totality. Crescents are shown at τ intervals of 0.01 for $\varepsilon = 0.05$ and (a) $\rho = 0.9$, and (b) $\rho = 0.5$.
7. An example demonstrating the relationship between the actual, normalized time to totality, τ_0, and the geometrical τ. The case shown is for $\varepsilon = 0.05$ and $\rho = 0$ to 1.2 at intervals of 0.1.
8. A slice through the Fourier transform of the crescent along the κ_x axis for (a) $\varepsilon + \tau = 0.1$, (b) $\varepsilon + \tau = 0.01$, and (c) $\varepsilon + \tau = 0.001$.
9. Scintillation efficiency profiles vs. distance from the observer. Figure 9a shows the evolution of the efficiency profile vs. τ. Figure 9b shows the effect of changing the wavelength for three different times. Figure 9c shows the efficiency profile for three different values of ε at two different times, τ.
10. Plot of the shadow band intensity fluctuation spectrum perpendicular to the solar crescent showing the three major scales.
11. Plot of the modified Hufnagel turbulence profile.
12. Scintillation index profile evolution.
13. Scintillation index evolution.
14. Dependence of the scintillation index on zenith angle.
15. Typical scattering distances vs. time and zenith angle.
16. Evolution of the characteristic scales vs. time and zenith angle.
17. Observed shadow band time series power spectrum compared to the approximate thin screen model.

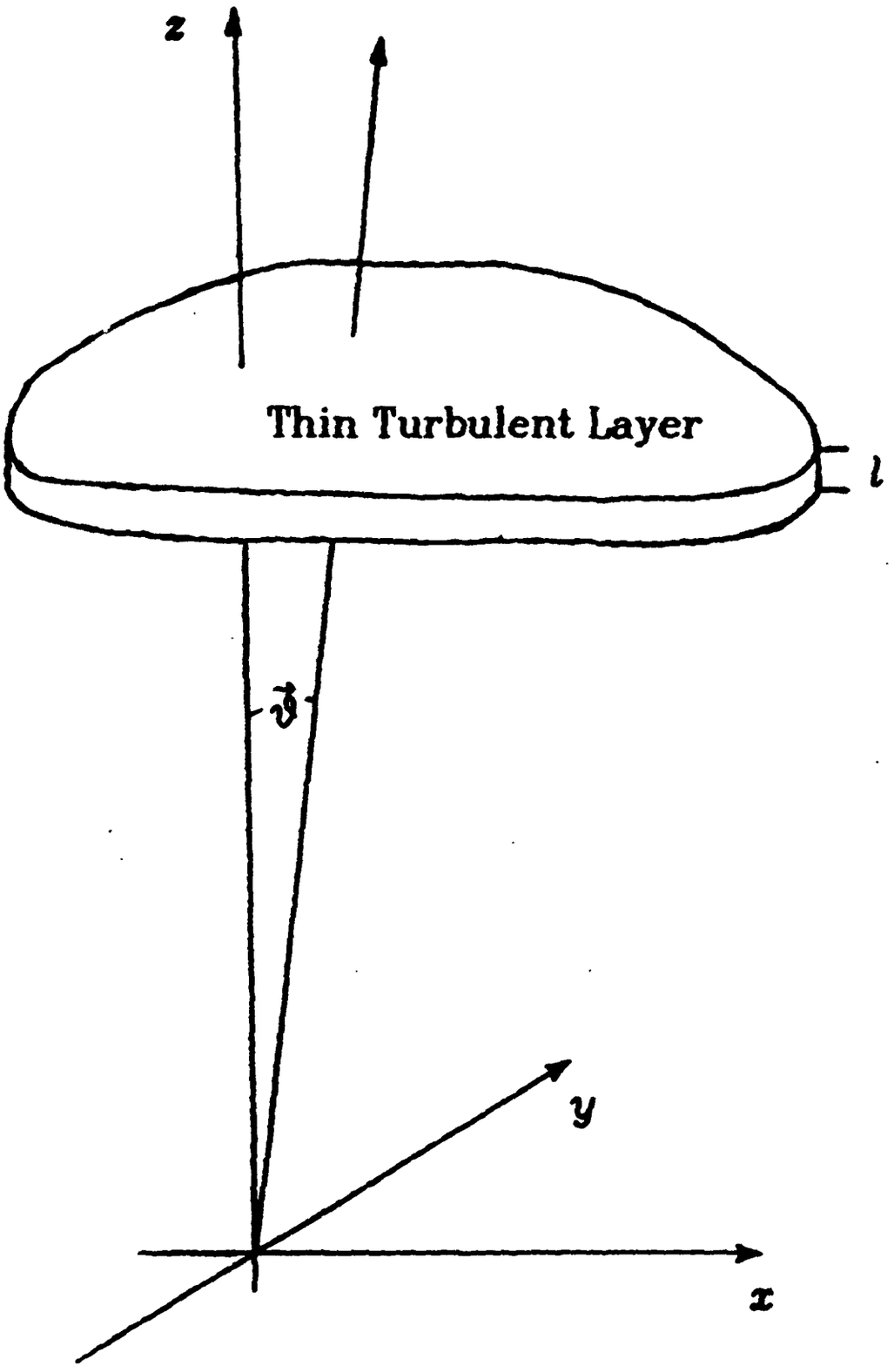
z
Thin Turbulent Layer
l
ϑ
y
x

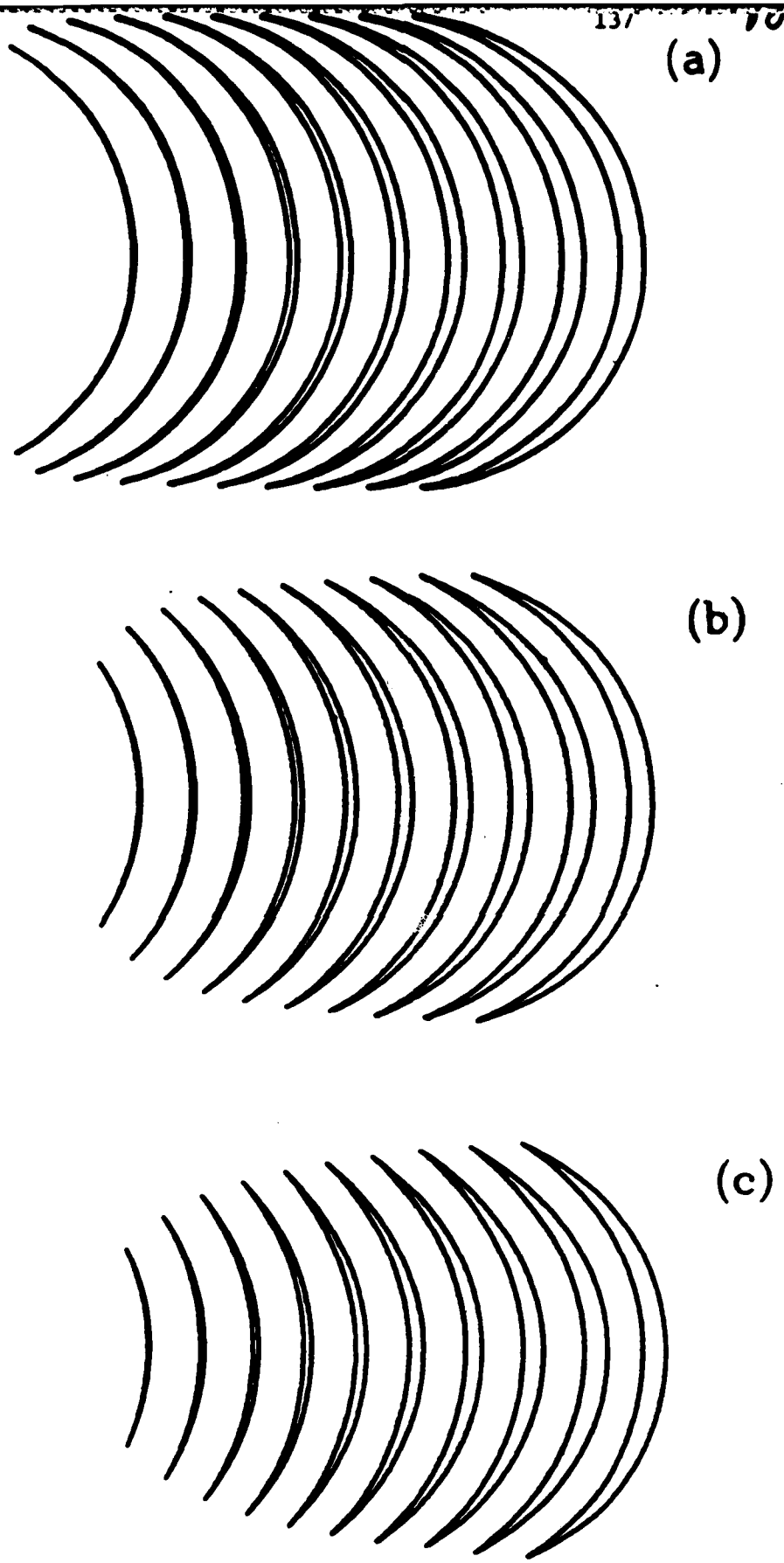
(a)
(b)
(c)

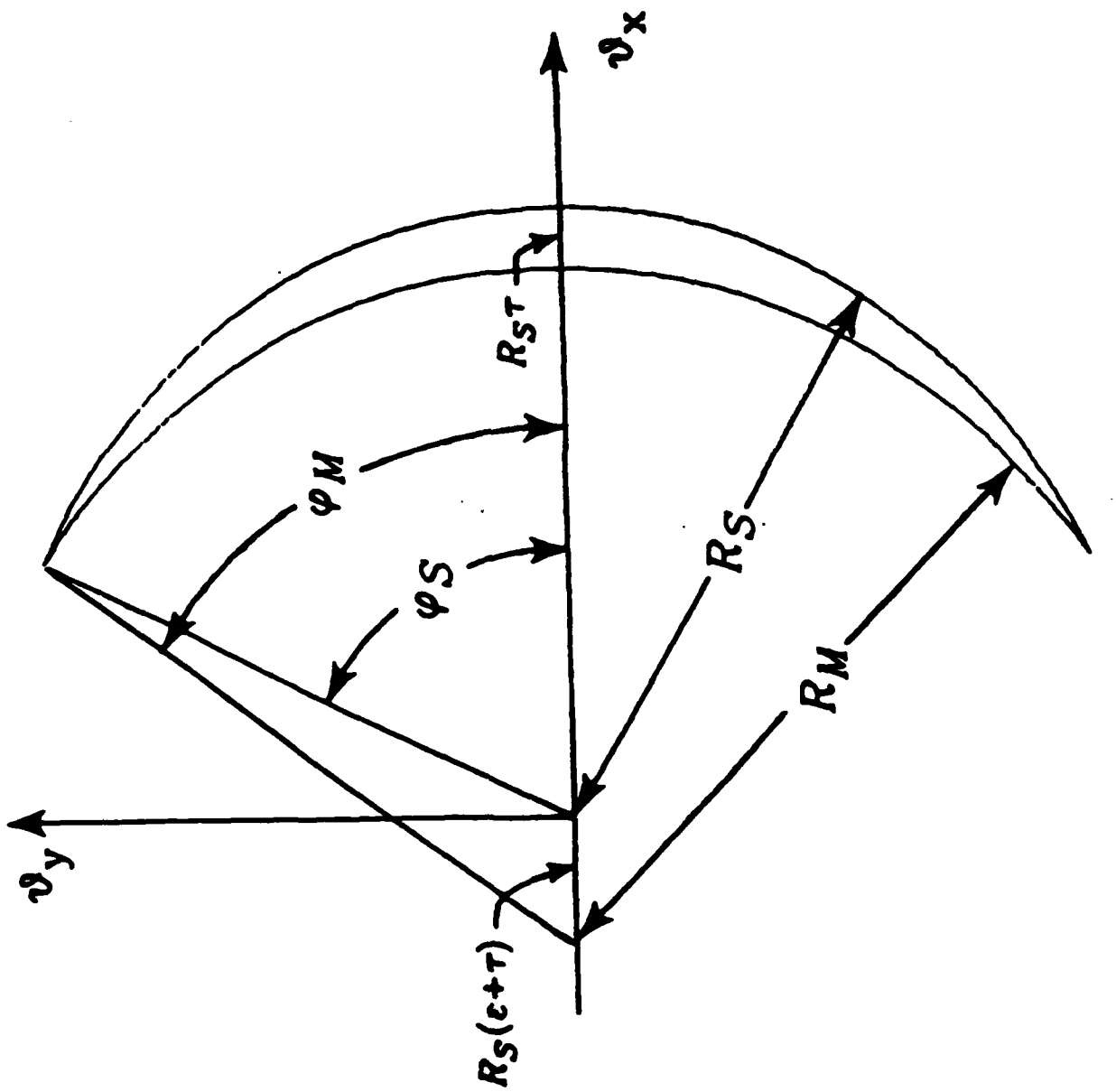
ϑ_x
R_{ST}
φ_M
φ_S
R_S
R_M
ϑ_y
$R_S(t+\tau)$

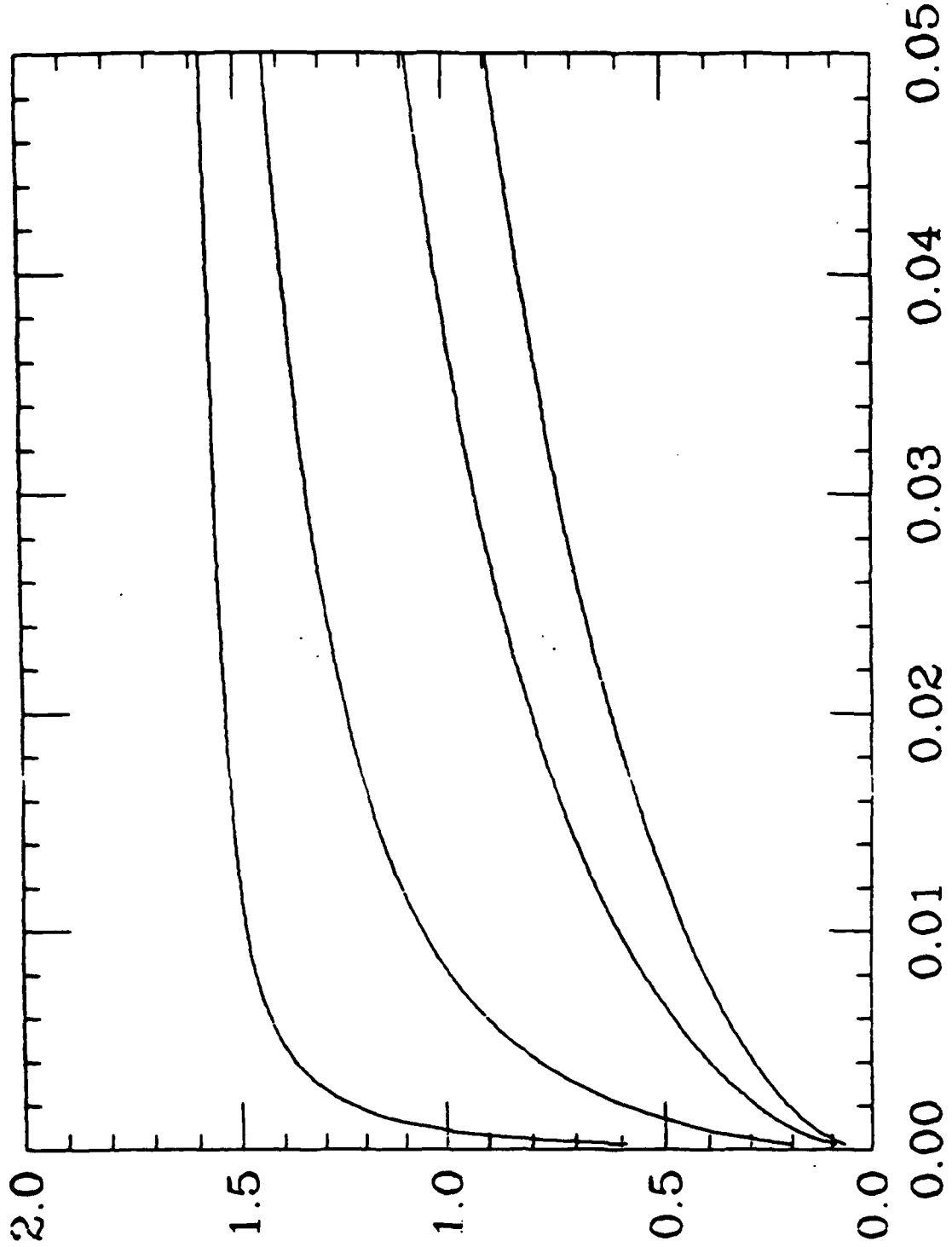
Crescent Horn Angle
2.0
1.5
1.0
0.5
0.0
0.00
0.01
0.02
0.03
0.04
0.05
τ

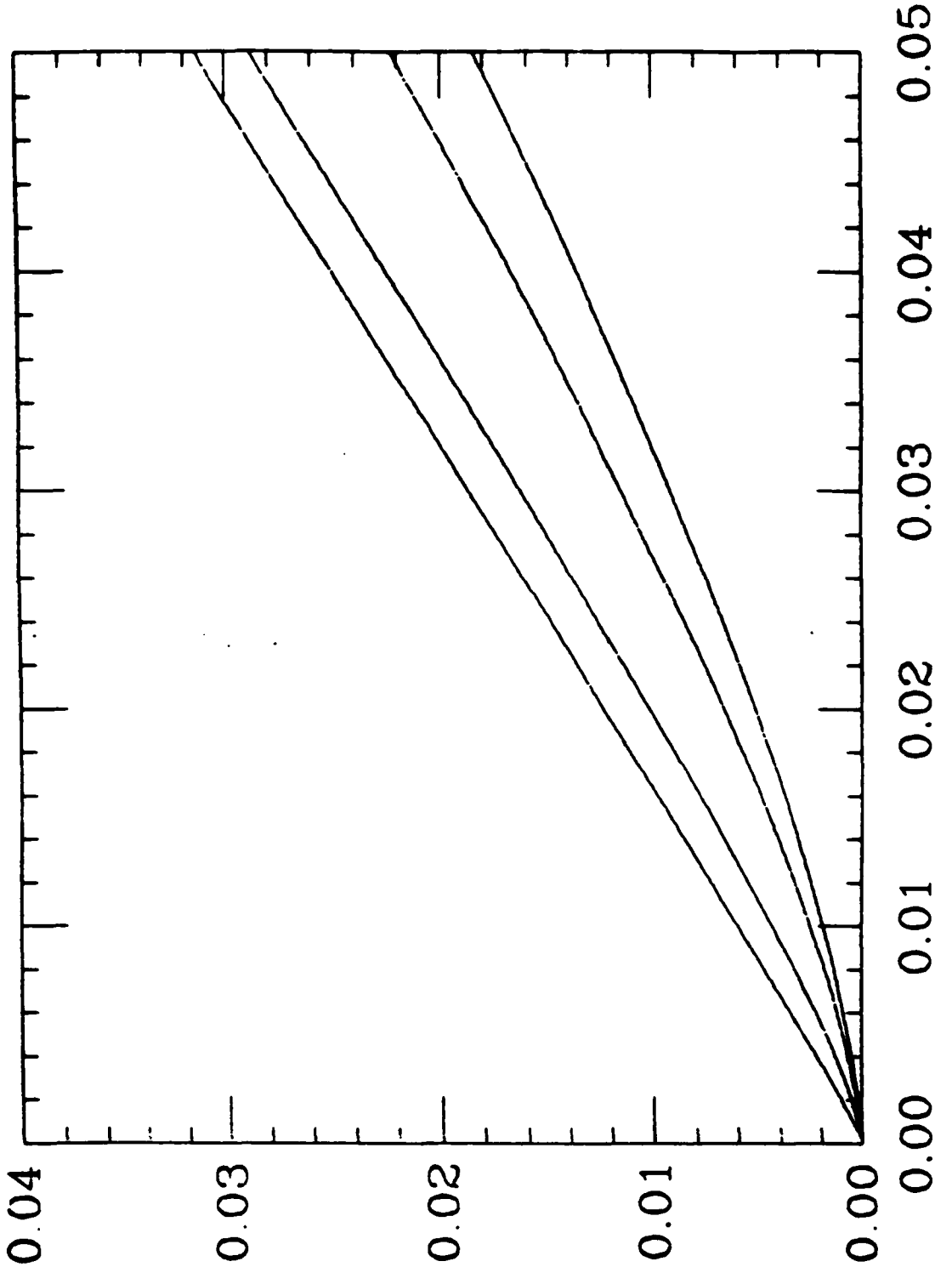
Mean Intensity
0.04
0.03
0.02
0.01
0.00
0.00
0.01
0.02
0.03
0.04
0.05
τ

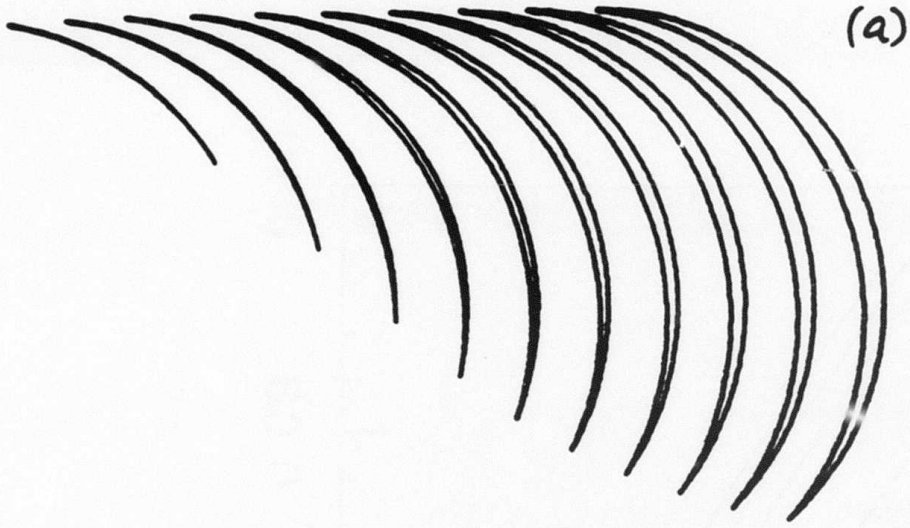
(a)

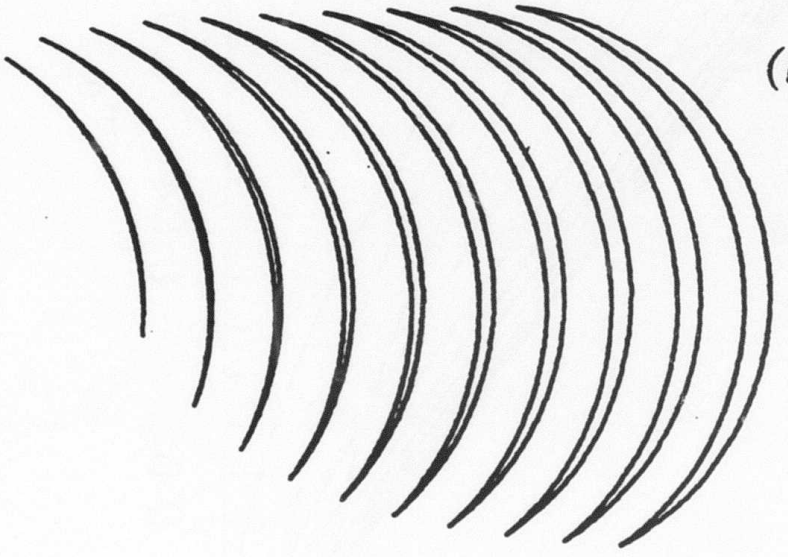
(b)

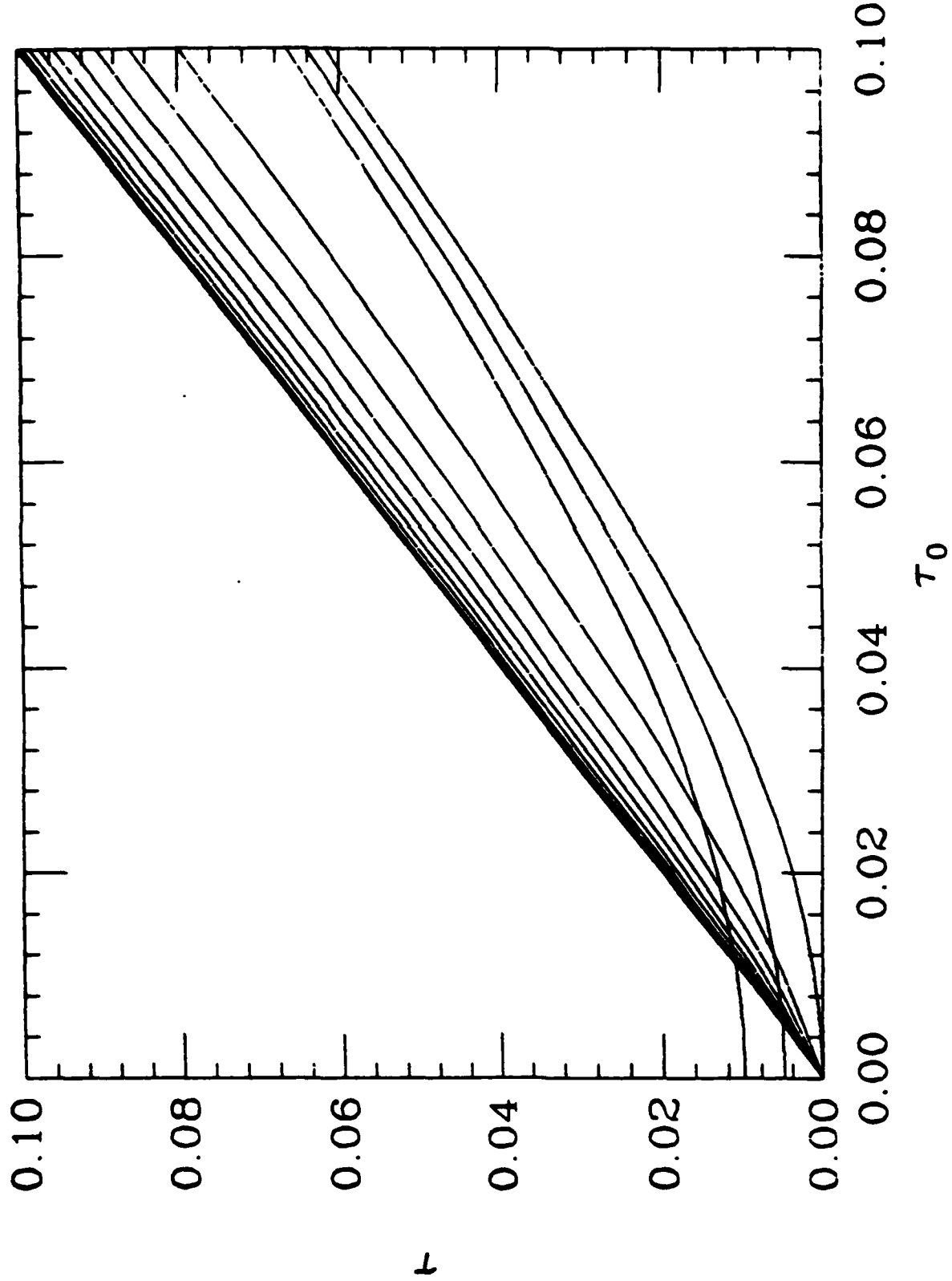
0.10
0.08
0.06
0.04
0.02
0.00
τ
0.00
0.02
0.04
0.06
0.08
0.10
τ_0

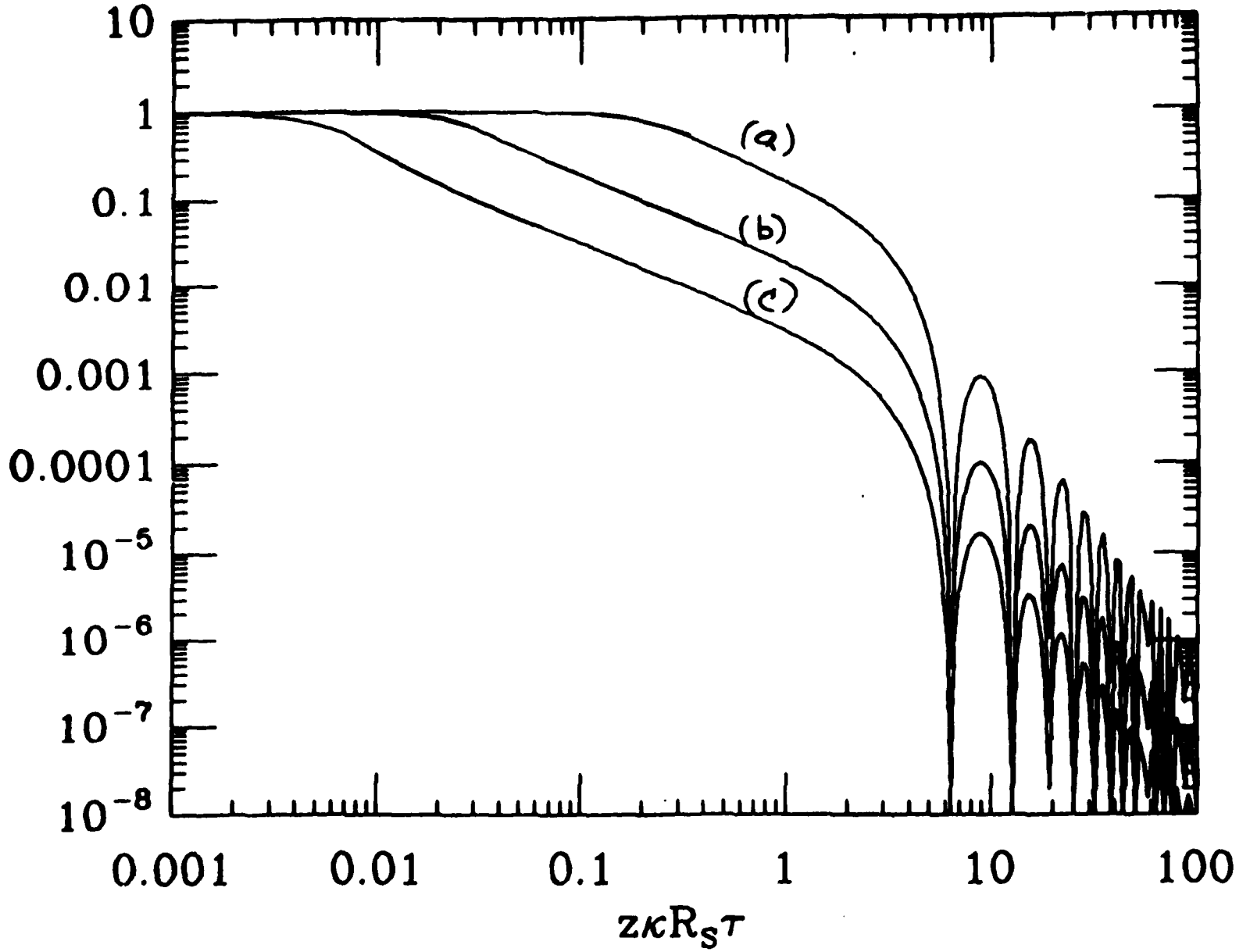
Normalized source spectrum
10
1
0.1
0.01
0.001
0.0001
10^{-5}
10^{-6}
10^{-7}
10^{-8}
(a)
(b)
(c)
0.001
0.01
0.1
1
10
100
$z\kappa R_S\tau$

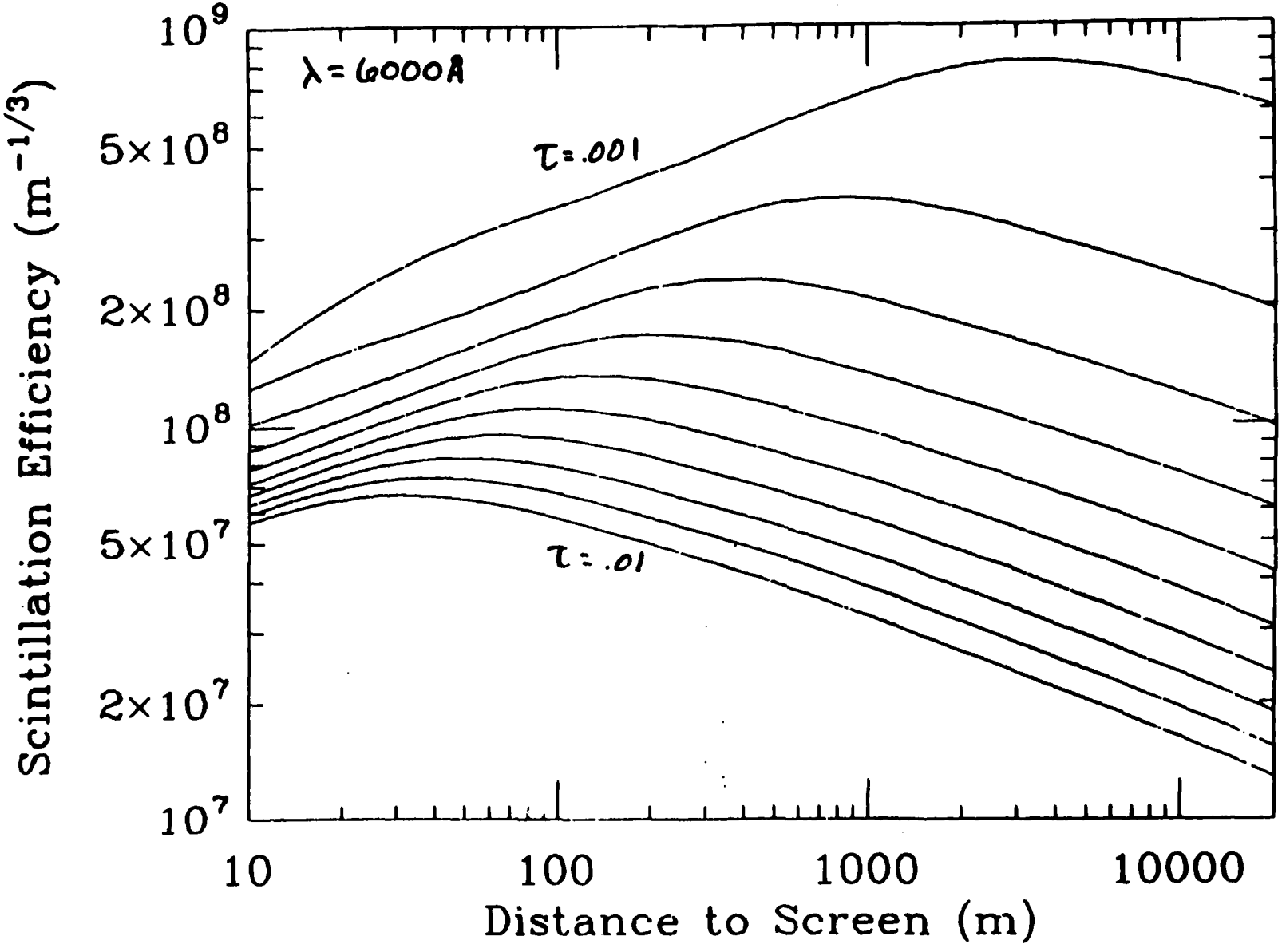
λ = 6000Å
τ = .001
τ = .01
Scintillation Efficiency (m^-1/3)
10^9
5×10^8
2×10^8
10^8
5×10^7
2×10^7
10^7
10
100
1000
10000
Distance to Screen (m)

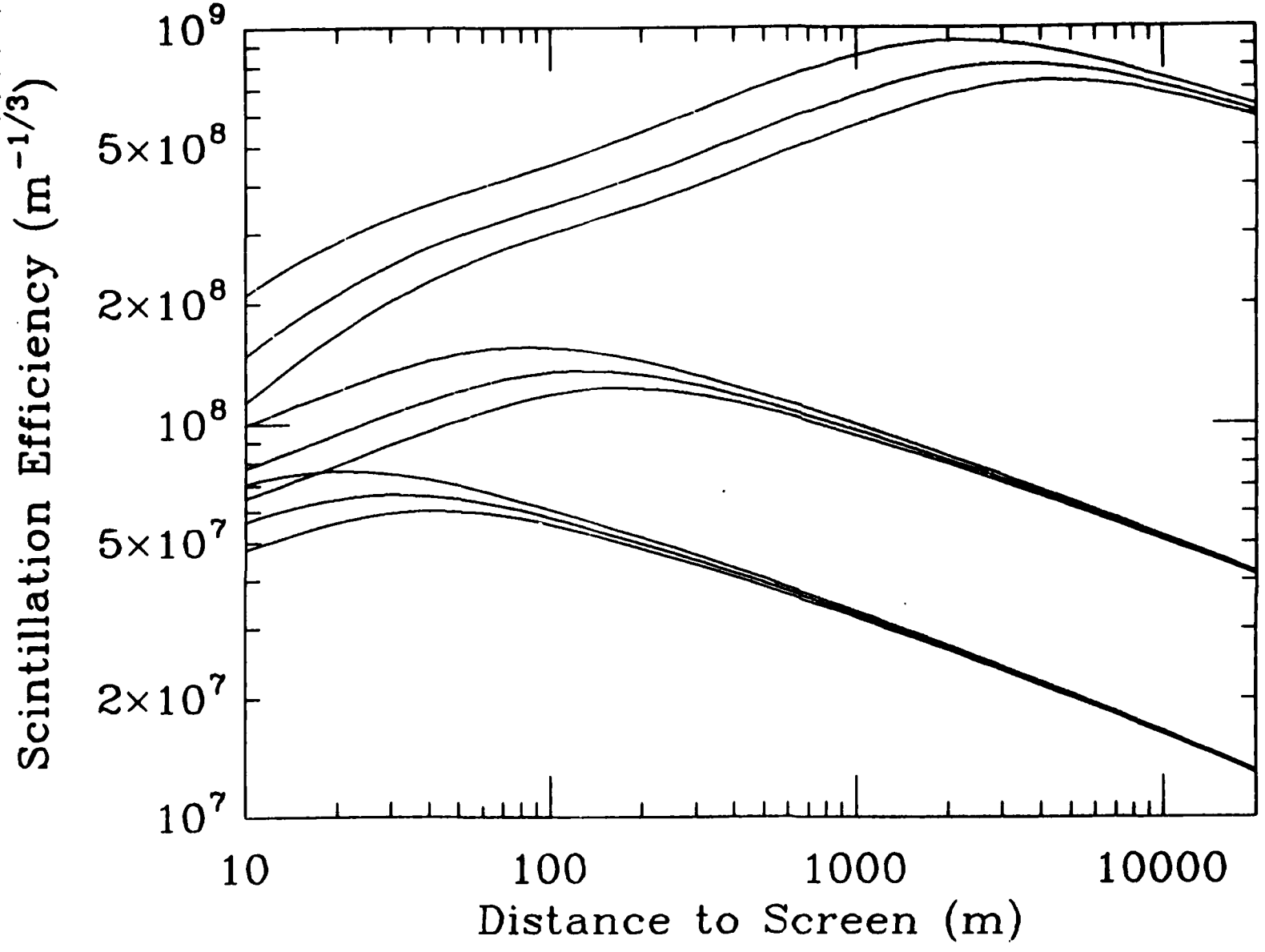
Scintillation Efficiency ($m^{-1/3}$)
10^9
5×10^8
2×10^8
10^8
5×10^7
2×10^7
10^7
10
100
1000
10000
Distance to Screen (m)

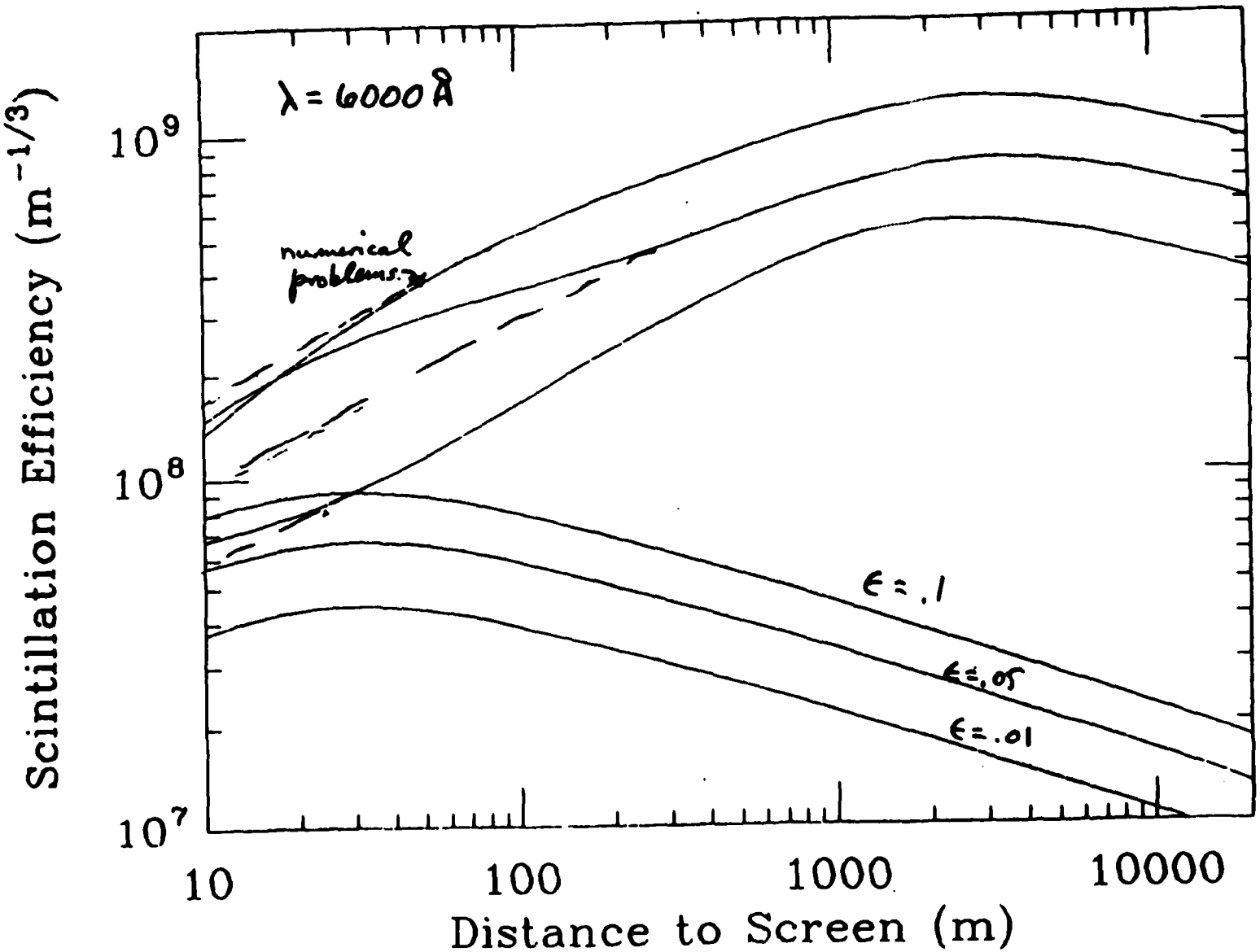
λ = 6000 Å
numerical problems
ε = .1
ε = .05
ε = .01
Scintillation Efficiency (m^-1/3)
10^9
10^8
10^7
10
100
1000
10000
Distance to Screen (m)

Figure 12

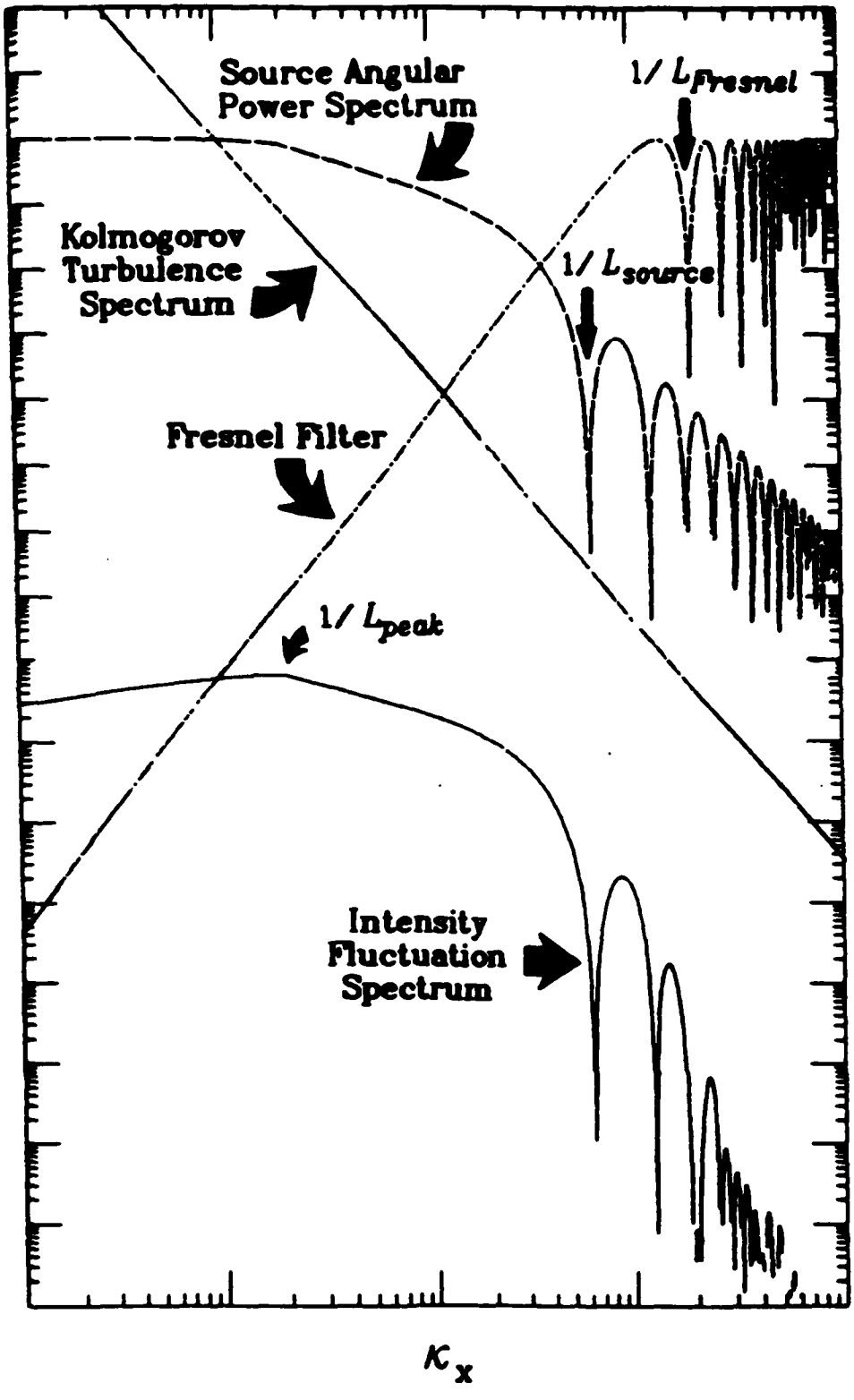
Source Angular
Power Spectrum
1/ $L_{Fresnel}$
Kolmogorov
Turbulence
Spectrum
1/ L_{source}
Fresnel Filter
1/ L_{peak}
Intensity
Fluctuation
Spectrum
Power
κ_x

figure 11

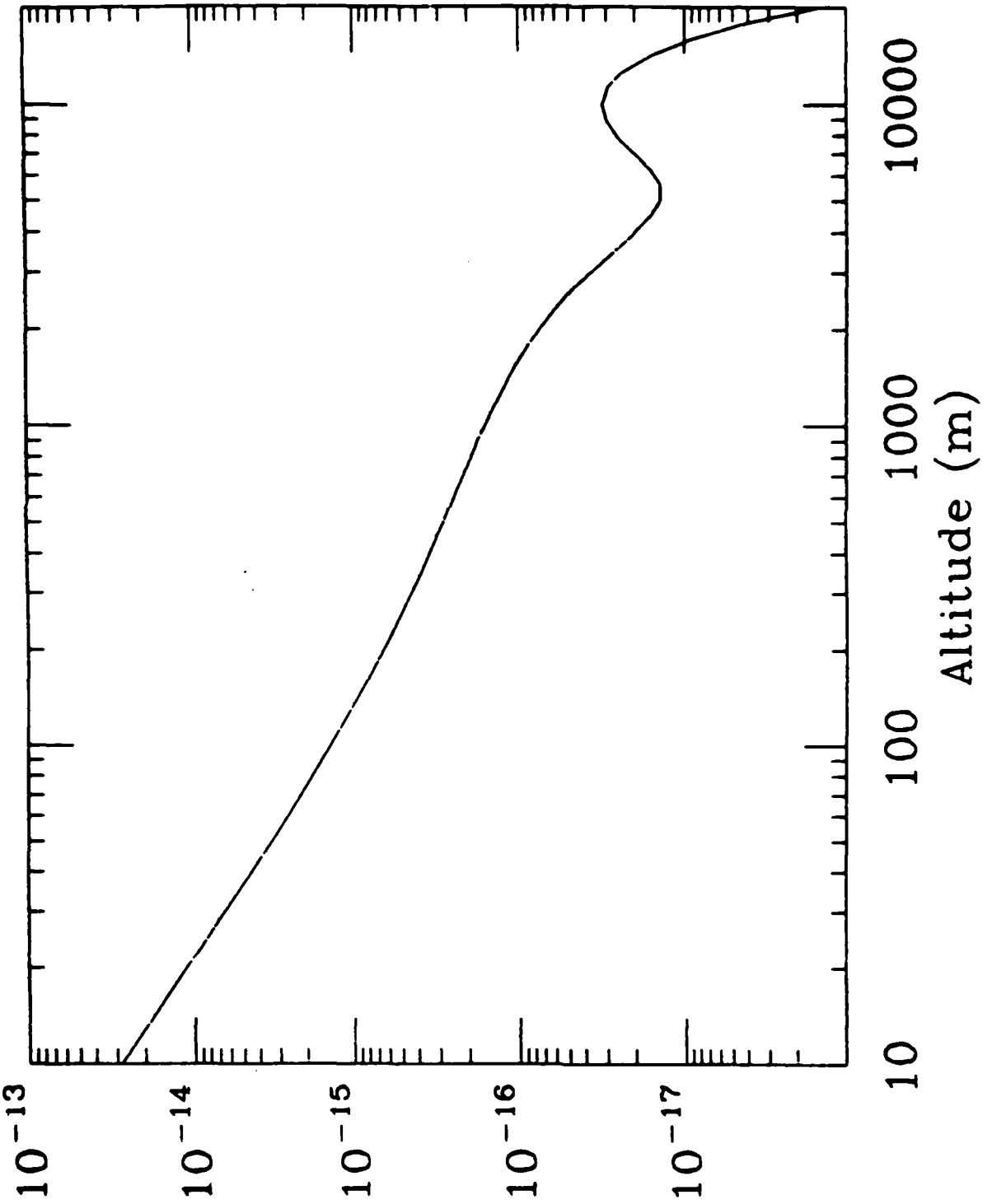

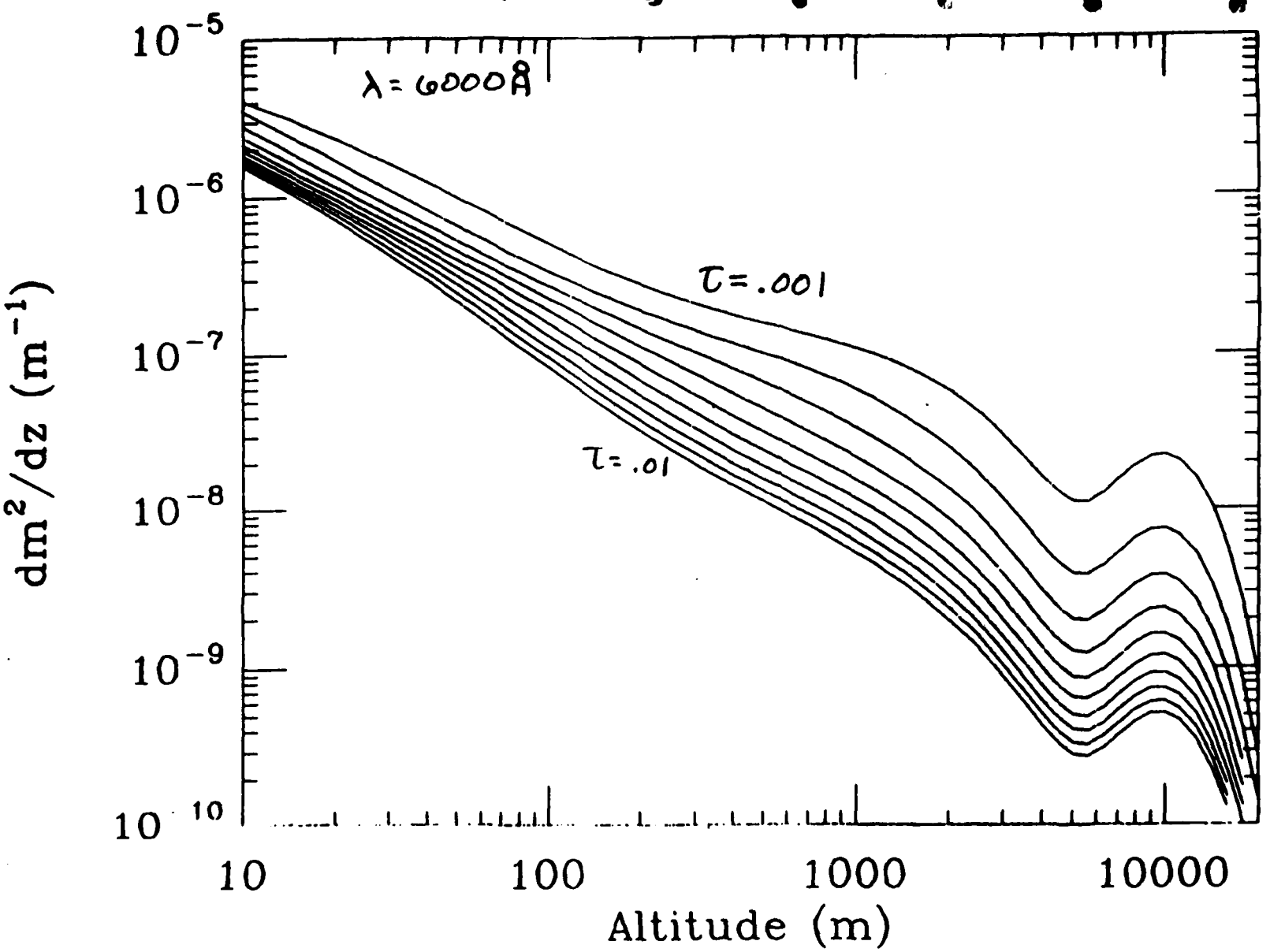
λ = 6000Å
τ = .001
τ = .01
10^{-5}
10^{-6}
10^{-7}
10^{-8}
10^{-9}
10^{-10}
$dm^2/dz\ (m^{-1})$
10
100
1000
10000
Altitude (m)

Figure 12a

Figure 26

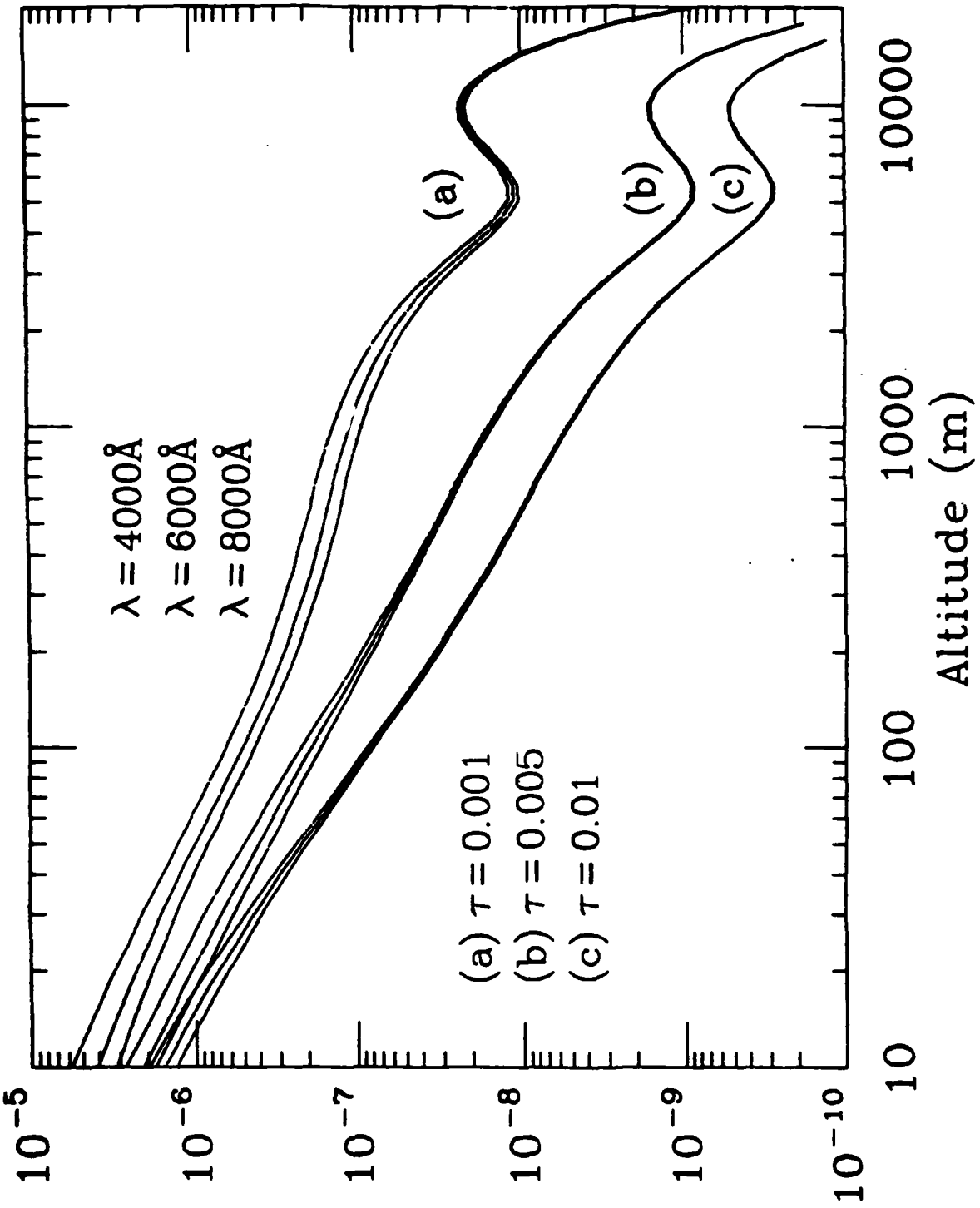
$dm^2/dz\ (m^{-1})$
10^{-5}
10^{-6}
10^{-7}
10^{-8}
10^{-9}
10^{-10}
10
100
1000
10000
Altitude (m)
(a)
(b)
(c)
λ = 4000Å
λ = 6000Å
λ = 8000Å
(a) τ = 0.001
(b) τ = 0.005
(c) τ = 0.01

figure 12c

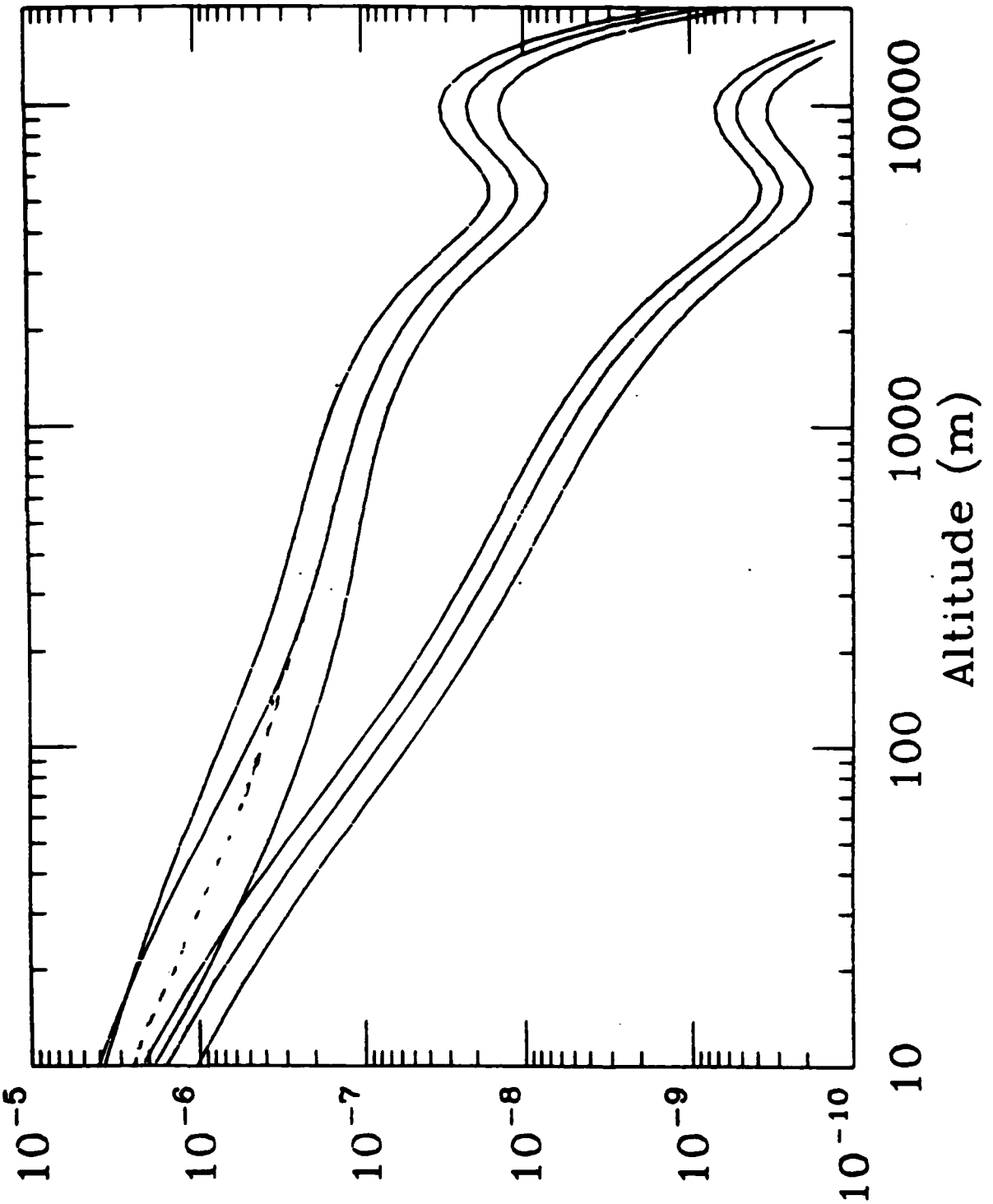

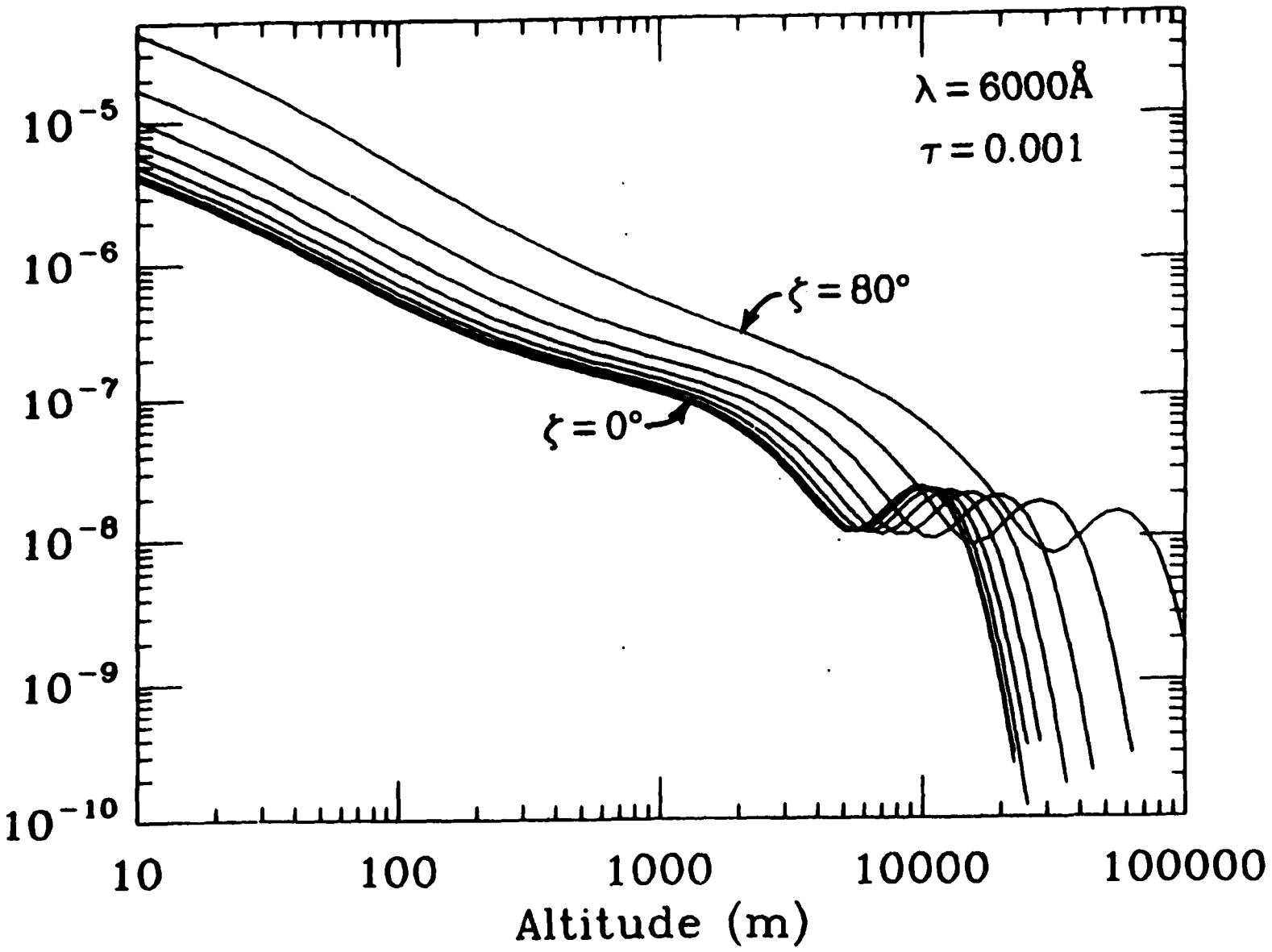
λ = 6000Å
τ = 0.001
ζ = 80°
ζ = 0°
10^{-5}
10^{-6}
10^{-7}
10^{-8}
10^{-9}
10^{-10}
$dm^2/dz\ (m^{-1})$
10
100
1000
10000
100000
Altitude (m)

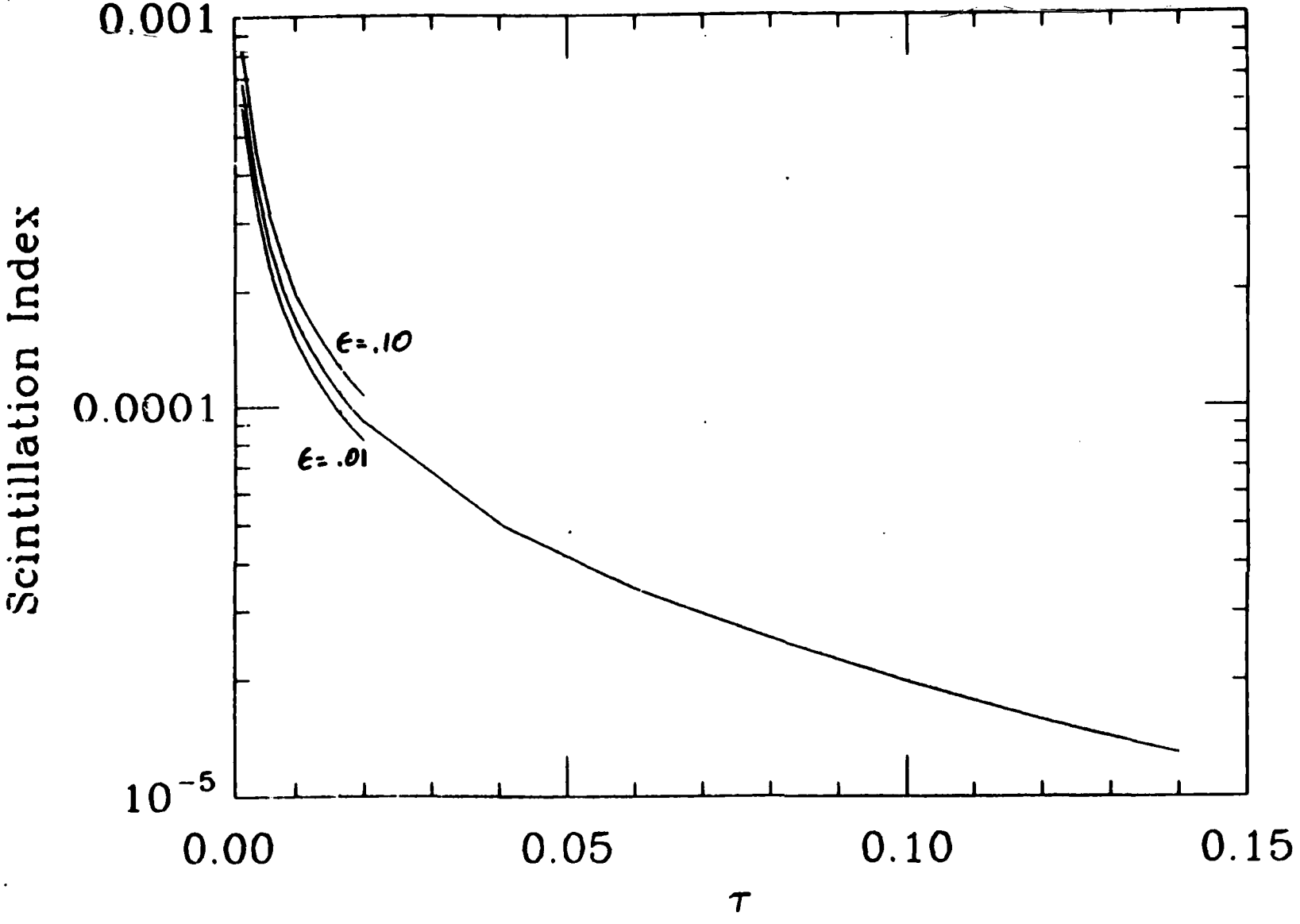
0.001
0.0001
10^{-5}
Scintillation Index
ϵ=.10
ϵ=.01
0.00
0.05
0.10
0.15
τ

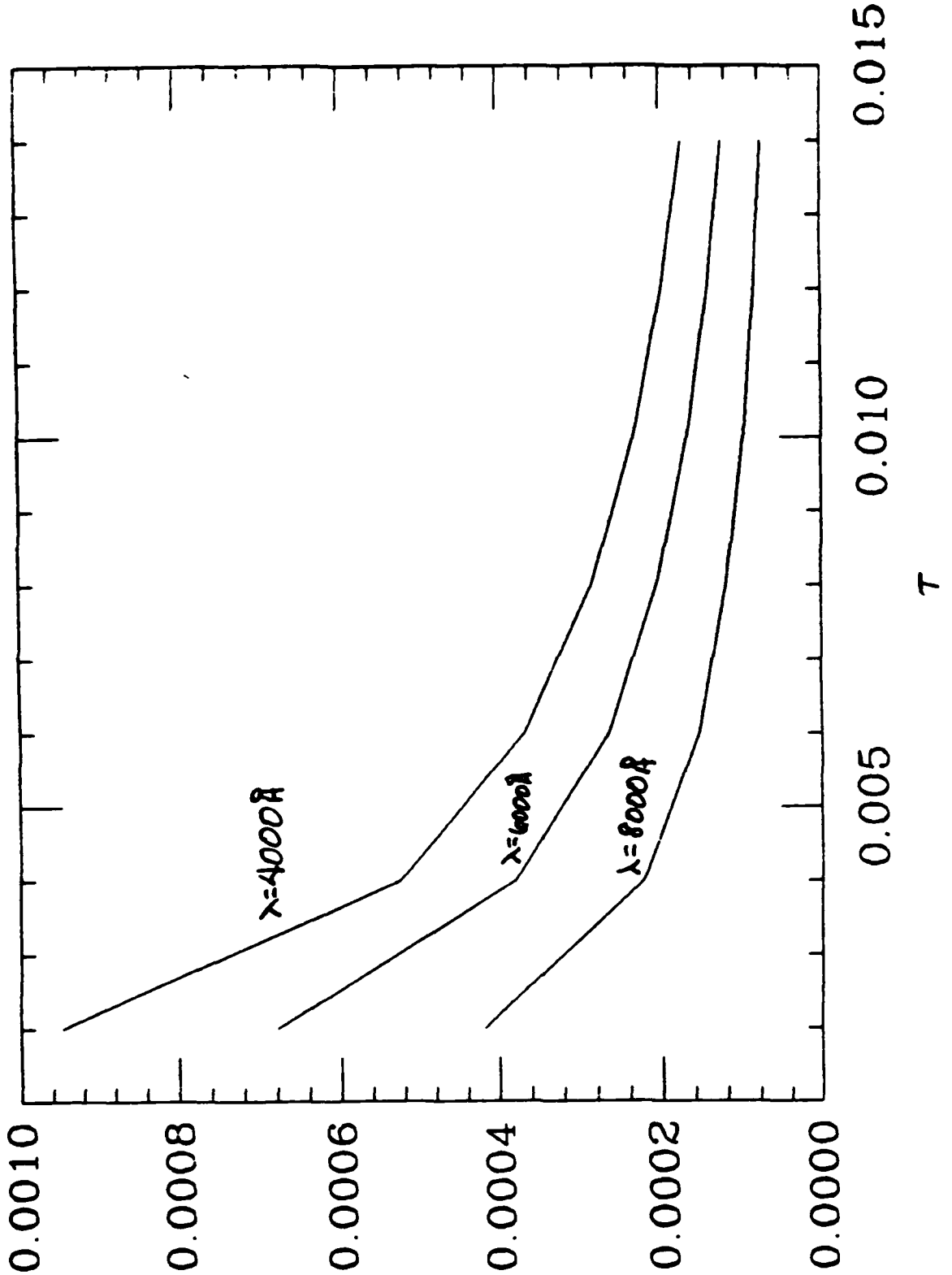
Scintillation Index
0.0010
0.0008
0.0006
0.0004
0.0002
0.0000
0.005
0.010
0.015
τ
λ=4000Å
λ=6000Å
λ=8000Å

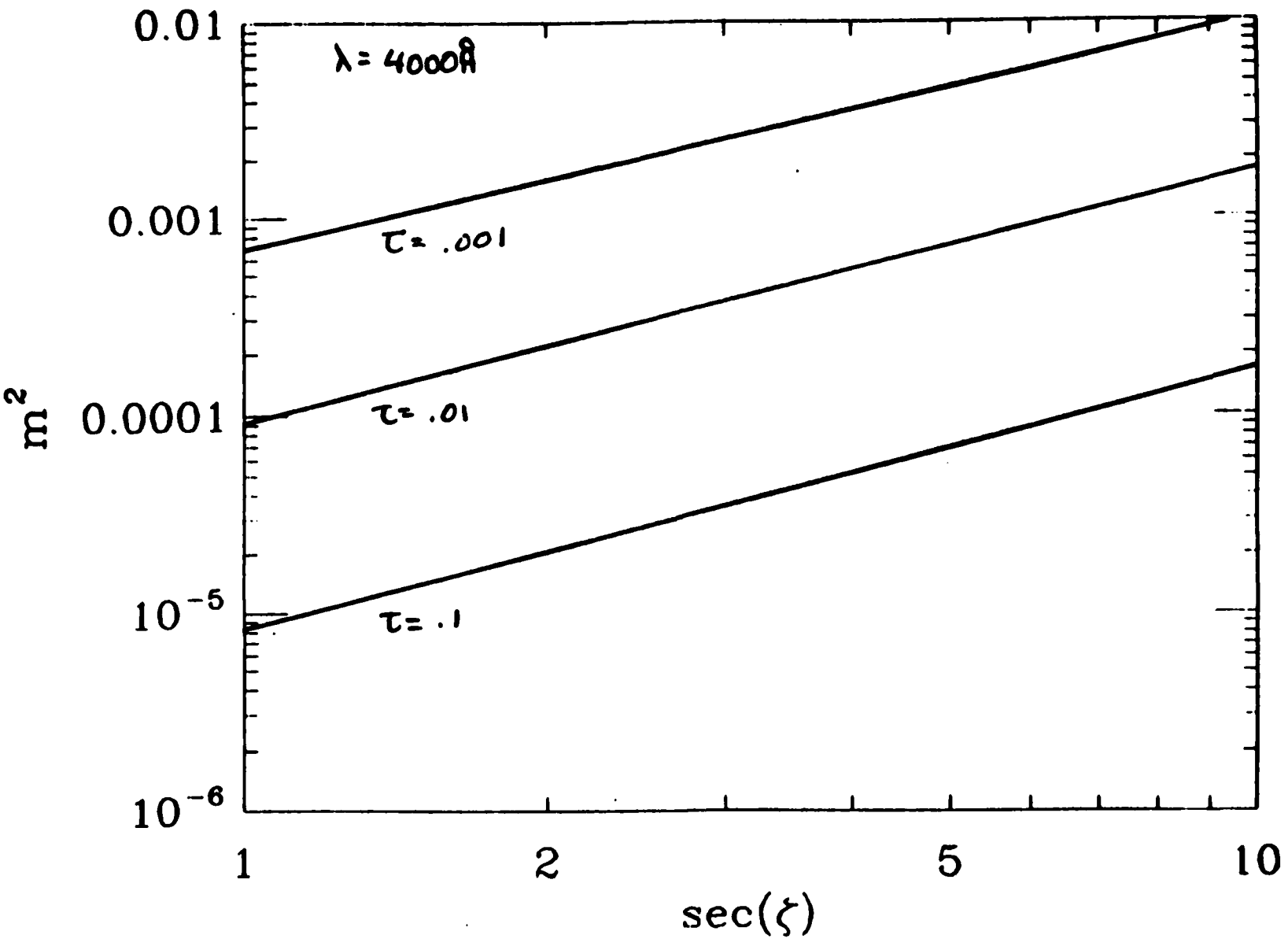
λ = 4000Å
τ = .001
τ = .01
τ = .1
0.01
0.001
0.0001
10^{-5}
10^{-6}
m^2
1
2
5
10
sec(ζ)

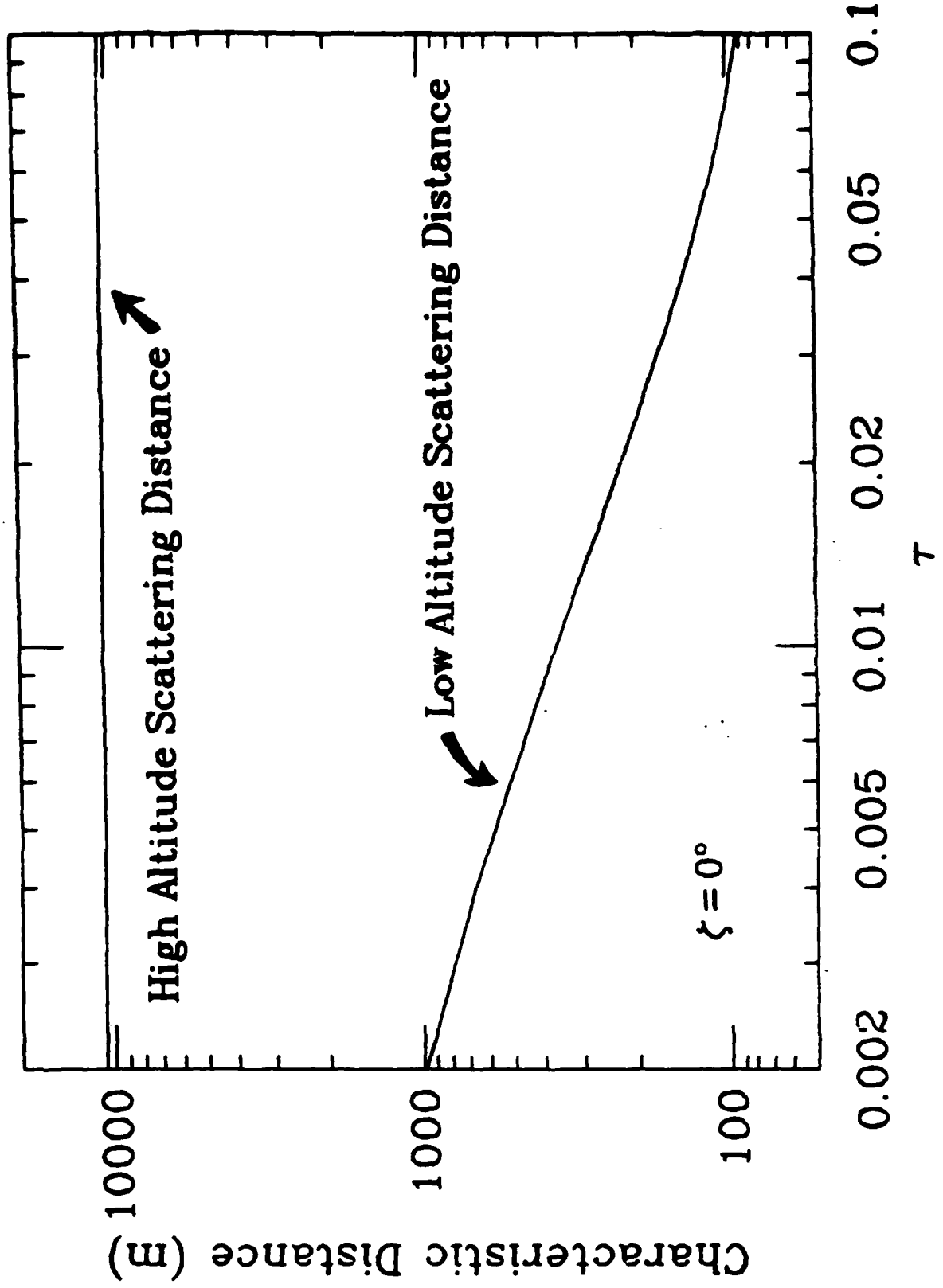
Characteristic Distance (m)
10000
1000
100
0.002
0.005
0.01
0.02
0.05
0.1
τ
ζ = 0°
High Altitude Scattering Distance
Low Altitude Scattering Distance

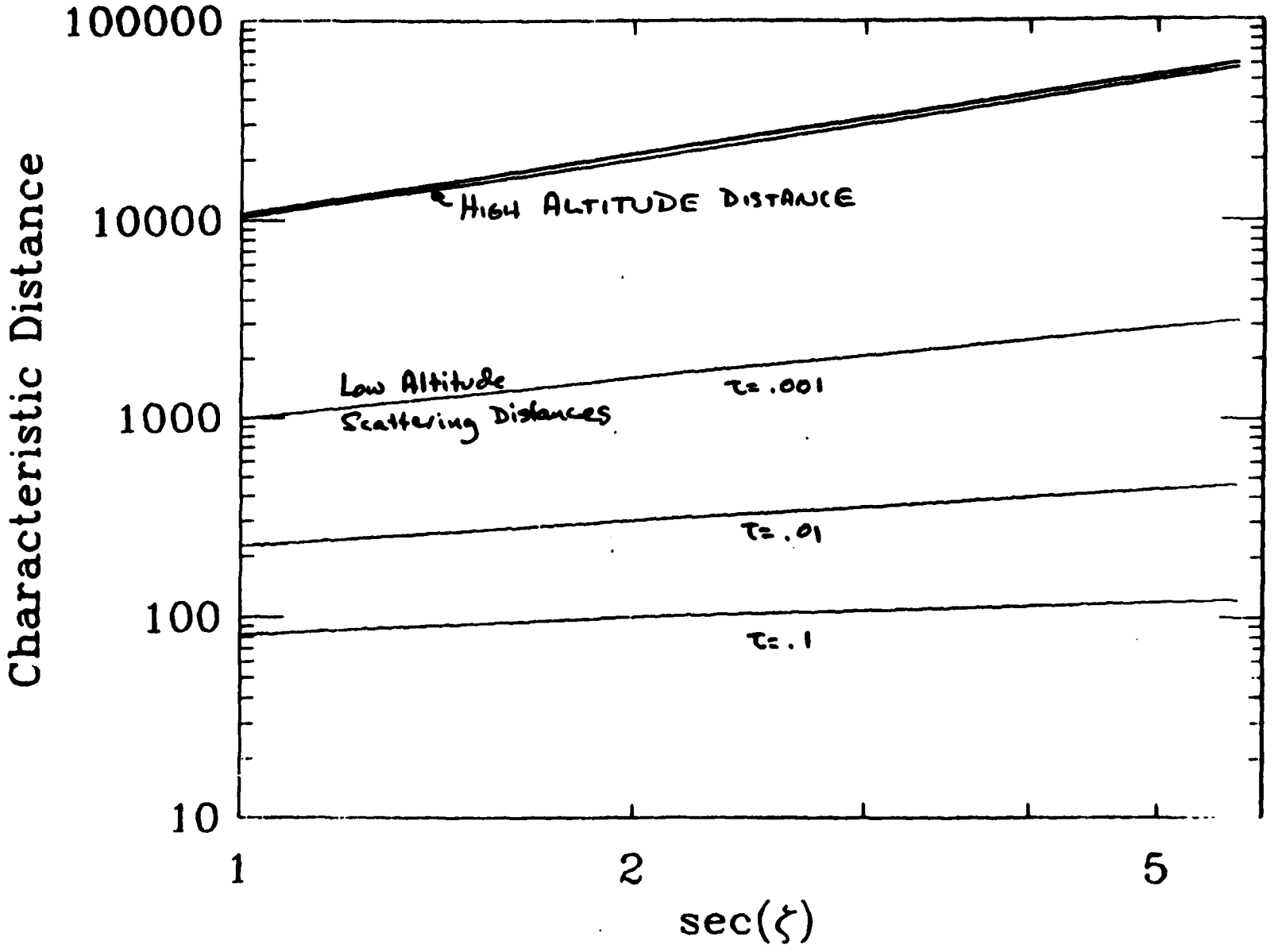
100000
10000
1000
100
10
Characteristic Distance
High Altitude Distance
Low Altitude
Scattering Distances
τ=.001
τ=.01
τ=.1
1
2
5
sec(ζ)

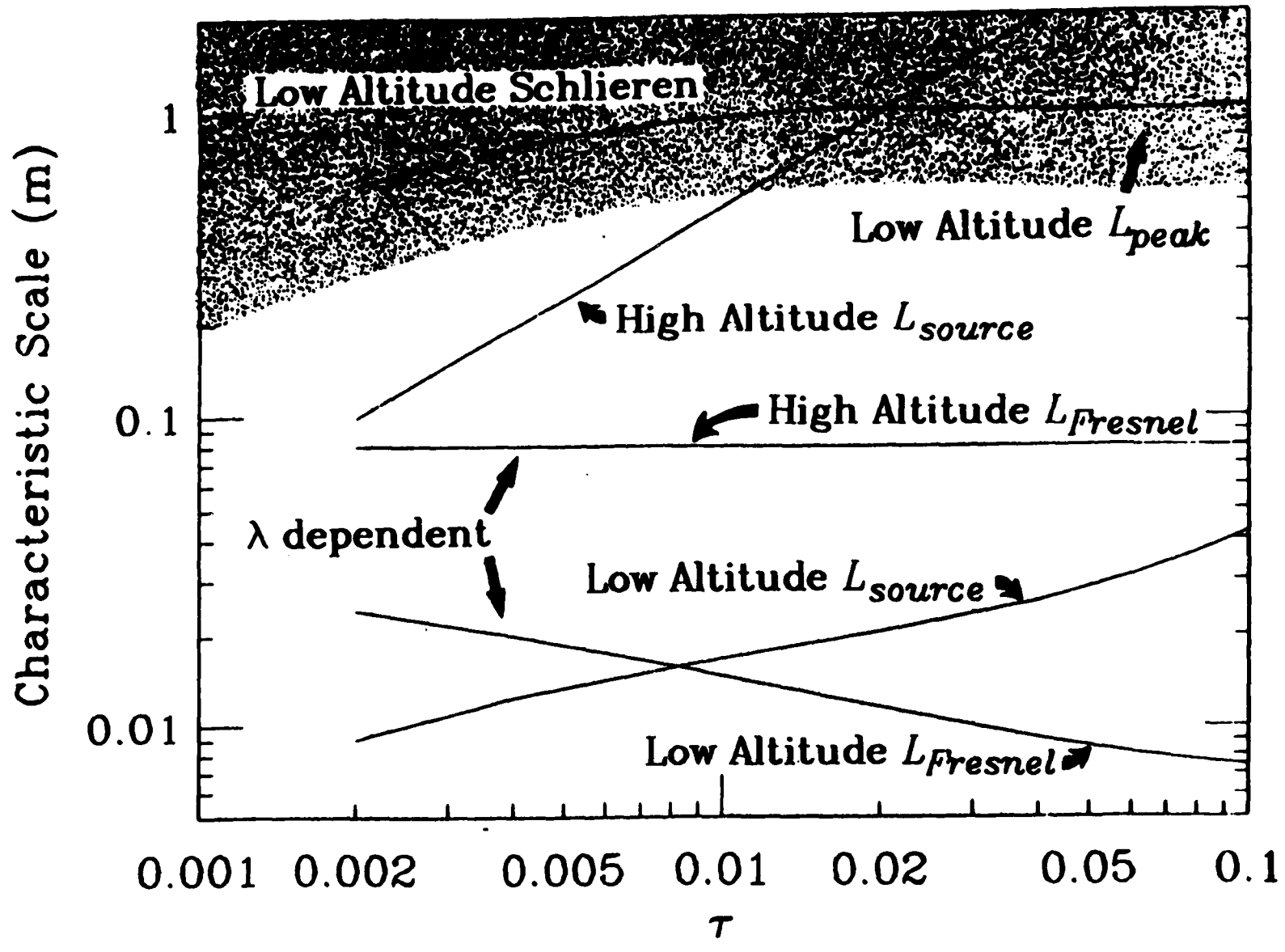
Low Altitude Schlieren
1
0.1
0.01
Characteristic Scale (m)
Low Altitude L_{peak}
High Altitude L_{source}
High Altitude $L_{Fresnel}$
λ dependent
Low Altitude L_{source}
Low Altitude $L_{Fresnel}$
0.001
0.002
0.005
0.01
0.02
0.05
0.1
τ

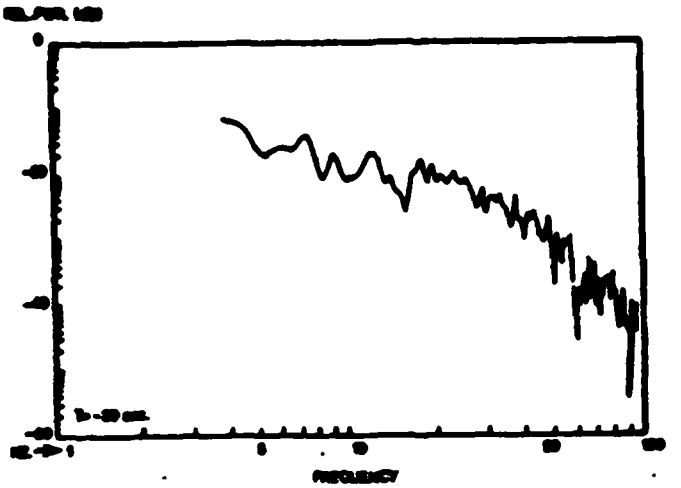

Fig. 3. Power spectrum (average of four channels) for a period of 8.192 sec beginning 30 sec before second contact.

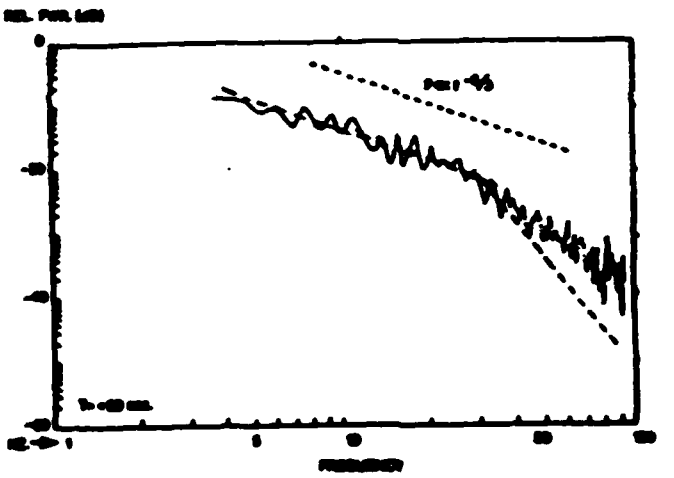

Fig. 4. Power spectrum (average of four channels) for a period of 8.192 sec beginning 20 sec after third contact. A line representing the relation $P = kF^{-\gamma}$ is shown for comparison with the results of Quenn and Daly.[16]